Uniwersytet im. Adama Mickiewicza w Poznaniu
Wydział Chemii

ROZPRAWA DOKTORSKA

mgr Dawid Lewandowski

Kontrolowane dostarczanie substancji biologicznie czynnych z wykorzystaniem modyfikowanych krzemionek

Controlled delivery of biologically active compounds using modified silicas

w formie spójnego tematycznie cyklu artykułów opublikowanych w czasopismach naukowych

Promotor: prof. dr hab. Grzegorz Schroeder
Promotor pomocniczy: dr Joanna Kurczewska

Poznań 2015

SPIS TREŚCI

WSTĘP

Hybrydowe materiały nieorganiczno-organiczne znalazły w ostatnim czasie zastosowanie jako układy dla kontrolowanego transportu substancji aktywnych biologicznie. Umożliwiają one przechowywanie substancji czynnych w formie o niezmienionej aktywności biologicznej, a także uwalnianie ze struktur hybrydowych pod wpływem czynników zewnętrznych, takich jak pH, światło, ultradźwięki, ciepło, reakcje redoks, enzymy czy pole magnetyczne, a także kombinacji dwóch lub więcej z nich. Wspomniana kontrola jest możliwa właśnie dzięki modyfikacjom tych materiałów. W przypadku krzemionek mezoporowatych, w pierwszej kolejności, wykorzystano reaktywność powierzchniowych grup silanolowych. Początkowo wprowadzano proste ugrupowania, zawierające w swojej strukturze pojedyncze grupy funkcyjne, takie jak aminową czy tiolową, które pozwalały na zmianę charakteru oddziaływań pomiędzy substancjami adsorbowanymi i zmodyfikowaną powierzchnią. Wraz z postępem w zakresie modyfikacji, zaczęto stosować coraz bardziej złożone układy, w tym cyklodekstryny oraz pseudorotaksany, będące składnikami tzw. przełączników molekularnych, regulujących precyzyjnie uwalnianie ładunku. W parze z modyfikacją powierzchni, rozwinięto inne sposoby wykorzystania materii organicznej do modyfikacji krzemionki. Możliwym stało się wplatanie niewielkich fragmentów organicznych w wewnętrzną strukturę nieorganicznej matrycy, nie zmieniając jej uporządkowania przy jednoczesnej istotnej zmianie właściwości sorpcyjnych. W celu zwiększenia użyteczności nieorganicznego nośnika opracowano również metody otrzymywania cząstek pustych w środku (tzw. hollow spheres), znacznie zwiększając przestrzeń dostępną dla adsorbujących cząsteczek, a także wprowadzono domieszkowanie innymi składnikami nieorganicznymi, np. nanocząstkami magnetytu, srebra, złota czy jonami lantanowców.

W tym nurcie badań zlokalizowana jest tematyka prowadzonych badań naukowych stanowiących pracę doktorską.

Celem naukowym rozprawy doktorskiej pod tytułem: "Kontrolowane dostarczanie substancji biologicznie czynnych z wykorzystaniem modyfikowanych krzemionek mezoporowatych" było:

1. opracowanie metod otrzymywania pochodnych związków biologicznie czynnych zawierających podstawniki zdolne do reakcji z powierzchnią krzemionki,

2. opracowanie metod otrzymywania modyfikowanych związkami biologicznie aktywnymi krzemionek mezoporowatych (MCM-41 i SBA-15),

3. ustalenie aktywności biologicznej otrzymanych układów hybrydowych pod kątem kontrolowanego dostarczania związków biologicznie czynnych do celów terapeutycznych lub diagnostycznych.

Badania prowadzone były dla związków biologicznie czynnych różniących się znacznie, zarówno strukturalnie jak i pod względem działania biologicznego. W badaniach stosowałem: barwniki używane do barwienia żywności (Chromotrop 2R - Chromotrope 2R, Żółcień pomarańczowa FCF - Sunset Yellow FCF, Błękit alcjanowy - Alcian Blue), nadtlenek wodoru, ryboflawinę (witaminę B_2), 3'-azydo-3'-deoksytymidynę (zydowudynę, AZT) oraz kwas galusowy. Wzory strukturalne wykorzystanych związków zostały przedstawione na rysunku 1.

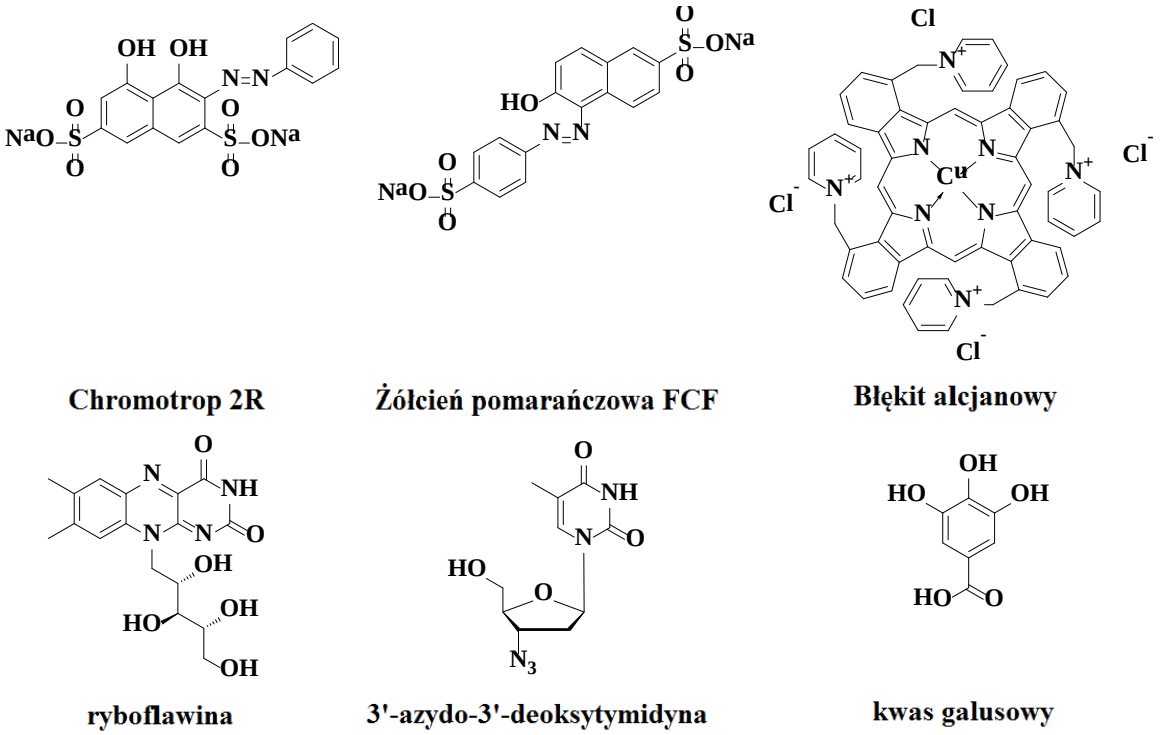

Rysunek 1. Wzory strukturalne związków biologicznie czynnych, wykorzystanych w pracy.

Barwniki zostały użyte jako związki modelowe do badania procesów adsorpcji/desorpcji na powierzchni krzemionki MCM-41, zmodyfikowanej kowalencyjnie przy pomocy związków posiadających naładowane dodatnio, jak i ujemnie grupy terminalne wpływające na ładunek powierzchniowy fragmentu nieorganicznego układu. W badaniach do modyfikacji powierzchni zastosowałem 1-metylo-3-(3-(trimetoksysililo)propylo)-1H-imidazol-3-ium, sól sodową kwasu N-(trimetoksysililopropylo)etylenodiaminotrioctowego, oraz jako układ odniesienia N-(3-

trietoksysililopropylo)glukonamid, wielokrotnie zwiększający ilość grup hydroksylowych na powierzchni krzemionki.

Mocznik z nadtlenkiem wodoru tworzy trwały kompleks o dużej stałej trwałości. Bazując na tej wiedzy, zaplanowałem otrzymanie trwałych połączeń mocznik-nadtlenek wodoru na powierzchni krzemionki mezoporowatej. Opracowałem różne metody modyfikacji powierzchni krzemionek MCM-41 i SBA-15, za pomocą N-(3-(trietoksysililo)propylo)mocznika.

Ponadto, w ramach swojej pracy doktorskiej, przeprowadziłem modyfikację powierzchni krzemionki SBA-15 ryboflawiną z użyciem łącznika izocyjanianopropylowego, a następnie zbadałem właściwości fluorescencyjne tak otrzymanego układu w obecności różnych nieorganicznych i organicznych kationów.

Azydotymidyna (AZT, 3'-azydo-3'-deoksytymidyna, zydowudyna) jest to związek chemiczny, pochodna tymidyny, w której grupa hydroksylowa w pozycji 3' zastąpiona jest grupą azydową. Związek ten jest stosowany jako lek antyretrowirusowy o działaniu anty-HIV. Działanie leku polega na przerwaniu procesu replikacji wirusa HIV w zainfekowanej komórce na zasadzie hamowania aktywności enzymu odwrotnej transkryptazy HIV, co wstrzymuje syntezę łańcucha DNA tego wirusa. Opracowałem metody syntezy krzemionek mezoporowatych modyfikowanych za pomocą AZT.

Zydowudynę, przy użyciu izocyjanianu 3-(trietoksysililo)propylu oraz, zamiennie, alkoholu propargilowego lub propargiloaminy, przekształciłem w pochodne zdolne do kowalencyjnego wiązania z powierzchnią krzemionki SBA-15. Następnie osadziłem je na powierzchni indywidualnie oraz w połączeniu z kwasem foliowym (przyłączonym przez łącznik propyloaminowy) i poddałem badaniu aktywności cytostatycznej wobec linii komórek nowotworowych HeLa i KB.

Kwas galusowy jest kwasem trójhydroksybenzoesowym, czyli należy do fenolokwasów. Kwas galusowy posiada właściwości przeciwwirusowe i antybakteryjne, wykazuje działanie przeciwzapalne po zastosowaniu doustnym lub zewnętrznym. Hamuje reakcje autoagresji immunologicznej. Ponadto, kwas galusowy hamuje rozwój grzybów pasożytniczych. W swojej pracy otrzymałem mezoporowate krzemionki modyfikowane kwasem galusowym. Proces ten przeprowadziłem według opracowanej metody syntezy. Kwas galusowy z blokowanymi grupami hydroksylowymi przekształciłem w jego chlorek kwasowy i, wykorzystując różne łączniki aminowe, wprowadzone przez: 3-(trimetoksysililo)propyloaminę, N-(2-aminoetylo)-3-(trimetoksysililo)-propyloaminę oraz

polietylenoiminę, zaszczepiłem na powierzchni krzemionki SBA-15. Po odblokowaniu grup fenolowych otrzymane materiały poddałem badaniu aktywności cytostatycznej wobec linii komórek nowotworowych HeLa i KB.

ŻYCIORYS NAUKOWY

Urodziłem się 9. listopada 1987 r. w Śremie. W 2006 r. ukończyłem I Liceum Ogólnokształcące im. Karola Marcinkowskiego w Poznaniu. W tym samym roku uzyskałem tytuł Laureata LII Olimpiady Chemicznej oraz rozpocząłem studia magisterskie na kierunku Chemia Podstawowa na Wydziale Chemii Uniwersytetu im. Adama Mickiewicza w Poznaniu. W 2007 roku, równolegle, rozpocząłem studia magisterskie na kierunku Farmacja na Wydziale Farmaceutycznym Uniwersytetu Medycznego im. Karola Marcinkowskiego w Poznaniu.

W maju 2011 roku uzyskałem tytuł magistra chemii, broniąc pracę pt. "Reakcja fuksyny z wybranymi eterami glicydowymi". Promotorem mojej pracy była dr hab. Bogusława Łęska, prof. UAM.

W 2011 roku rozpocząłem studia doktoranckie na Wydziale Chemii Uniwersytetu im. Adama Mickiewicza w Poznaniu w Zakładzie Chemii Supramolekularnej.

W maju 2012 roku uzyskałem tytuł magistra farmacji, broniąc pracę pt. "Próby zastosowania spektrometrii mas w analizie leków miejscowo znieczulających sterylizowanych radiacyjnie". Promotorem mojej pracy była prof. zw. dr hab. Barbara Marciniec.

W maju 2013 po odbyciu stażu w aptece uzyskałem Prawo Wykonywania Zawodu Farmaceuty.

Jestem współautorem sześciu publikacji w czasopismach z listy filadelfijskiej oraz czterech rozdziałów w monografiach naukowych. Brałem udział w trzech konferencjach międzynarodowych oraz pięciu konferencjach krajowych.

LISTA PUBLIKACJI

PUBLIKACJE WCHODZĄCE W SKŁAD ROZPRAWY DOKTORSKIEJ

Publikacje w czasopismach z listy filadelfijskiej:

1) Lewandowski D., Olejnik A., Schroeder G., "Adsorption studies and release of selected dyes from functionalized mesoporous MCM-41 silica", Central European Journal of Chemistry 2014;12:233-241 (IF = 1,329; punkty MNiSW = 25).
2) Lewandowski D., Bajerlein D., Schroeder G., "Adsorption of hydrogen peroxide on functionalized mesoporous silica surfaces", Structural Chemistry 2014;25(5):1505-1512 (IF = 1,837; punkty MNiSW = 25).
3) Lewandowski D., Schroeder G., Sawczak M., Ossowski T., "Fluorescence properties of riboflavin-functionalized mesoporous silica SBA-15 and riboflavin solutions in presence of different metal and organic cations", Journal of Physics and Chemistry of Solids 2015;85:56-61 (IF = 1,853; punkty MNiSW = 25).
4) Lewandowski D., Lewandowska M., Ruszkowski P., Pińska A., Schroeder G., "Immobilization of zidovudine derivatives on the SBA-15 mesoporous silica and evaluation of their cytotoxic activity", PLoS ONE 2015;10(5):e0126251 (IF = 3,234; punkty MNiSW = 40).
5) Lewandowski D., Ruszkowski P., Pińska A., Schroeder G., Kurczewska J., "SBA-15 mesoporous silica modified with gallic acid and evaluation of its cytotoxic activity", PLoS ONE 2015;10(7):e0132541 (IF = 3,234; punkty MNiSW = 40).

Rozdziały w monografiach:

1) Lewandowski D., Schroeder G., "Mesoporous silicas as carriers in controlled release systems in biomedicine and cosmetics", W: Rybachenko V. I. (red.), From molecules to functional architecture. Supramolecular interactions, East Publisher House, Donetsk 2012, s. 229-268, ISBN 978-966-317-155-5.
2) Lewandowski D., Schroeder G., "Application of mesoporous silica nanoparticles for drug delivery", W: Rybachenko V. I. (red.), New trends in supramolecular chemistry, East Publisher House, Donetsk 2014, s. 113-146, ISBN 978-966-317-208-8.

POZOSTAŁE PUBLIKACJE

Publikacje w czasopismach z listy filadelfijskiej:

1) Kurczewska J., Lewandowski D., Olejnik A., Schroeder G., Nowak I., "Double barrier as an effective method for slower delivery rate of ibuprofen", International Journal of Pharmaceutics 2014;472(1-2):248-250.

Rozdziały w monografiach:

1) Lewandowski D., Łęska B., Schroeder G., "Etery glicydowe jako prekursory modyfikacji powierzchni", W: Schroeder G. (red.), Chemiczna funkcjonalizacja powierzchni dla potrzeb nanotechnologii, Cursiva, Poznań 2011, s. 101-130, ISBN 978-83-62108-07-7.

2) Lewandowski D., Schroeder G., "Synteza układów makrocyklicznych z zastosowaniem metod klasycznej i dynamicznej chemii kombinatorycznej", W: Schroeder G. (red.), Syntetyczne receptory molekularne – strategie, syntezy, metody badawcze, BETAGRAF P.U.H., Poznań 2007, s. 49-60, ISBN 83-89936-18-6.

KONFERENCJE NAUKOWE

Międzynarodowe konferencje naukowe:

1) Lewandowski D., Cegłowski M., Schroeder G.: "Adsorption of phthalocyanine and 5,10,15,20-tetra(4-pyridyl)-21H,23H-porphine on carboxyl functionalized SBA-15 mesoporous silica" Fourth International Conference on Multifunctional, Hybrid and Nanomaterials, 9-13 marca 2015 r., Sitges.
2) Cegłowski M., Lewandowski D., Schroeder G.: "Preparation of porous polymer with Schiff base chelating groups for removal of heavy metal ions from aqueous solutions" Fourth International Conference on Multifunctional, Hybrid and Nanomaterials, 9-13 marca 2015 r., Sitges.
3) Kurczewska J., Lewandowski D., Olejnik A., Schroeder G., Nowak I.: "Double barrier as an effective method for slower delivery rate of a drug" BaltSilica, 1-3 czerwca 2014 r., Poznań.
4) Lewandowski D., Bajerlein D., Schroder G.: "Adsorption of H_2O_2 on mesoporous MCM-41 and MSU-H silicas functionalized with heterorganic moieties able to form hydrogen bonds" 16^{th} International Symposium "Advances in the Chemistry of Heteroorganic Compounds", 15. listopada 2013 r., Łódź.

Krajowe konferencje naukowe:

1) Lewandowski D., Lewandowska M., Ruszkowski P., Pińska A., Schroeder G.: "Immobilization of zidovudine derivatives on the SBA-15 mesoporous silica and evaluation of their cytotoxic activity" 7. Krajowa Konferencja Nanotechnologii, 25-27 czerwca 2015 r., Poznań.
2) Lewandowski D., Schroeder G.: "Analiza adsorpcji nadtlenku wodoru na zmodyfikowanych krzemionkach mezoporowatych MCM-41 i MSU-H", 56. Zjazd Naukowy Polskiego Towarzystwa Chemicznego i Stowarzyszenia Inżynierów i Techników Przemysłu Chemicznego, 16-20 września 2013 r., Siedlce.
3) Lewandowski D., Schroeder G.: "Analiza uwalniania wybranych barwników z modyfikowanych krzemionek mezoporowatych" 55. Zjazd Naukowy Polskiego

Towarzystwa Chemicznego i Stowarzyszenia Inżynierów i Techników Przemysłu Chemicznego, 16-20 września 2012 r., Białystok.

4) Schroeder G., Gierczyk B., Łęska B., Pankiewicz R., Cegłowski M., Lewandowski D.: "Synteza i właściwości podandów polioksaetylenowych", 50. Zjazd Naukowy Polskiego Towarzystwa Chemicznego i Stowarzyszenia Inżynierów i Techników Przemysłu Chemicznego, 9-12 września 2007 r., Toruń.

5) Gierczyk B., Łęska B., Pankiewicz R., Schroeder G., Cegłowski M., Lewandowski D.: "Zastosowanie nowych, nieorganicznych estrów surfaktantu niejonowego - Triton-X w katalizie przeniesienia międzyfazowego" I Krajowa Konferencja Nanotechnologii, 25-28 kwietnia 2007 r., Wrocław.

KONTROLOWANE DOSTARCZANIE SUBSTANCJI BIOLOGICZNIE CZYNNYCH Z WYKORZYSTANIEM KRZEMIONEK

Systemy kontrolowanego uwalniania mają ogromne znaczenie w dziedzinie dostarczania leków. Pozwalają utrzymać osoczowe stężenie substancji leczniczych na odpowiednim poziomie, znacznie zmniejszają częstotliwość zażywania kolejnych dawek leków (doustnie lub parenteralnie) oraz niejednokrotnie obniżają całkowity koszt terapii. Badane i wykorzystywane do tej pory rozwiązania oparte na materii organicznej, takie jak micele, liposomy czy też nanocząstki polimerowe, cechuje niewielka stabilność związana z podatnością na atak biochemiczny. W związku z tym, coraz więcej uwagi naukowców kieruje się ku nanocząstkom nieorganicznym, a pośród nich - krzemionkom mezoporowatym. Od początku lat 90. XX wieku, kiedy to pracownikom Mobil Oil Corporation [1] udało się opracować prostą i wydajną metodę syntezy krzemionek mezoporowatych z rodziny MCM, znajdują one coraz więcej zastosowań.

W warunkach fizjologicznych powierzchnia niezmodyfikowanej krzemionki naładowana jest ujemnie ze względu na obecność kwaśnych grup silanolowych, które można podzielić na dwie grupy, różniące się wartością pK_a [2]. Ten ładunek powierzchniowy ma duży wpływ na możliwość fizycznej adsorpcji cząsteczek związków biologicznie czynnych - decyduje o ilości substancji, która może zostać zaadsorbowana oraz reguluje kinetykę procesu desorpcji. Problemem badawczym rozwiązanym i opisanym w pracy pt. *"Adsorption studies and release of selected dyes from functionalized mesoporous MCM-41 silica"* było ustalenie wpływu różnych modyfikacji powierzchni krzemionki MCM-41 na procesy adsorpcji/desorpcji wybranych związków modelowych - dwóch barwników azowych, różniących się nieznacznie kształtem oraz rozmiarem cząsteczki, oraz jednego ftalocyjaninowego. Barwniki azowe, w warunkach prowadzenia adsorpcji/desorpcji, pozostawały zdysocjowane w formie jonów sulfonianowych, natomiast cząsteczki barwnika ftalocyjaninowego występowały jako czterokrotnie naładowane kationy. Powierzchnię krzemionek zmodyfikowałem następującymi związkami: dodatnio naładowanym 1-metylo-3-(3-(trimetoksysililo)propylo)-1H-imidazol-3-ium (IMID), obojętnym - N-(3-(trietoksysililo)propylo)glukonamidem (GLUK) oraz naładowaną ujemnie solą sodową kwasu N-(3-(trimetoksysililo)propylo)etylenodiaminotrioctowego (EDTA). Ze względu

na różną reaktywność tych odczynników względem powierzchni oraz posiadany przez nie ładunek i objętość, uzyskałem różną gęstość obsadzenia, co miało wpływ na uzyskane wyniki. Barwnik ftalocyjaninowy adsorbował efektywnie na powierzchni krzemionki bez względu na zastosowaną modyfikację (nawet w przypadku IMID, ze względu na stosunkowo niewielką gęstość obsadzenia powierzchni, ilość zaadsorbowanego barwnika była duża) i nie desorbował lub desorbował w bardzo niewielkim stopniu przy obu wartościach pH wykorzystanych w badaniu (pH = 4.5 - bufor octanowy i pH = 6.8 - bufor fosforanowy). Barwniki azowe natomiast adsorbowały zgodnie z oczekiwaniami: jako aniony najchętniej osadzały się na powierzchni zmodyfikowanej IMID, następnie GLUK i ostatecznie - EDTA. W ostatnim przypadku ilości zaadsorbowane nie wystarczały na przeprowadzenie analizy desorpcji. W pozostałych dał się zauważyć znaczny wzrost szybkości desorpcji (kilkukrotnie większy dla Chromotrop 2R niż Żółcieni pomarańczowej) przy pH = 6.8 względem pH = 4.5, co można wytłumaczyć przez większy stopień dysocjacji barwników przy wyższej wartości pH. Porównanie kinetyki desorpcji dla obu przeprowadzonych modyfikacji, tj. IMID i GLUK, dostarcza ciekawych wniosków. Jedynie dla Żółcieni pomarańczowej i wartości pH = 4.5, desorpcja następuje szybciej dla GLUK, niż dla IMID (co sugerowałyby oddziaływania elektrostatyczne między barwnikami i powierzchnią), natomiast pozostałe pomiary wskazywały na szybsze uwalnianie barwników z powierzchni krzemionki zmodyfikowanej IMID. Wszystkie uzyskane krzywe kinetyczne dobrze korelują z pierwszorzędową kinetyką uwalniania, co wskazuje na fakt adsorpcji barwników na zewnętrznej powierzchni krzemionki oraz w pobliżu ujścia mezoporów. Podsumowując, badanie pokazało, że zarówno adsorpcja fizyczna, jak i następcza desorpcja, zależą od wielu czynników, takich jak rozmiar cząsteczek, ich właściwości kwasowo-zasadowe, średnica porów, ładunek elektryczny powierzchni czy warunki zewnętrzne (pH środowiska), dlatego też nie można wyników uzyskanych dla jednego związku przenosić bezpośrednio na inny, nawet bardzo podobny strukturalnie.

Próbę wykorzystania adsorpcji fizycznej w celu kontrolowanego dostarczenia substancji biologicznie czynnej zastosowałem również wobec nadtlenku wodoru, co zostało opisane w pracy pt. *„Adsorption of hydrogen peroxide on functionalized mesoporous silica surfaces”*. Zainspirowany informacjami na temat znanego już od dawna połączenia kompleksowego mocznika z nadtlenkiem wodoru (UHP) [3], postanowiłem sprawdzić, czy możliwe jest wytworzenie tego typu połączenia na

powierzchni krzemionki mezoporowatej, co pozwoliłoby dostarczać nadtlenek wodoru na stabilnym nośniku nieorganicznym. W tym celu zmodyfikowałem izocyjanian 3-(trietoksysililo)propylu, przy pomocy gazowego amoniaku, do N-(3-(trietoksysililo)propylo)mocznika, a następnie osadziłem na powierzchni krzemionki SBA-15. Kolejno, próbki tak otrzymanego materiału zawieszałem w wodnych roztworach nadtlenku wodoru o różnych stężeniach na okres 24 godzin, a następnie suszyłem w nieznacznie podwyższonej temperaturze. Gotowy materiał zanalizowałem pod kątem obecności nadtlenku wodoru, wykorzystując metodę tiocyjanianową [4]. Otrzymane wyniki pozwoliły ustalić, że maksimum adsorpcji było obserwowane przy stężeniu roztworu nadtlenku wodoru 25% - powyżej tej wartości dochodziło najprawdopodobniej do utlenienia części organicznej i utraty możliwości wiązania nadtlenku wodoru. Ponadto, krzemionka SBA-15, ze względu na średnicę porów, a co za tym idzie znacznie większą przestrzeń zdolną pomieścić adsorbat, była w stanie przyjąć dwukrotnie więcej nadtlenku wodoru, niż MCM-41. Mimo wszystko, zawartość procentowa nadtlenku wodoru w otrzymanym materiale była znacznie mniejsza, niż dla kompleksu UHP.

Dużo stabilniejsze połączenia adsorbent-adsorbat otrzymywane są na drodze chemisorpcji, dlatego też część mojej pracy doktorskiej była poświęcona dostarczaniu substancji biologicznie czynnych związanych z powierzchnią kowalencyjnie. W pracy pt. *"Fluorescence properties of riboflavin-functionalized mesoporous silica SBA-15 and riboflavin solutions in presence of different metal and organic cations"* problemem badawczym, jaki podjąłem, było kowalencyjne przyłączenie cząsteczek ryboflawiny (witaminy B_2) do powierzchni krzemionki SBA-15 przez łącznik izocyjanianopropylowy (w określonych warunkach temperatury, środowiska i czasu prowadzenia reakcji - ryboflawinę cechuje słaba rozpuszczalność w większości rozpuszczalników, a ponadto ulega degradacji w podwyższonej temperaturze) i analiza właściwości fluorescencyjnych tak otrzymanego materiału. Otrzymałem bladożółty proszek, zawierający - co ustalono przy pomocy analizy elementarnej - 34,6 μmol witaminy B_2 na każdy gram użytej krzemionki. Wykazywał on - w formie zawiesiny w roztworze wodnym - znaczne różnice w intensywności emisji oraz położeniu maksimum emisji fluorescencji w obecności poszczególnych kationów, zarówno nieorganicznych, jak i organicznych. Intensywność emisji zawierała się w zakresie od 10 do 180% względem zawiesiny w czystej wodzie demineralizowanej (dla ryboflawiny rozpuszczonej w wodzie wartości te wynosiły od 87 do 101% - wyjątkowo dla jonów srebra - 10%, rtęci(II) - 33% i kationu benzokainowego -

64%), a maksima emisji były przesunięte od -30,6 do +20,3 nm względem maksimum w wodzie demineralizowanej (w roztworze, dla ryboflawiny, wartości te oscylowały w zakresie od -2,2 do -0,1 nm).

Chemisorpcji na powierzchni krzemionki mezoporowatej SBA-15 dokonałem również z wykorzystaniem substancji o właściwościach przeciwnowotworowych. W pracy pt. *"Immobilization of zidovudine derivatives on the SBA-15 mesoporous silica and evaluation of their cytotoxic activity"* problemem naukowym, którego się podjąłem, było otrzymanie pochodnych znanego leku przeciwnowotworowego, 3'-azydo-3'-deoksytymidyny (zydowudyny), zdolnych do kowalencyjnego związania się z powierzchnią krzemionki, a następnie zbadanie aktywności cytostatycznej otrzymanych materiałów. W tym celu izocyjanian 3-(trietoksysililo)propylu poddałem działaniu, równolegle, alkoholu propargilowego i propargiloaminy, by otrzymać produkty pośrednie, widoczne na rysunku 2.

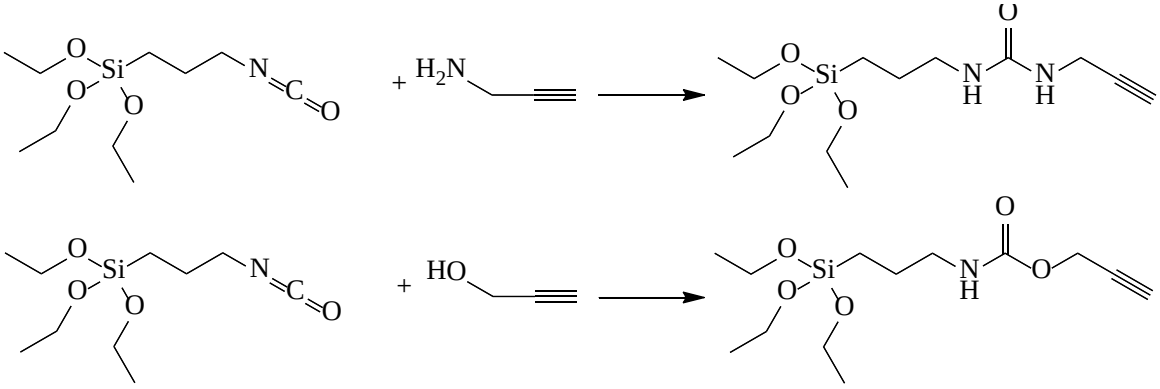

Rysunek 2. Schemat syntezy produktów pośrednich, pochodnych zydowudyny.

Następnie oba połączyłem, wykorzystując reakcję 1,3-dipolarnej cykloaddycji Huisgena, z zydowudyną otrzymując produkty ostateczne. Zarówno związki pośrednie, jak i ostateczne, zostały zbadane z wykorzystaniem ESI MS, FT-IR, ^{1}H NMR, ^{13}C NMR oraz pomiaru temperatury topnienia, co potwierdziło uzyskanie zamierzonych związków o wysokiej czystości. Drugi etap syntezy został przedstawiony schematycznie na rysunku 3.

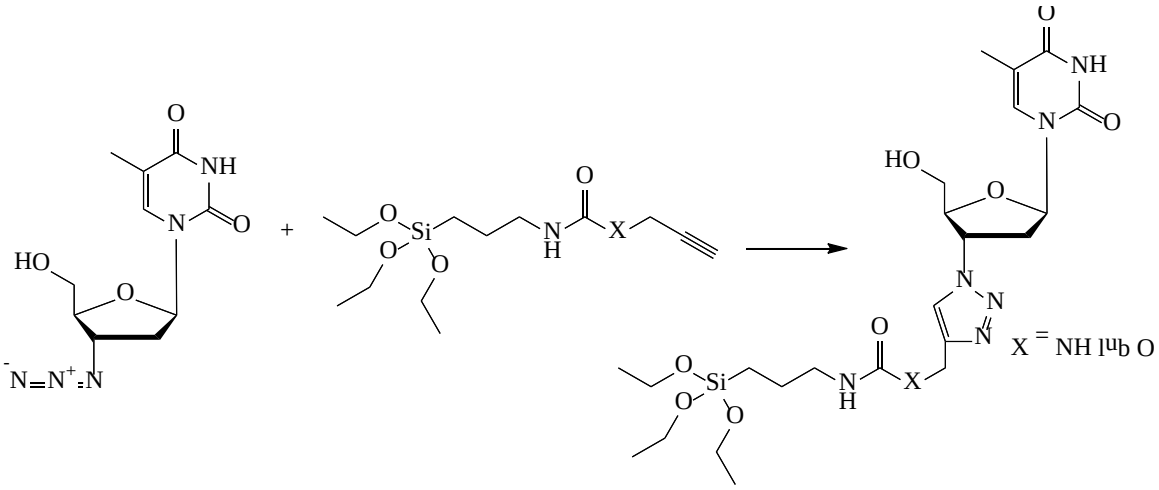

Rysunek 3. Schemat drugiego etapu syntezy pochodnych zydowudyny.

Związki ostateczne osadziłem na powierzchni krzemionki indywidualnie oraz z dodatkiem kwasu foliowego, przyłączonego kowalencyjnie przez łącznik aminopropylowy. Dodatek kwasu foliowego, docelowo, miał wspomóc proces endocytozy cząstek krzemionki przez oddziaływania specyficzne z błonowymi receptorami folianowymi (wiele linii komórek nowotworowych - w tym również obie wykorzystane w badaniu - cechuje nadekspresja błonowych receptorów folianowych [5]). Badania aktywności cytostatycznej wobec linii HeLa i KB wykazały wysoką, zależną od stężenia, aktywność otrzymanych materiałów. Najaktywniejszy z produktów uzyskał wyniki na poziomie 69 i 65% spowolnienia wzrostu komórek dla linii, odpowiednio, HeLa i KB, przy stężeniu zawiesiny krzemionki 10 $\mu g*ml^{-1}$. Zgodnie z oczekiwaniami, próbki z dodatkiem kwasu foliowego były aktywniejsze od tych pozbawionych obecności kwasu.

Drugą z substancji cytostatycznych, osadzonych na powierzchni, był kwas galusowy. W pracy pt. *"SBA-15 mesoporous silica modified with gallic acid and evaluation of its cytotoxic activity"* opisałem procedurę związania kwasu na powierzchni, polegającą w pierwszej kolejności na blokadzie grup fenolowych grupami octanowymi przy użyciu bezwodnika octowego. Następnie przekształciłem produkt pośredni w chlorek kwasowy, korzystając z nadmiaru chlorku tionylu, i ostatecznie związałem z powierzchnią przez łączniki zawierające aminowe atomy azotu. Związkami wykorzystanymi w pracy były: 3-(trimetoksysililo)propyloamina, N-(2-aminoetylo)-3-(trimetoksyililo)propyloamina oraz polietylenoimina, którą zaszczepiłem na powierzchni

przez 3-chloropropylotrimetoksysilan. Przed poddaniem materiałów analizie cytotoksyczności odblokowałem grupy fenolowe w nasyconym metanolowym roztworze węglanu potasu. Ze względu na różną gęstość obsadzenia powierzchni przez cząsteczki łączników, a przez to różną ilość i jakość (rzędowość) atomów azotu, otrzymane materiały różniły się zawartością kwasu galusowego w przeliczeniu na gram materiału. Ostateczna aktywność finalnych produktów była wysoka i zależała od wielu czynników. Okazało się, że zawartość kwasu galusowego nie przekładała się bezpośrednio na aktywność, ponieważ wpływ mógł mieć tutaj również łącznik i obecność odsłoniętych silanolowych grup powierzchniowych. Udowodniono w literaturze [6], że polietylenoimina wpływa pozytywnie na przenikanie nanocząstek do wnętrza komórek nowotworowych, co zapewne przesądziło o największej aktywności materiału, w którym łącznikiem była właśnie PEI - do 65% spowolnienia wzrostu komórek dla obu linii przy stężeniu 10 $\mu g*ml^{-1}$.

Literatura

[1] C. T. Kresge, M. E. Leonowicz, W. J. Roth, J. C. Vartuli, J. S. Beck, Ordered mesoporous molecular sieves synthesized by a liquid-crystal template mechanism, Nature, 359 (1992) 710-712.

[2] J. M. Rosenholm, T. Czuryszkiewicz, F. Kleitz, J. B. Rosenholm, M. Lindén, On the Nature of the Brønsted Acidic Groups on Native and Functionalized Mesoporous Siliceous SBA-15 as Studied by Benzylamine Adsorption from Solution, Langmuir, 23 (2007) 4315-4523.

[3] S. Tanatar, J. Russ. Phys.-chem. Soc., 40L (1906) 376.

[4] D. F. Boltz, J. A. Howell, Colorimetric Determination of Nonmetals, 2nd Edition, Wiley, New York.

[5] C. J. Weber, S. Müller, S. A. Safley, K. B. Gordon, P. Amancha, F. Villinger et al., Expression of functional folate receptors by human parathyroid cells, Surgery, 154 (2013) 1385-1393.

[6] J. S. Park, K. Na, D. G. Woo, H. N. Yang, J. M. Kim, J. H. Kim et al., Non-viral gene delivery of DNA polyplexed with nanoparticles transfected into human mesenchymal stem cells, Biomaterials, 31 (2010) 124-132.

PODSUMOWANIE

Celem naukowym rozprawy doktorskiej pod tytułem "Kontrolowane dostarczanie substancji biologicznie czynnych z wykorzystaniem modyfikowanych krzemionek" była modyfikacja powierzchni krzemionek mezoporowatych MCM-41 i SBA-15 przy pomocy substancji biologicznie czynnych. Tak otrzymane materiały miały być wykorzystane do kontrolowanego dostarczania zaadsorbowanych substancji w celach terapeutycznych lub analitycznych.

Na podstawie przeglądu literatury przedstawiłem w rozdziale monografii pt. *"Mesoporous silicas as carriers in controlled release systems in biomedicine and cosmetics"* możliwości zastosowania krzemionek mezoporowatych w systemach kontrolowanego uwalniania w biomedycynie i przemyśle kosmetycznym, natomiast w rozdziale monografii pt. *"Application of mesoporous silica nanoparticles for drug delivery"* skupiłem się na zastosowaniu krzemionek mezoporowatych w celu dostarczania leków.

Uzyskane oryginalne wyniki przedstawiłem w pięciu oryginalnych publikacjach naukowych. W wyniku przeprowadzonych badań opracowałem metody syntezy i otrzymałem:

- krzemionkę MCM-41 zmodyfikowaną grupami wpływającymi na powierzchniowy ładunek elektryczny oraz określiłem wpływ modyfikacji na procesy adsorpcji/desorpcji modelowych związków w postaci barwników,
- krzemionki MCM-41 i SBA-15 zmodyfikowane silanową pochodną mocznika, zdolną do adsorpcji nadtlenku wodoru, co zostało również określone ilościowo,
- krzemionkę SBA-15 zmodyfikowaną ryboflawiną oraz określiłem właściwości fluorescencyjne otrzymanego materiału w obecności wybranych kationów nieorganicznych i organicznych,
- krzemionkę SBA-15 zmodyfikowaną związkami o charakterze cytostatycznym, tj. zydowudyną i kwasem galusowym, oraz określiłem ich aktywność przeciwnowotworową wobec linii komórkowych HeLa i KB, a także oceniłem wpływ wybranych czynników na ich aktywność.

Otrzymane materiały posiadały przewidywane przed syntezą właściwości i mogą znaleźć zastosowanie w dziedzinach takich, jak medycyna czy chemia analityczna. Opublikowane prace stanowią bazę do dalszych badań nad krzemionkami mezoporowatymi dla transportu, przechowywania oraz uwalniania substancji biologicznie aktywnych.

Streszczenie rozprawy doktorskiej pt.

"Kontrolowane dostarczanie substancji biologicznie czynnych z wykorzystaniem modyfikowanych krzemionek"

mgr Dawid Lewandowski

promotor: prof. dr hab. Grzegorz Schroeder

Krzemionki mezoporowate znalazły do tej pory wiele zastosowań, m. in. jako adsorbenty, w katalizie, chromatografii oraz jako sensory. Obiecujące wyniki badań *in vitro* oraz *in vivo* na zwierzętach pozwalają sądzić, że w niedalekiej przyszłości krzemionki mezoporowate znajdą również swoje stałe miejsce w medycynie. Ich wykorzystanie jako nośniki leków, substancji diagnostycznych czy też enzymów możliwe będzie dzięki wysokiej odporności chemicznej, termicznej oraz mikrobiologicznej, wysokiej powierzchni właściwej, łatwości modyfikacji powierzchni oraz wielkości cząstek, pozwalającej na penetrację barier wewnątrz ludzkiego organizmu.

Zmodyfikowane krzemionki mezoporowate mogą pełnić szczególną rolę, jako nośniki leków uwalnianych w sposób kontrolowany. Duża powierzchnia właściwa oraz objętość porów pozwalają na adsorpcję znacznych ilości substancji terapeutycznych, a powierzchniowe grupy silanolowe umożliwiają zastosowanie modyfikacji regulujących proces desorpcji ładunku.

Celem mojej pracy naukowej była modyfikacja krzemionek mezoporowatych (MCM-41 oraz SBA-15) umożliwiająca kontrolowane dostarczanie wybranych substancji biologicznie czynnych. W pracy skupiłem się zarówno na adsorpcji fizycznej, jak i chemicznej wybranych substancji.

W ramach fizysorpcji ustaliłem wpływ ładunku elektrycznego wnoszonego przez modyfikację na powierzchni krzemionki na procesy adsorpcji i desorpcji wybranych związków modelowych - dwóch barwników azowych oraz jednego ftalocyjaninowego. Wyznaczyłem ilości zaadsorbowanych związków oraz kinetykę desorpcji w roztworze wodnym przy dwóch różnych wartościach pH, a także oceniłem wpływ innych, poza modyfikacją powierzchni, czynników na procesy adsorpcji/desorpcji. Adsorpcją fizyczną zająłem się również w kontekście możliwości dostarczania nadtlenku wodoru na nośniku nieorganicznym. W tym celu zmodyfikowałem powierzchnię krzemionek MCM-41 i SBA-15 ugrupowaniem zawierającym fragment zbliżony strukturalnie do mocznika, który tworzy z nadtlenkiem wodoru znane od dawna połączenie kompleksowe. Tak

otrzymany materiał zawiesiłem w roztworach wodnych nadtlenku wodoru o różnych stężeniach. Analiza ilości zaadsorbowanego nadtlenku wodoru metodą tiocyjanianową pozwoliła ustalić, że na powierzchni krzemionki SBA-15 osadziło się ponad dwukrotnie więcej substancji, niż na MCM-41. Mimo, że uzyskane zawartości procentowe nadtlenku wodoru w materiale są dużo niższe od tych w czystym kompleksie UHP (urea-hydrogen peroxide), to opis i wyniki tego badania mogą posłużyć jako baza do dalszego rozwoju tego zagadnienia.

Przy pomocy chemisorpcji umieściłem na powierzchni krzemionki ryboflawinę, tj. witaminę B_2. Dokonałem tego poprzez reaktywny łącznik, zawierający grupę izocyjanianową. Powstały materiał wykazywał ciekawe właściwości fluorescencyjne, a mianowicie znaczną zmienność zarówno intensywności emisji fluorescencji, jak i położenia maksimum emisji w obecności różnych kationów nieorganicznych i organicznych. Obserwowane różnice były znacznie większe, niż dla ryboflawiny w postaci roztworu wodnego. Krzemionkę mezoporowatą SBA-15 zmodyfikowałem również przy pomocy, specjalnie zsyntezowanych w dwuetapowym procesie, pochodnych zydowudyny (3'-azydo-3'-deoksytymidyny, AZT). Otrzymane materiały, z dodatkiem (lub bez) kwasu foliowego przyłączonego do powierzchni dodatkowym łącznikiem, wykazały wysoką aktywność przeciwnowotworową wobec linii komórkowych HeLa i KB. Próbki zawierające kwas foliowy były przy tym aktywniejsze od tych pozbawionych kwasu. Podobnie, poprzez wiązanie kowalencyjne, przyłączyłem do powierzchni krzemionki SBA-15 inny związek o działaniu cytostatycznym - kwas galusowy. Dokonałem tego przy pomocy jego chlorku kwasowego z zablokowanymi grupami fenolowymi, który otrzymałem na drodze dwuetapowej syntezy. Wiązanie z powierzchnią zostało przeprowadzone z użyciem trzech różnych łączników, zawierających grupy aminowe pierwszo-, drugo- i trzeciorzędowe. Wszystkie materiały wykazały wysoką aktywność przeciwnowotworową, przy czym najwyższą zaobserwowano dla próbki, w której łącznikiem azotowym była polietylenoimina.

Summary of doctoral dissertation on:

"Controlled delivery of biologically active compounds using modified silicas"

Dawid Lewandowski

PhD supervisor: Prof. Grzegorz Schroeder

Mesoporous silicas have found numerous applications, among others as adsorbents, in catalysis, chromatography and as sensors. Promising results of *in vitro* and *in vivo* animal tests allow to guess that in the near future the mesoporous silicas will also find their firm place in medicine. Their use as carriers of drugs, diagnostic agents or enzymes will be possible due to their high chemical, thermal and microbiological stability, high surface area, an ease in surface modification and particle size allowing to penetrate barriers inside the human organism.

Modified mesoporous silicas can play a particular role as carriers of drugs released in a controlled manner. High surface area and pores volume allow to adsorb significant amounts of therapeutics and the surface silanol groups enable the use of modifications regulating the cargo desorption process.

The aim of my doctoral dissertation was the modification of mesoporous silicas (MCM-41 and SBA-15) allowing controlled delivery of chosen biologically active compounds. The study focused on both, the physical and chemical adsorption of chosen substances.

In the matter of physisorption I established the influence of electrical charge, introduced with the modification onto the silica surface, on adsorption and desorption processes of chosen model compounds - two azo dyes and a phthalocyanine one. I determined the amounts of the compounds adsorbed and desorption kinetics in aqueous solution at two different pH values and assessed the influence of other, beside the surface modification, factors on the adsorption/desorption processes. I also dealt with the physical adsorption in terms of possible delivery of hydrogen peroxide on the inorganic carrier. To do this, I modified the surface of MCM-41 and SBA-15 silicas with the moiety containing a part structurally similar to urea, which has been known to form a complex with hydrogen peroxide. I suspended the prepared material in aqueous solutions of hydrogen peroxide of various concentrations. The analysis of amounts of adsorbed hydrogen peroxide, performed using the thiocyanate method, allowed to determine, that over twice

as much hydrogen peroxide deposited on the surface of SBA-15 in compare to MCM-41. Although the resulting percentage of hydrogen peroxide in the material is far much lower than that of pure UHP (urea-hydrogen peroxide) complex, the description and results of this study can be a basis for further development of this issue.

With the use of chemisorption I managed to place riboflavin, it is vitamin B_2, on the silica surface. I achieved this using reactive linker, containing isocyanate group. The obtained material showed interesting fluorescence properties, namely significant variability of fluorescence emission intensity, as well as the location of emission maxima in presence of different inorganic and organic cations. Observed differences were much higher than those obtained for riboflavin in aqueous solution. I also modified the SBA-15 mesoporous silica with, specially synthesized in a two-step process, zidovudine (3'-azido-3'-deoxythymidine, AZT) derivatives. Obtained materials with (or without) the addition of folic acid, attached to the surface through the additional linker, showed high anticancer activity against HeLa and KB cell lines. The samples containing folic acid were more active than those lacking it. Similarly, by a covalent bond, I attached to the SBA-15 silica surface another cytostatic compound - gallic acid. I managed to do this with the use of its acid chloride with blocked phenolic groups obtained via the two-step synthesis. The binding with the surface was conducted using three different linkers, containing primary, secondary and tertiary amino groups. Two materials showed high antitumor activity, with the highest observed for the sample, where polyethyleneimine was used as a nitrogen linker.

Cent. Eur. J. Chem. • 12(2) • 2014 • 233-241
DOI: 10.2478/s11532-013-0361-x

VERSITA

Central European Journal of **Chemistry**

Adsorption studies and release of selected dyes from functionalized mesoporous MCM-41 silica

Research Article

Dawid Lewandowski*, Anna Olejnik, Grzegorz Schroeder

Faculty of Chemistry,
Adam Mickiewicz University,
61-614 Poznan, Poland

Received 24 June 2013; Accepted 4 October 2013

Abstract: Functionalized mesoporous MCM-41 silica was subjected to adsorption and release studies of encapsulated guest molecules of three chosen dyes. These mesoporous systems were composed of three different capping reagents introduced by grafting method on the silica surface to control the release of dye molecules at two different pH values. The amounts of dyes adsorbed on the silica surface were measured using ultraviolet-visible (UV-VIS) spectrophotometry. The efficiency of grafting was calculated on the basis of differential thermal analysis (TG) results and elemental analysis. The release profiles were determined for all obtained systems using USP Dissolution Apparatus 2. Adsorption of the two azo dyes used was the most efficient after the positively charged functionalization and lower after functionalization with neutral and negatively charged capping reagents, while the phthalocyanine dye adsorption was almost functionalization-independent. Grafting efficiency was the highest for neutral capping reagent and much lower for electrically charged molecules of other reagents. Release studies showed clearly that desorption was pH-dependent for azo dyes and pH independent for Alcian Blue. The adsorption and release seem to be connected with the electrical charge of all constituents of these systems. Results obtained can be used for further analysis of different electrically charged molecules.

Keywords: •

1. Introduction

Discovery of the M41S silica family by Mobil Corporation in 1992 [1] has attracted much attention to mesoporous materials because of their numerous interesting properties. Large surface area (~1000 $m^2\ g^{-1}$), uniform and controllable pore size, large pore volume (~1 $cm^3\ g^{-1}$), narrow particle size, open pore structures [2], chemical stability, possibility of control surface functionalization and resistance to microbial attack made them very useful in a wide variety of potential applications. Mesoporous silicas can be used in several fields such as adsorption (modified mesoporous nanoparticles found their application in timber industry to control termites with imidacloprid loaded into modified mesoporous silica [2]), ion exchange, catalysis - cracking abilities of unmodified mesoporous silicas can be used in petrochemical industry and Al supported on MCM-41 is useful for organic synthesis [3], sensing (modified mesoporous silica nanoparticles as biosensors have many advantages over homogenous fluorescent and staining dyes. They are resistant to fluorescent self-quenching and other diffusion-related problems, moreover they can be modified with wide range of cell-recognition or other site-directing compounds [4], *e.g.* glucose oxidase- and horseradish peroxidase-loaded mesoporous silica has been used as a selective sensor for glucose detection [5] or myoglobin and hemoglobin were introduced on a surface of silica-modified electrodes to be used as a sensor for H_2O_2 and NO_2^- [6]), polymerization processes, separation (chromatography) [7], enzyme supporters, delivery carriers and controlled drug/gene release [8]. The last application is especially interesting, because it provides powerful tools for the treatment of cancer, chronic diseases, pain and many other ailments.

Uniform and small particle size allows easy uptake by lysosomes in cancer cells [9]. Also pH in lysosomes (4.8-6.4) is significantly lower than physiological cells (~7.4), which makes it possible to make pH-sensitive systems for selective drug delivery [10], *i.e.*, benzimidazole

* *E-mail: dawid_le@amu.edu.pl*

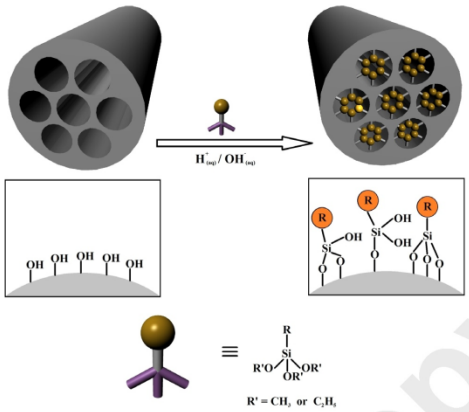

Figure 1. Scheme shows grafting as one of the methods for the modification of mesoporous silica.

moiety capped with β-cyclodextrin susceptible to pH values similar to its pK_a=5.64 [11]. Silica nanoparticles are also more stable than lyposome carriers and are more resistant to drug leakage [12]. More sophisticated systems, with insulin as a cap of mesoporous pores, that can be removed by the presence of glucose or photo-susceptible azobenzene caps are also known [9]. Unmodified mesoporous nanoparticles express toxicity due to interactions of surface silanol groups with cellular membranes. Toxicity can be reduced by coating particles with a polymer shell that also provides colloidal stability, handles for chemoligation and improved blood circulation lifetimes. Unfortunately, the polymer shell limits drug loading and release properties [13].

Controlled drug release demands functionalization of the mesoporous silica surface in order to avoid premature diffusion of the drug into the environment. There are three general methods to achieve this [14].

Postsynthetic functionalization (the so called "grafting") modifies the inner surfaces of mesoporous silica and is carried out by reaction of organosilanes, chlorosilanes or silazanes with the free silanol groups of the pore surfaces (Fig. 1). The main advantage of this method is that the mesostructure of the starting material is retained, but the lining of the walls causes a reduction in the porosity of the hybrid material, depending upon the size of the organic residue and the degree of occupation. If the substrates react at the pore openings, the diffusion of organosilanes deeper into the pores can be impaired or even stopped leading to complete closure of the pores (pore blocking).

Co-condensation is an alternative method to synthesize organically modified mesoporous silicas. It is a one-pot synthesis, which can be carried out by the reaction of tetraalkoxysilanes (tetramethoxysilane - TMOS or tetraethoxysilane - TEOS) with terminal trialkoxyorganosilanes in the presence of structure-directing agents. It leads to materials with organic residues anchored covalently to the pore walls. When using this method, the pore blocking is not a problem, because organic functionalities are direct components of silica matrix and are distributed more homogeneously than in the materials synthesized with the grafting process. Co-condensation has also some disadvantages: the use of too high a concentration of organosilanes in the reaction mixture can lead to totally disordered products, also the proportion of organic groups incorporated is lower than that corresponding to the starting concentration of the reaction mixture. Moreover, in most cases only extraction can be used to remove residual surfactant without destroying the organic functionality – calcination cannot be applied.

Condensation reactions of bridged organosilica precursors (Fig. 3) have been known for a long time from sol-gel chemistry. They are used in preparation of the so-called Periodic Mesoporous Organosilicas, which have organic units incorporated in the silica matrix through two covalent bonds and in this way distributed more homogeneously in the pore walls.

Depending on the method of production, the functionalized mesoporous silicas show different cargo releasing profiles [15]:

Profile *a* (Fig. 4) is characteristic of an unmodified silica matrix and presents initial burst release and slow release afterwards, profile *b* is associated with

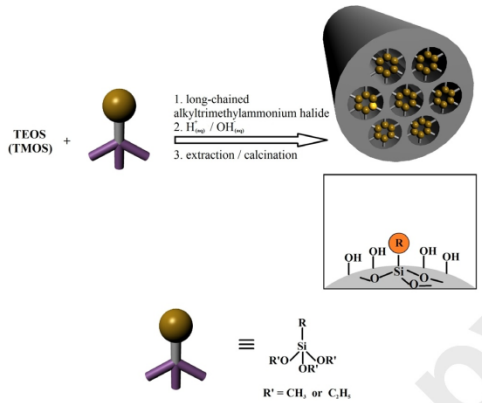

Figure 2. Co-condensation as one of the methods for the modification of mesoporous silica.

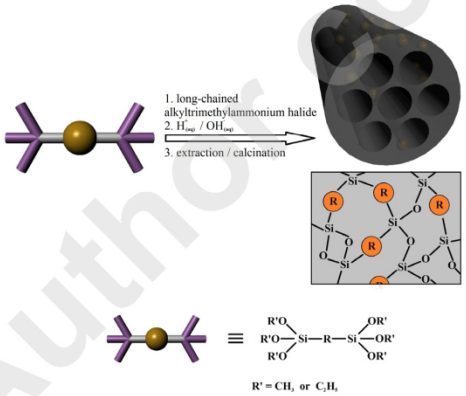

Figure 3. Preparation of periodic mesoporous silica.

a diffusion process and generally follows first-order kinetics for drug concentration. An example of a material showing this profile can be MCM-41 silica loaded with alendronate [16]. Profile *c* shows zero-order kinetics, which can be exemplified as amino-functionalized SBA-15 mesoporous silica loaded with alendronate [16]. Profile *d* corresponds to more sophisticated systems sensitive to different external stimuli.

Functionalized mesoporous silica systems can operate under a range of stimuli including pH [11,17-22], competitive binding [18], light [23-28], redox control [29-32] and enzymes [33] changing the cargo diffusion process between "on" and "off" states.

The aim of this work was to obtain functionalized mesoporous silicas of MCM-41 type and analyze the influence of pH value on the process of cargo release. We have used the grafting method and different reagents - positively charged ionic liquid 1-methyl-3-(3-(trimethoxysilyl)propyl)-1H-imidazol-3-ium, neutral N-(3-(triethoxysilyl)propyl)gluconamide and negatively charged N-(3-(trimethoxysilyl)-propyl)ethylenediamine triacetic acid trisodium salt. Two azo dyes (Sunset Yellow FCF and Chromotrope 2R) and copper phthalocyanine called Alcian Blue were used as cargo. pH value for cargo release was set to 4.5 and 6.8, which are very popular values in pharmaceutical studies.

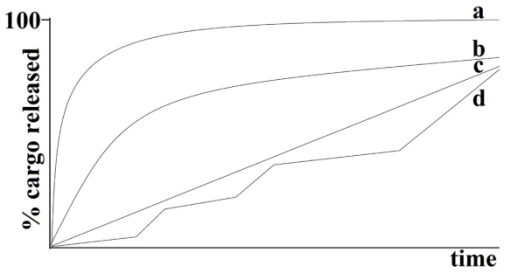

Figure 4. Cargo releasing profiles dependent on the method of functionalization.

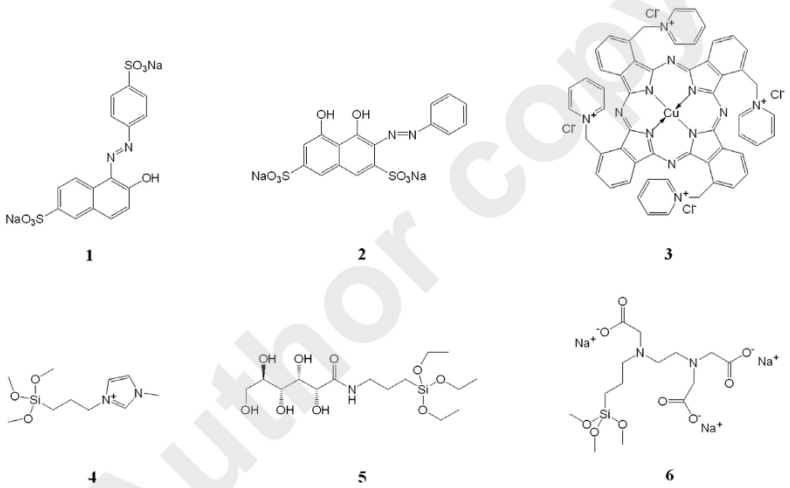

Figure 5. Dyes and capping reagents used in the experiment.

2. Experimental procedure

2.1. Materials

Dyes (Sunset Yellow FCF (**1**), Chromotrope 2R (**2**), and Alcian Blue-tetrakis(methylpyridinium) chloride (**3**)) were purchased from Sigma-Aldrich. Capping reagents (1-methyl-3-(3-(trimethoxysilyl)propyl)-1H-imidazol-3-ium (**4**), N-(3-(triethoxysilyl)propyl)gluconamide (**5**), and N-(3-(trimethoxysilyl)-propyl)ethylenediamine triacetic acid trisodium salt (**6**)) were obtained from ABCR and methanol was used from Stanlab.

2.2. Preparation of the modified silica

MCM-41 silica had been prepared for the grafting reaction by activating it in a boiling mixture of water and concentrated nitric acid (1:1) for 6 h. Then it was filtered off and washed by large amount of water to remove the residual acid. A portion of 10 mg (about 0.02 mmol of **1** and **2** or about 0.008 mmol of **3**) of a dye was dissolved in 25 mL of methanol and 100 mg of activated silica was then suspended. The mixture was stirred at room temperature for 24 h. Then 40 mg (0.163 mmol) of **4** or 130 mg of 50% ethanol solution of **5** (*i.e.*, 65 mg of pure substance, which is 0.163 mmol) or 163 mg of 45% water solution of **6** (*i.e.*, 73 mg of pure substance, which is 0.163 mmol) was added and stirred at 60°C for 2 h and then at room temperature for the next 2 h. Suspensions were filtered through fibre glass filters and washed by small amounts of methanol. The filters, together with their contents, were dried at 90°C

Table 1. The amounts of dyes adsorbed on functionalized silicas prepared.

Capping reagent	Dye adsorbed	Percentage of total mass occupied by the dye
4	1	3.4
	2	3.3
	3	9.0
5	1	0.7
	2	0.4
	3	5.5
6	1	0.4
	2	0.2
	3	8.5

Table 2. Results of elemental analysis for carbon, hydrogen and nitrogen.

Compound	Mass percentages for selected elements			Mass ratios C:H:N
	carbon [%]	hydrogen [%]	nitrogen [%]	
4	1.676	1.135	0.415	4.04:2.73:1
	1.641	1.124	0.403	4.07:2.79:1
5	8.142	1.851	1.038	7.84:1.78:1
	8.157	1.786	1.062	7.68:1.68:1
6	3.946	1.421	0.562	7.02:2.53:1
	3.980	1.520	0.651	6.11:2.33:1
pure MCM-41	0.030	0.832	0.034	0.88:24.54:1
	0.043	0.879	0.043	1:20.44:1

and colourful precipitates were obtained. Neutral pH (methanol solution) was used, except for **6,** which had alkaline solutions, because of its dissociation.

2.3. Adsorption analysis

The amount of dye adsorbed was measured on an UV-VIS Agilent 8453 Spectrophotometer, at the following wavelengths: for **1** λ_{max} = 480 nm, for **2** λ_{max} = 508 nm and for **3** λ_{max} = 602 nm.

2.4. TG analysis

All modified silicas (with capping reagents and without dyes) and the unmodified one as a reference were subjected to TG analysis using Setsys 1200 apparatus (Setaram, US). The samples were analysed in the range 15-1000°C at the heating speed 10°C min^{-1} and in air atmosphere, but particular attention was paid to the observations in the range 120-800°C, in which organic parts of capping reagents undergo decomposition (water desorbs in lower temperatures and in 800-1000°C temperature range no differences between curves were observed).

2.5. Release analysis

Release analysis was performed with an USP Dissolution Apparatus 2 (Varian Vankel 7010), which is very often used in pharmaceutical dissolution tests. In all cases, the potassium acetate buffer at pH 4.5 and potassium phosphate buffer at pH 6.8 were used as a receptor media. The medium (200 mL) was maintained at 37.0±0.5°C and stirred at 100 rpm. The samples were filtered through 35 µm high-density polyethylene (HDPE) Full-Flow filters and the concentration of released dye was spectrophotometrically monitored at 480 nm for **1**, at 508 nm for **2** and 602 nm for **3**. The absorbance of the sample aliquots was used to assess the amount of dye release at each time point.

3. Results and discussion

Three different mesoporous systems were obtained through the following procedure: mesoporous material was filled with the dye (**1-3**) and then capped with alkoxysilanes of different properties (first of all the electric charge). These systems were then tested to determine their sorption properties, the efficacy of capping as well as the release kinetics.

3.1. Adsorption analysis

The amounts of dyes **1-3** adsorbed on mesoporous silica were determined on the basis of spectrophotometric analysis.

3.2. Elemental analysis

Elemental analysis of capped materials (without dyes) for carbon, hydrogen and nitrogen allowed determination of the amounts of capping reagents, which had reacted with the silica surface. Results are presented in Table 2.

The presence of trace amounts of carbon and nitrogen was attributable to the residues of surfactant left after processing or adsorbed from the air, while the presence of hydrogen is understood as it is a component of silanol groups on the surface of silica.

From the carbon : nitrogen ratios it was possible to determine the mode of capping reagents attachment to the surface, whether through one, two or three Si–O–Si bonds, and from carbon and nitrogen percentages the total amounts of capping compounds bound to silica could be calculated. Hydrogen mass percentage was

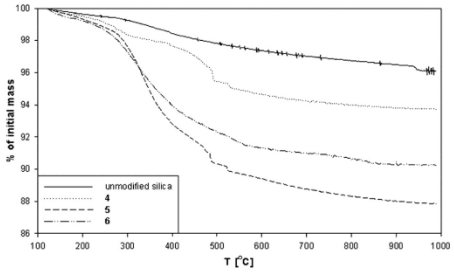

Figure 6. Adjusted curve emphasizes the mass loss.

Table 3. Calculations for the grafting process of different capping reagents on the MCM-41 silica's surface.

Capping reagent	Molecular weight [Da]	Molecular mass of fragment eliminated in DTA analysis [Da] (assuming bonding through all three bonds)	Difference in mass decrease comparing to unmodified silica [%]	Capping reagent:silica molar ratio
4	245.4	139.2	2.75	1:78
5	399.5	251.3	8.45	1:41
6	448.4	273.3	6.05	1:65

used to estimate the amount of silanol groups replaced during the grafting process. Thus, reagent **4** is probably attached through only one bond in a total amount of 3.30±0.29 g per 100 g of grafted silica and replaced about 1% of silanol groups. Capping compound **5** is connected through three bonds, in 29.37±0.86 g per 100 g of grafted silica. It replaced approximately 40-45% of silanol groups population. Carbon:nitrogen ratio in compound **6** was too high and could not be attributed to any of the possible combinations. Compound **6** could partly undergo basic hydrolysis (which occurs usually at higher temperatures [34]) and result in 2-((2-hydroxyethyl)(3-trimethoxysilyl)propyl) amino)acetic acid, which could have already been assigned. The hydrolysis product is still a negatively charged molecule. However, no mass calculations for **6** were performed.

3.3. TG analysis

The amount of capping groups introduced onto the mesoporous material was also estimated from TG results. The mass loss related to decomposition of organic residues from the surface was observed in the range from 120ºC until 800ºC. Above 800ºC all curves were parallel to each other and below 120ºC the elimination of physically adsorbed water was observed. The TG curves (Fig. 6) were modified (percentages of initial mass was set to 100% at 120ºC) to emphasize mass loss as a consequence of thermal decomposition of organic components. The part of each curve corresponding to the temperature range between 800ºC and 1000°C is parallel to that recorded for unmodified silica, which means that the mass loss in this range is not related to the presence of carbon containing compounds but to the destruction of silica matrix.

From the differences in mass loss observed for unmodified and modified silicas it was easy to calculate the mass of chemically adsorbed capping reagents and the molar ratio of substrates used.

TG results generally agree with those from elemental analysis and show that binding of **4** is the weakest – only 1:80 in molar ratio. It is caused probably by the steric hindrance and electrostatic repulsion of methylimidazolium rings, which have only short three-membered carbon chains joining them with the surface. This makes them unable to take optimal positions. The TG results obtained for compound **5** show better coverage than for compound **6** because of smaller steric hindrance in **5** (**6** is strongly branched, even hydrolysed, **5** has no branches), the absence of undesirable electrostatic interactions – **6** is a trisodium salt and has three (hydrolysis product – one) carboxylic groups – and the presence of hydrogen bonds binding the molecules of **5**. After analysis of the capping process, the release analysis was performed.

3.4. Release analysis

Results of release analysis of **1** from modified MCM-41 silica for pH= 4.5 are shown in Fig. 7, for pH= 6.8 in Fig. 8.

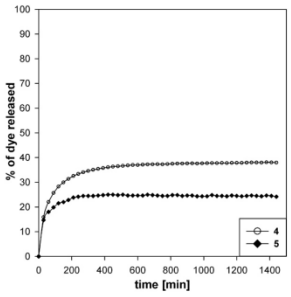

Figure 7. Release of **1** from modified MCM-41 silica at pH= 4.5.

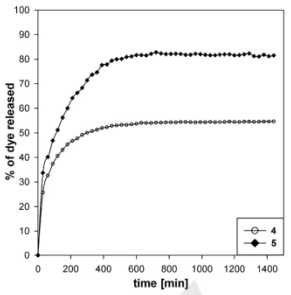

Figure 9. Release of **2** from modified MCM-41 silica at pH= 4.5.

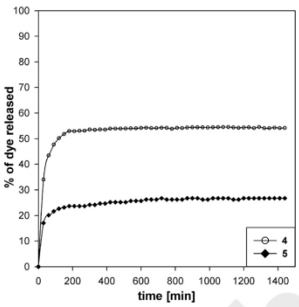

Figure 8. Release of **1** from modified MCM-41 silica at pH= 6.8.

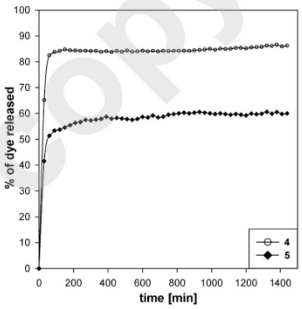

Figure 10. Release of **2** from modified MCM-41 silica at pH= 6.8.

Because of the very small amount of dye adsorbed with the use of **6** as a capping reagent and possible considerable errors, the release analysis was not performed .

Results of release analysis of **2** from modified MCM-41 silica for pH= 4.5 are shown in Fig. 9, for pH= 6.8 in Fig. 10.

Because of the very small amount of dye adsorbed with the use of **6** as a capping reagent and possible considerable errors, the release analysis was not performed.

The release of **3** was very low (under 10%) and the release curves were irregular so they are not presented. Except for instantly released small amounts of the dye (residue after filtering and washing or molecules which are closest to the pore openings), no diffusion of **3** from modified MCM-41 silica takes place, irrespectively of the capping reagent used. It may be caused by steric fit of molecule **3** molecule to the diameter of silica channel, which is illustrated in Fig. 11.

A molecule of **3** is square-shaped, with concave sides of about 1.8 nm in length (calculated using HyperChem),

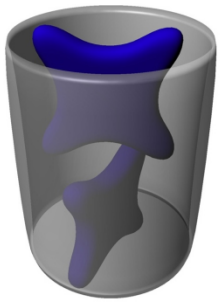

Figure 11. Model of **3** molecule inside of MCM-41 channel.

while the diameter of the MCM-41 channel is, according to the manufacturer, 2.3-2.7 nm. Therefore electrostatic interactions between lone pairs of oxygen atoms from the channel's wall and positively charged nitrogen atoms from molecules of **3** may occur. Hydrogen bonds between these oxygen atoms and hydrogen atoms from **3** may be also significant.

Table 4. Fitting parameters of release experiments carried out with a first order release model, described by the equation $f(t) = 1 - e^{-kt}$.

Dye	Capping reagent	pH = 4.5		Dye	Capping reagent	pH = 6.8	
		k [h^{-1}]	R^2			k [h^{-1}]	R^2
1	4	0.7414	0.9717	1	4	1.7237	0.9918
	5	1.3405	0.9758		5	1.5626	0.9222
2	4	0.7699	0.9602	2	4	4.7722	0.9961
	5	0.5037	0.9650		5	2.1757	0.9688

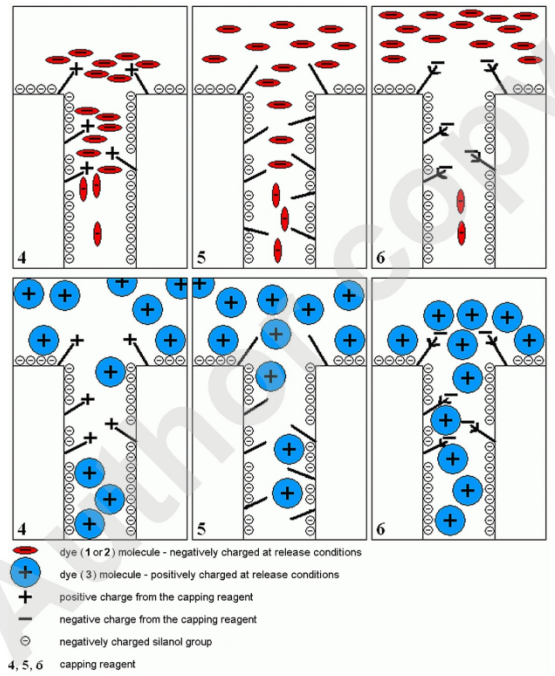

Figure 12. The interactions between the molecules of capping reagents and those of the dyes trapped in the MCM-41 silica channels and on its outer surface – channel diameter and size of the molecules match.

Interpretation of the release curves for **1** and **2** allows the following conclusions: for pH= 4.5 the release is partial, fast and reaches a plateau in about 10 hours. The kinetics of this process are similar to that of the first order reactions. For pH= 6.8 the release curves reach a plateau in about 3-4 hours but in general they are similar to those from the analysis for pH= 4.5. Higher pH value makes the dissociation of dye molecules more significant, which increases their total negative charge and accelerates desorption.

4. Conclusions

Major differences in amounts of dyes adsorbed during the adsorption process can be explained by differences in their physicochemical interactions with the silica surface.

Large amounts of **3** adsorbed due to a good fit of the molecule size to the size of the channel and favorable intermolecular interactions (oxygen atoms from MCM-41 channels, negatively charged surface, for **6** - additionally negatively charged carboxylic ions,

even after hydrolysis). Large amounts of dye adsorbed for positively charged **4** is caused probably by its low surface coverage.

The presence of minimum amounts of dyes **1** and **2** adsorbed on the silica modified with capping reagent **6**, can be explained as a result of negative electrostatic interactions of carboxylic ions and negatively charged dye molecules (deprotonated sulfonic groups) and repulsing ion-dipole interactions between dyes and oxygen atoms from silica channels. For **5** there is no electrostatic repulsion of dye molecules and that is why more dye is adsorbed – the amount is similar to that for unmodified mesoporous silica. The highest amount of dye was adsorbed on MCM-41 silica modified with **4**, which can be attributed to the positive electrostatic interactions.

As follows from all the above results, dye binding can take place mostly on the outer surface of the pores and the outer surface of silica particles, between the molecules of the capping compound.

References

[1] J.S. Beck, J.C. Vartuli, W.J. Roth, M.E. Leonowicz, C.T. Kresge, K.D. Schmitt, C.T.W. Chu, D.H. Olson, E.W. Sheppard, J. Am. Chem. Soc. 114, 10834 (1992)

[2] A. Popat, J. Liu, Q. Hu, M. Kennedy, B. Peters, G. Qing, M. Lu, S.Z. Qiao, Nanoscale 4, 970 (2012)

[3] A. Taguchi, F. Schuth, Microporous and Mesoporous Materials 77, 1 (2005)

[4] I.I. Slowing, B.G. Trewyn, S. Giri, V.S.-Y. Lin, Adv. Funct. Mater. 17, 1225 (2007)

[5] Y. Wei, H. Dong, J. Xu, Q. Feng, Chem. Phys. Chem. 3, 802 (2002)

[6] Z. Dai, S. Liu, H. Ju, H. Chen, Biosens. Bioelectron. 19, 861 (2004)

[7] N. Kishor Mal, M. Fujiwara, Y. Tanaka, T. Taguchi, M. Matsukata, Chem. Mater. 15, 3385 (2003)

[8] Q. He, J. Shi, J. Mater. Chem. 21, 5845 (2011)

[9] K.K. Coti, M.E. Belowich, M. Liong, M.W. Ambrogio, Y.A. Lau, H.A. Khatib, J.I. Zink, N.M. Khashab, J. F. Stoddart, Nanoscale 1, 16 (2009)

[10] L. Du, H. Song, S. Liao, Microporous and Mesoporous Materials 147, 200 (2012)

[11] H. Meng, M. Xue, T. Xia, Y.L. Zhao, F. Tamanoi, J.F. Stoddart, J.I. Zink, A.E. Nel, J. Am. Chem. Soc. 132, 12690 (2010)

[12] Q. He, Y. Gao, L. Zhang, Z. Zhang, F. Gao, X. Ji, Y. Li, J. Shi, Biomaterials 32, 7711 (2011)

[13] N. Singh, A. Karambelkar, L. Gu, K. Lin, J.S. Miller, C.S. Chen, M.J. Sailor, S.N. Bhatia, J. Am. Chem. Soc. 133, 19582 (2011)

[14] F. Hoffmann, M. Cornelius, J. Morell, M. Fröba, Angew. Chem. Int. Ed. 45, 3216 (2006)

[15] M. Vallet-Regí, F. Balas, D. Arcos, Angew. Chem. Int. Ed. 46, 7548 (2007)

[16] F. Balas, M. Manzano, P. Horcajada, M. Vallet-Regí, J. Am. Chem. Soc. 128, 8116 (2006)

[17] T.D. Nguyen, K.C.F. Leung, M. Liong, C.D. Pentecost, J.F. Stoddart, J.I. Zink, Org. Lett. 8, 3363 (2006)

[18] K.C.F. Leung, T.D. Nguyen, J.F. Stoddart, J.I. Zink, Chem. Mater. 18, 5919 (2007)

[19] C. Park, K. Oh, S.C. Lee, C. Kim, Angew. Chem. Int. Ed. 46, 1455 (2007)

[20] S. Angelos, N.M. Khashab, Y.W. Yang, A. Trabolsi, H.A. Khatib, J.F. Stoddart, J.I. Zink, J. Am. Chem. Soc. 131, 12912 (2009)

[21] P. Demuth, M. Hurley, C. Wu, S. Galanie, M.R. Zachariah, P. Deshong, Microporous and Mesoporous Materials 141, 128 (2011)

[22] S. Angelos, Y.W. Yang, K. Patel, J.F. Stoddart, J.I. Zink, Angew. Chem. Int. Ed. 47, 2222 (2008)

[23] N.K. Mal, M. Fujiwara, Y. Tanaka, Nature 421, 350 (2003)

[24] M. Liu, D.R. Dunphy, P. Atanassov, S.D. Bunge, Z. Chen, G.P. López, T.J. Boyle, C.J. Brinker, Nano Lett. 4, 551 (2004)

[25] T.D. Nguyen, K.C.F. Leung, M. Liong, Y. Liu, J.F. Stoddart, J.I. Zink, Adv. Funct. Mater. 17, 2101 (2007)

[26] J. Lu, E. Choi, F. Tamanoi, J.I. Zink, Small 4, 421 (2008)

[27] D. Ferris, Y.L. Zhao, N.M. Khashab, H.A. Khatib, J.F. Stoddart, J.I. Zink, J. Am. Chem. Soc. 131, 1686 (2009)

[28] J. Lai, X. Mu, Y. Xu, X. Wu, C. Wu, C. Li, J. Chen, Y. Zhao, Chem. Commun. 46, 7370 (2010)

[29] R. Hernandez, H.R. Tseng, J.W. Wong, J.F. Stoddart, J.I. Zink, J. Am. Chem. Soc. 126, 3370 (2004)

[30] T.D. Nguyen, H.R. Tseng, P.C. Celestre, A.H. Flood, Y. Liu, J.F. Stoddart, J.I. Zink, Proc. Natl. Acad. Sci. USA 102, 10029 (2005)

[31] T. D. Nguyen, Y. Liu, S. Saha, K.C.F. Leung, J.F. Stoddart, J.I. Zink, J. Am. Chem. Soc. 129, 626 (2007)

[32] Z. Luo, K. Cai, Y. Hu, L. Zhao, P. Liu, L. Duan, W. Yang, Angew. Chem. 123, 666 (2011)

[33] K. Patel, S. Angelos, W.R. Dichtel, A. Coskun, Y.W. Yang, J.I. Zink, J.F. Stoddart, J. Am. Chem. Soc. 130, 2382 (2008)

[34] R.J. Motekaitis, D. Hayes, A.E. Martell, W.W. Frenier, Can. J. Chem. 57, 1018 (1978)

Struct Chem
DOI 10.1007/s11224-014-0428-0

ORIGINAL RESEARCH

Adsorption of hydrogen peroxide on functionalized mesoporous silica surfaces

Dawid Lewandowski · Dawid Bajerlein · Grzegorz Schroeder

Received: 7 November 2013 / Accepted: 19 March 2014

Abstract MCM-41 and MSU-H mesoporous silicas were successfully functionalized with hydrogen bonds forming organic moieties, which have been proven by elemental analysis. Both moieties, based on oxygen and nitrogen containing groups, were introduced with high efficiency—the amount of carbon in all cases exceeded 10 % and the elemental ratios suggest binding to the surface through two or three Si–O–Si bonds. Hydrogen peroxide adsorption was conducted in its aqueous solutions and the amount adsorbed was determined using the ferric thiocyanate method. Results are presented as a function of hydrogen peroxide concentration in aqueous solution from 5 to 30 %. Both functionalized silicas show increased adsorption capacity when compared with that of their unfunctionalized analogues. The surface modified with nitrogen-based organic moiety revealed better adsorption properties as well as higher resistance against oxidation. MSU-H silica, due to its larger pore diameter, provides more space to bind hydrogen peroxide molecules and thus was found to have higher adsorption capacity: it adsorbed up to four times more hydrogen peroxide than MCM-41.

Keywords MCM-41 · MSU-H · Hydrogen peroxide · Adsorption

Introduction

Hydrogen peroxide is a very useful oxidizer that has been employed in many different fields, such as chemistry of atmosphere [1], autodissociation dynamics [2, 3], and bleaching [4]. It is reasonably stable, readily available, inexpensive, and generates only water as a by-product [5]. Although its molecule is similar to water, it has not been much studied in a pure state because of its instability. However, like water, it forms hydrogen bonds with nitrogen- and oxygen-containing compounds [6, 7].

To avoid the stability issues, hydrogen peroxide can be transformed into a number of complexes with organic compounds. Urea–hydrogen peroxide complex (UHP) has already been used in many oxidation processes [8–11] as a source of anhydrous hydrogen peroxide. It is a stable and inexpensive solid that has been first prepared by Tanatar [12] and now is sold by a number of chemical manufacturers. Its crystals are composed of molecules of urea and hydrogen peroxide in 1:1 ratio, connected through multiple hydrogen bonds [13]. Hydrogen peroxide forms also complexes with melamine [14] and DABCO-di-*N*-oxide [15]. Some polymer-supported systems containing hydrogen peroxide are known as well. The most prominent among them is polyvinylpyrrolidone-hydrogen peroxide complex (PVP-H_2O_2), introduced by Pourali and Ghanei [16] that has already been successfully used for iodination of aromatic compounds as well as for oxidation of α,β-enones [17]. It can be easily prepared from 30 % aqueous solution of hydrogen peroxide and polyvinylpyrrolidone K-30, it contains up to 23 % of hydrogen peroxide by weight [18] and is insoluble in organic solvents [19]. It is stable for several months while stored in a refrigerator, without losing its weight or activity [16]. Hydrogen peroxide can also be encapsulated in different silica xerogel systems to serve as an oxidant in the presence of metal catalyst [20–22] or without it, with a hydrogen peroxide content up to 68 % [23].

Mesoporous materials developed in the 1990s, show numerous advantages: large surface area ($\sim$1,000 m^2/g),

D. Lewandowski (✉) · D. Bajerlein · G. Schroeder
Department of Chemistry, Adam Mickiewicz University, Umultowska 89b, 61-614 Poznan, Poland
e-mail: dawid_le@amu.edu.pl

Published online: 08 April 2014

uniform and controllable pore size, large pore volume ($\sim$1 cm^3/g), narrow particle size, open pore structures [24], chemical and biological stability, and possibility of control of surface functionalization, which makes them very useful in a wide variety of applications such as adsorption, catalysis, ion exchange, sensing [25], chromatography [26], delivery carriers, and controlled drug/gene release [27]. There are three general paths to achieve surface functionalization of mesoporous silica surface [28]: postsynthetic functionalization (the so-called "grafting") and two methods involved in the silica preparation process—co-condensation and condensation of bridged organosilica precursors forming periodic mesoporous organosilicas. The use of grafting method usually preserves the mesostructure of the starting silica phase, but the distribution of organic moieties anchored to the silica surface is solvent dependent [29] and sometimes leads to pores blockage [30]. Another advantage of this method is that it can be applied to a diversity of organic molecules, from small ones like aminopropyltrimethoxysilane [29] or compounds used in our experiment, to large moieties as dendrimers [31] and fullerenes [32]. Co-condensation is a convenient direct method of synthesis when the total amount of the organic part is supposed to be rather small. It provides better homogeneity of organic moieties, but can alter the matrix structure leading sometimes to totally disordered products [28]. It also allows the use of extraction as the only method for surfactant removal, as calcination could destroy organic compounds. After pioneering works of the groups of Mann and co-workers [33] and MacQuarrie [34], many different organically modified mesoporous silicas have been prepared by co-condensation, including those modified with alkyl, thiol, vinyl/allyl [35], amino, cyano/isocyano [36], alkoxy [37], organophosphine, and aromatic groups [38]. Periodic mesoporous organosilicas (PMOs) are materials with modified matrices but preserved organized pore system and narrow pore size distribution. They were first synthesized in 1999 by three groups working independently [39–41]. Until now, various PMOs are known: ethane- [39], ethene- [40], benzene- [42], bisphenyl-bridged [43], etc. They have found their application in chromatography [44] and catalysis [45].

The study was conducted to verify the ability of organic moieties grafted onto the mesoporous silicas of MCM-41 and MSU-H types to adsorb hydrogen peroxide from its aqueous solutions at different concentrations. Silica was chosen for the experiment, as it can be easily functionalized and has native silanol groups, able to form desired hydrogen bonds. Furthermore, both types of silica used differ in the pore diameter and noticeably in the surface area. We have used the method of postsynthetic modification to anchor nitrogen- and oxygen-containing groups that are able to form hydrogen bonds as grafting method offers higher coverage efficiency than direct synthesis methods and do not influence the order of mesoporous silica structure. Nitrogen-based compound (1-[3-(triethoxysilyl)propyl]urea) with urea-like moiety was chosen to permit comparison of the ability of hydrogen peroxide binding of this moiety and pure urea. Oxygen-based compound (*N*-(3-triethoxysilylpropyl)gluconamide) has many hydroxyl groups, and it was chosen to verify their influence on binding hydrogen peroxide.

This study is the first on hydrogen peroxide adsorption (not decomposition) on the surface of organically modified mesoporous silica. It is supposed to be the basis for future articles covering the presented issue.

Experimental details

Materials

Mesoporous silicas—MCM-41 (2.1–2.7 nm in diameter and 1,000 m^2/g surface area) and MSU-H ($\sim$7.1 nm in diameter and 750 m^2/g surface area), 30 % stock solution of hydrogen peroxide and 3-(triethoxysilyl)propyl isocyanate used for the synthesis of 1-[3-(triethoxysilyl)propyl]urea (**1**) were all purchased from Sigma-Aldrich, and *N*-(3-triethoxysilylpropyl)gluconamide (**2**) was purchased from ABCR GmbH & Co. KG. The structures of compounds used are presented in Fig. 1. Water used for the preparation of diluted hydrogen peroxide solutions had been degassed and deionized.

Preparation of reagents

Both mesoporous silicas had been prepared for grafting by activation in boiling mixture of nitric acid and water (1:1) for a few hours, filtered off, washed by large amount of water, and dried in 60 °C for several hours.

A portion of 2 g of 3-(triethoxysilyl)propyl isocyanate was dissolved in 20 ml of acetonitrile and reacted with dry gaseous ammonia. The substrates reacted vigorously, so the solution was mixed and the flask was held in a cool water bath. After 1 h, the reaction was stopped, and both ammonia and acetonitrile were evacuated under vacuum. Gelatinous, quickly crystallizing solid, identified as *N*-[3-(triethoxysilyl)propyl]urea, was obtained. Figures 2, 3, and 4 present the spectra obtained for the isolated compound.

^{1}H NMR spectrum was taken on an NMR Varian VNMR-S 400 MHz spectrometer at 298 K with TMS as a reference. ^{1}H NMR(400 MHz, $CDCl_3$), δ: 0.62–0.67 (t, 2H), 1.20–1.25 (t, 9H), 1.57–1.66 (quin, 2H), 3.11–3.17 (q, 2H), 3.79–3.85 (q, 6H), 4.74–4.77 (s, 2H), 5.20–5.28 (s, 1H).

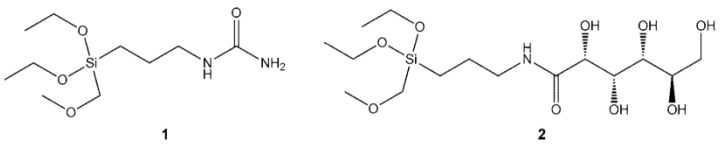

Fig. 1 Molecules grafted on selected mesoporous silicas surface—**1** stands for 1-[3-(triethoxysilyl)propyl]urea and **2** is *N*-(3-triethoxysilylpropyl)gluconamide

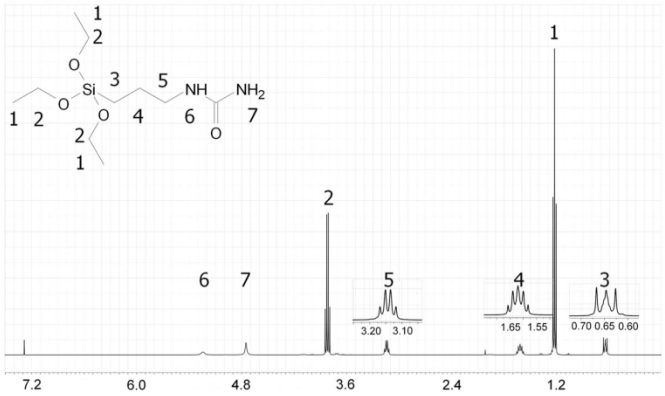

Fig. 2 ^{1}H NMR spectrum of *N*-[3-(triethoxysilyl)propyl]urea

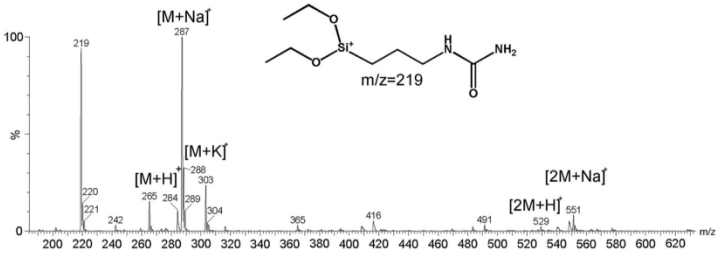

Fig. 3 ESI MS spectrum of *N*-[3-(triethoxysilyl)propyl]urea

ESI MS spectrum was obtained on a Waters/Micromass ZQ Mass Detector using 10^{-3} M methanol solution. ESI analysis parameters were the following: cone voltage—30 V, capillary voltage—3 kV, ion source temperature—393 K, desolvation temperature—573 K, and nitrogen was used as the nebulizing and desolving gas at flow rate of 80 l/min. ESI MS *m/z*: $[M+H]^+$ 265, $[M+Na]^+$ 287, $[M+K]^+$ 303.

IR spectrum was obtained on a Bruker FT-IR IFS 66/s spectrometer using 1.2 mg of the compound mixed with 200 mg of KBr and formed into a pellet. IR: 3670–3440 cm^{-1} N–H amide stretching, 2975–2885 cm^{-1} C–H alkyl stretching, 1668 cm^{-1} C=O amide stretching, 1593, 1526 cm^{-1} N–H amide bending.

Preparation of modified silica

The procedure of modifying both silicas with each of grafting reagents used was as follows: 250 mg of the grafting reagent was dissolved in 10 ml of toluene, and then 250 mg of unmodified mesoporous silica was suspended. The mixture was stirred under reflux for 6 h, cooled to room temperature, filtered off, washed with pure toluene, and dried in 60 °C for several hours.

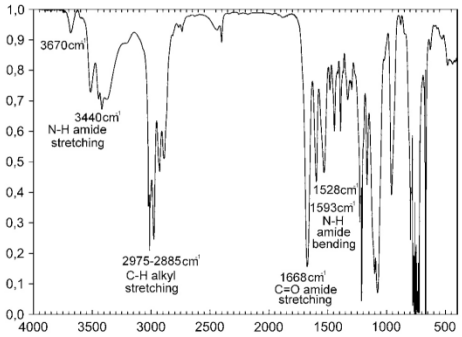

Fig. 4 IR spectrum of *N*-[3-(triethoxysilyl)propyl]urea

Hydrogen peroxide adsorption analysis

A series of hydrogen peroxide solutions with concentrations increasing from 5 to 30 % and pure, deionized, and degassed water were prepared for both unmodified and modified silica systems. Each system was composed of 35 mg of a selected silica suspended in 6 ml of hydrogen peroxide solution in a phial and stirred with a magnetic stirrer at room temperature for 24 h. Then, the phial contents were filtered off, washed with decent amount of water, and dried in 50 °C for 2 h to avoid hydrogen peroxide decomposition. The amount of hydrogen peroxide adsorbed was determined using the ferric thiocyanate method [46]. Before absorbance measurement on an UV–Vis Agilent 8453 Spectrophotometer, the silica suspensions were centrifuged to avoid disturbances caused by silica particles, and only clear solution from over the precipitate was taken for measurement.

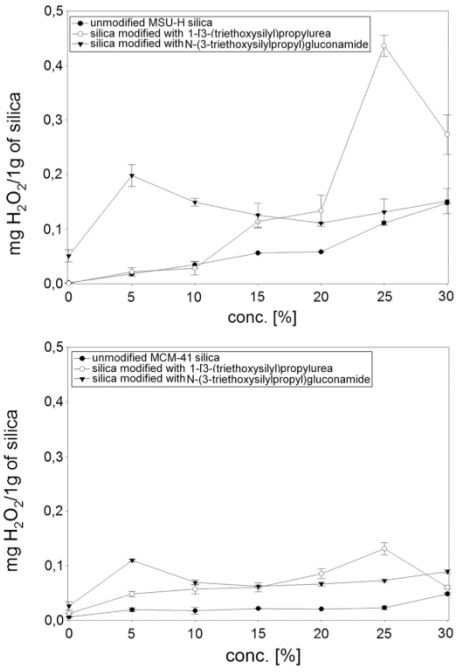

Fig. 5 Amount of hydrogen peroxide adsorbed on each functionalized silica as a function of hydrogen peroxide concentration in aqueous solution

Table 1 Comparison of grafting efficiency for all obtained systems

Grafting compound	Mesoporous silica type	Mass percentages of selected elements			Mass ratios C:H:N
		Carbon (%)	Hydrogen (%)	Nitrogen (%)	
1-[3-(Triethoxysilyl) propyl]urea	MCM-41	11.70	3.044	4.371	2.68:0.70:1
		11.74	3.065	4.276	2.75:0.72:1
	MSU-H	12.31	3.160	6.310	1.95:0.50:1
		12.27	3.190	6.250	1.96:0.51:1
N-(3-Triethoxysilylpropyl) gluconamide	MCM-41	15.68	3.786	1.925	8.14:1.97:1
		15.71	3.954	1.969	7.98:2.01:1
	MSU-H	16.17	3.498	1.939	8.34:1.80:1
		16.21	3.534	1.877	8.64:1.88:1
Pure MCM-41		0.030	0.832	0.034	0,88:24.54:1
		0.043	0.879	0.043	1.00:20.44:1
Pure MSU-H		0.089	1.215	0.044	2.02:27.61:1
		0.093	1.242	0.012	7.75:103.50:1

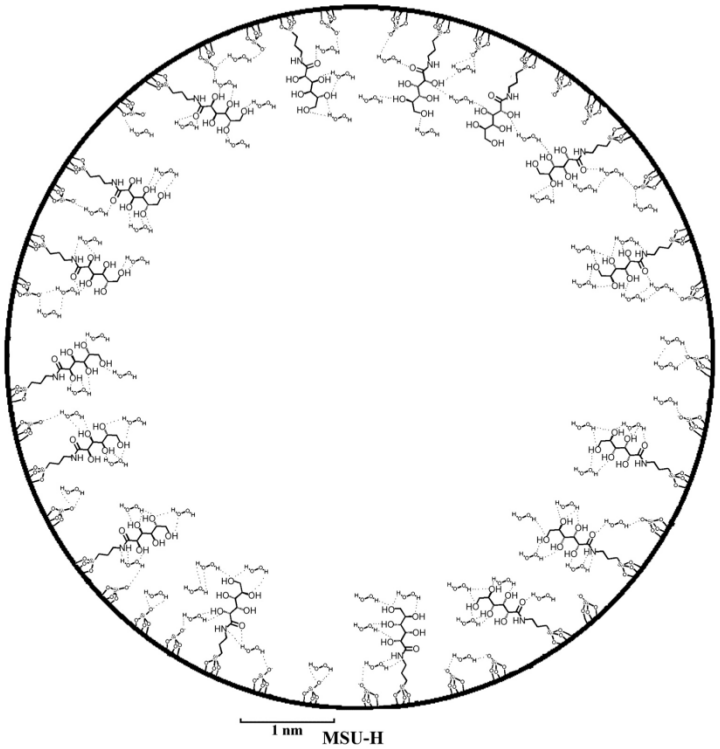

Fig. 6 Cross-section of MSU-H silica, functionalized with *N*-(3-triethoxysilylpropyl)gluconamide, explaining the possible organization of grafted molecules and hydrogen peroxide adsorbed in the pores. Channel diameter and size of the molecules match

Results and discussion

Elemental analysis

Elemental analysis for carbon, hydrogen, and nitrogen content allowed determination of the amounts of grafting reagents that had reacted with the silica surface. Results are presented in Table 1.

The presence of carbon in pure silicas can be a residue of surfactant used in the manufacturing process. Nitrogen observed in pure silica can be either adsorbed from the air or a surfactant residue, and hydrogen is a component of silanol groups densely covering the surface. The number of Si–O–Si bonds linking the grafted molecules to the surface could be easily calculated from the carbon:nitrogen ratio as hydrogen balance was more difficult to calculate. Hydrogen was removed from the surface silanol groups and added with grafted molecules in the amount depending on the total amount of the given compound grafted, hydrolysis of its alkoxy-groups, and the amount of Si–O–Si links formed.

The unbound 1-[3-(triethoxysilyl)propyl]urea of the molecular formula $C_{10}H_{24}N_2O_4Si$ and the carbon:nitrogen ratio equal to 4.29:1 can be linked through one (with one ethoxy-group removed), two, or three Si–O–Si links with carbon:nitrogen ratios equal to 3.43:1, 2.57:1, and 1.71:1, respectively. The carbon:nitrogen ratios obtained for this compound suggest binding through two Si–O–Si links, when grafted on MCM-41, and through two or three (two links:three links ratio is 0.29:0.71) links, when grafted on MSU-H silica. Similar analysis conducted for binding of *N*-(3-triethoxysilylpropyl)gluconamide led to the following results: unbound compound of the molecular formula $C_{15}H_{33}NO_9Si$ and the carbon:nitrogen ratio equal to

12.86:1 can be linked through one, two, or all three links with carbon:nitrogen ratios equal to 11.14:1, 9.43:1, and 7.71:1, respectively. The carbon:nitrogen ratios for this compound suggest binding to the surface of both silicas through two or three Si–O–Si links (for MCM-41 two links:three links ratio is 0.21:0.79 and for MSU-H 0.45:0.55).

The silicas obtained contain large amounts of grafted compounds on their surface, comparable to those of simple organic compounds grafted in the previous studies on functionalization of mesoporous surfaces [47, 48], that could be estimated from the amount of nitrogen as its content is not dependent on the binding degree. 1-[3-(Triethoxysilyl)propyl]urea accounts for 32.11 % of total mass of modified MCM-41 and 41.71 % of MSU-H, which is 1.37 molecules/nm^2 of MCM-41 surface and 3.09 molecules/nm^2 of MSU-H surface. *N*-(3-Triethoxysilylpropyl)gluconamide accounts for 44.51 % of total mass of modified MCM-41 and 45.32 % of MSU-H, which is 1.51 molecules/nm^2 of MCM-41 surface and 2.00 molecules/nm^2 of MSU-H. These results show clearly that the pore size is an important factor, influencing the total amount of compounds grafted.

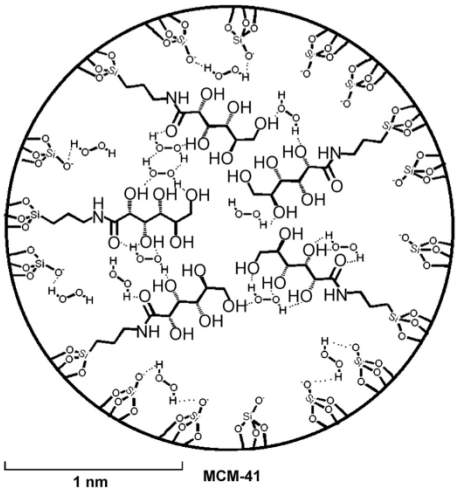

Fig. 7 Cross-section of MCM-41 silica, functionalized with *N*-(3-triethoxysilylpropyl)gluconamide, explaining the possible organization of grafted molecules and hydrogen peroxide adsorbed in the pores. Channel diameter and size of the molecules match

Hydrogen peroxide adsorption analysis

The graphs presented in Fig. 5 for different mesoporous silicas show clearly that surface modification influenced the amounts of hydrogen peroxide adsorbed on its surface, which after modification increased several times. The adsorption capacity of silicas modified with 1-[3-(triethoxysilyl)propyl]urea was increasing nonlinearly up to a hydrogen peroxide concentration of 25 %, and then it dropped to values similar to those obtained for unmodified silica, probably because of the destruction of organic moiety anchored to the silica surface (loss of the "urea" part makes it unable to form hydrogen bonds). The silicas modified with *N*-(3-triethoxysilylpropyl)gluconamide have their maximum adsorption at 5 % concentration of hydrogen peroxide, and then it decreases slightly to become almost equal to the adsorption of unmodified silica at 30 % hydrogen peroxide concentration. A large number of hydroxyl groups included in gluconamide moiety are oxidized, even at lower concentrations, and partially lose their ability to form hydrogen bonds (carbonyl group, without a hydrogen atom, can only be an electron donor). The average contents of carbon, hydrogen, and nitrogen for samples bathed in a 30 % solution of hydrogen peroxide are, respectively, 7.468, 2.261, and 3.897 %. The carbon:nitrogen ratio is much smaller than that for the unoxidized sample, which proves a major destruction to the organic part and the loss of ability to bind hydrogen peroxide. Small increase in the amount of hydrogen peroxide adsorbed at 25 and 30 % concentrations in comparison to that adsorbed from hydrogen peroxide solutions of concentrations 20 and 25 % may be caused by adsorption on the uncovered part of the silica surface.

Also, MSU-H silica was found to adsorb much higher amounts of hydrogen peroxide, although it has smaller surface area. The influence of pore diameter on the amounts of hydrogen peroxide adsorbed is also indicated by the results obtained for each silica separately. The maximum amounts of hydrogen peroxide for MCM-41 are similar because of available space limitations. Grafted molecules occupy most of the pore volume, so there is not much space to bind H_2O_2 and its diffusion may be impaired. MSU-H provides much more space for both grafted organic moieties and hydrogen peroxide adsorbed as can be seen comparing Figs. 6 and 7, and the amount of H_2O_2 is only limited by the binding abilities of grafted molecules.

The amount of hydrogen peroxide adsorbed on unmodified silica surface almost linearly increases with increasing hydrogen peroxide concentration. This phenomenon can be explained by formation of hydrogen bonds between free silanol groups and hydrogen peroxide. In the experimental conditions, almost all of silanol groups were ionized as mesoporous silanol groups existed in two forms, Si-$(OH)_2$ and Si-(OH) with pK_a values, respectively, 8.2 and 2.0 [49].

Conclusions

Two different molecules able to form hydrogen bonds were successfully grafted on the surface of two different mesoporous silicas of MCM-41 and MSU-H types. The amounts of hydrogen peroxide adsorbed on their surface were measured, and MSU-H sample was found to have a higher adsorption capacity, as about 2–3 times more hydrogen peroxide got adsorbed on its surface. Unmodified silica showed also some adsorption abilities dependent on the concentration of hydrogen peroxide solution. Functionalized surface was not resistant enough and the compounds deposited underwent oxidation, changing the silicas adsorption properties in higher hydrogen peroxide concentrations. Increased amount of hydroxyl groups introduced with *N*-(3-triethoxysilylpropyl)gluconamide indeed has enhanced the adsorption of hydrogen peroxide. Although the content of hydrogen peroxide bound by the systems obtained was small in comparison with that of PVP or urea complexes, results of this study can initiate further development in this field.

Acknowledgments The authors would like to thank the National Science Center of Poland (Grant No. 2011/03/B/ST5/01573) for financial support.

References

1. Wayne RP (1991) Chemistry of atmospheres. Clarendon Press, Oxford
2. Gericke K-H, Klee S, Comes FJ, Dixon RN (1986) Dynamics of H_2O_2 photodissociation: OH product state and momentum distribution characterized by sub-Doppler and polarization spectroscopy. J Chem Phys 85:4463–4479
3. Docker MP, Hodgson A, Simons JP (1986) Photodissociation of H_2O_2 at 248 nm: translational anisotropy and oh product state distributions. Chem Phys Lett 128:264–269
4. Hart PW, Rudie AW (2012) The bleaching of pulp, 5th edn. Tappi Press, Norcross
5. Kureshy RI, Khan NH, Abdi SHR, Patel ST, Jasra RV (2001) Enantioselective epoxidation of non-functionalised alkenes using a urea–hydrogen peroxide oxidant and a dimeric homochiral Mn(III)-Schiff base complex catalyst. Tetrahedron Asymmetry 12:433–437
6. Goebel JR, Ault BS, Del Bene JE (2001) Matrix isolation and ab initio study of 1:1 hydrogen-bonded complexes of H_2O_2 with NH_3 and $N(CH_3)_3$. J Phys Chem A 105:6430–6435
7. Goebel J, Ault BS, Del Bene JE (2000) Matrix isolation and ab initio study of the hydrogen-bonded complex between H_2O_2 and $(CH_3)_2O$. J Phys Chem A 104:2033–2037
8. Boehlow TR, Spilling CD (1996) The regio- and stereo-selective epoxidation of alkenes with methyl trioxorhenium and urea–hydrogen peroxide adduct. Tetrahedron Lett 37:2717–2720
9. Hasaninejad A, Zolfigol MA, Chehardoli G, Mokhlesi M (2010) Molybdatophosphoric acid as an efficient catalyst for the catalytic and chemoselective oxidation of sulfides to sulfoxides using urea hydrogen peroxide as a commercially available oxidant. J Serb Chem Soc 75:307–316
10. Varma RS, Naicker KP (1999) The urea–hydrogen peroxide complex: solid-state oxidative protocols for hydroxylated aldehydes and ketones (Dakin reaction), nitriles, sulfides, and nitrogen heterocycles. Org Lett 1:189–192
11. Caron S, Do NM, Sieser JE (2000) A practical, efficient, and rapid method for the oxidation of electron deficient pyridines using trifluoroacetic anhydride and hydrogen peroxide–urea complex. Tetrahedron Lett 41:2299–2302
12. Tanatar S (1906) J Russ Phys Chem Soc 40L:376
13. Lu C-S, Hughes EW, Giguère PA (1941) The crystal structure of the urea–hydrogen peroxide addition compound $CO(NH_2)_2$ H_2O_2. J Am Chem Soc 63:1507–1513
14. Chehardoli G, Zolfigol MA (2009) Melamine hydrogen peroxide (MHP): novel and efficient reagent for the chemo- and homoselective and transition metal-free oxidation of thiols and sulfides. Phosphorus Sulfur Silicon Relat Elem 185:193–203
15. Zolfigol MA, Salehi P, Mallakpour SE, Torabi M (2003) 1,4-Diazabicyclo[2.2.2]octane 1,4-bis(oxide)-bis(hydrogen peroxide)/MCl_x as a novel heterogeneous system for the oxidation of urazoles under mild conditions. Bull Chem Soc Jpn 76:1673–1674
16. Pourali AR, Ghanei M (2006) Direct Iodination of aromatic compounds with polyvinylpyrrolidone supported hydrogen peroxide (PVP-H_2O_2) and potassium iodide or molecular iodine. Chin J Chem 24:1077–1079
17. Pourali AR, Ghanei M (2006) Efficient epoxidation of α, β-enones with polyvinylpyrrolidone supported hydrogen peroxide (PVP-H_2O_2). Bull Korean Chem Soc 27:1674–1676
18. Merianos JJ (1991) Anhydrous complexes of PVP and hydrogen peroxide. US Patent 5,008,093
19. Ghorbani-Choghamarani A, Azadi G (2011) Polyvinylpolypyrrolidone-supported hydrogen peroxide (PVP-H_2O_2), silica sulfuric acid and catalytic amounts of ammonium bromide as green, mild and metal-free oxidizing media for the efficient oxidation of alcohols and sulfides. JICS 8:1082–1090
20. Kochkar H, Figueras F (1997) Synthesis of hydrophobic TiO_2–SiO_2 mixed oxides for the epoxidation of cyclohexene. J Catal 171:420–430
21. Barbosa GN, MacLeod TCO, Guedes DFC, Assis MD, Oliveira HP (2008) Preparation, characterization and catalytic studies of V_2O_5–SiO_2 xerogel composite. J Sol–Gel Sci Technol 46:99–105
22. Neumann R, Levin-Elad M (1997) Metal oxide (TiO_2, MoO_3, WO_3) substituted silicate xerogels as catalysts for the oxidation of hydrocarbons with hydrogen peroxide. J Catal 166:206–217
23. Bednarz S, Ryś B, Bogdał D (2012) Application of hydrogen peroxide encapsulated in silica xerogels to oxidation reactions. Molecules 17:8068–8078
24. Popat A, Liu J, Hu Q, Kennedy M, Peters B, Lu GQM, Qiao SZ (2012) Adsorption and release of biocides with mesoporous silica nanoparticles. Nanoscale 4:970–975
25. Vallet-Regi M, Ramila A, Real RPd, Perez-Pariente J (2001) A new property of MCM-41: drug delivery system. Chem Mater 13:308–311
26. Mal NK, Fujiwara M, Tanaka Y (2003) Photocontrolled reversible release of guest molecules from coumarin-modified mesoporous silica. Nature 421:350–353
27. He Q, Gao Y, Zhang L, Zhang Z, Gao F, Ji X, Li Y, Shi J (2011) A pH-responsive mesoporous silica nanoparticles-based multi-drug delivery system for overcoming multi-drug resistance. Biomaterials 32:7711–7720

28. Hoffmann F, Cornelius M, Morell J, Froba M (2006) Silica-based mesoporous organic–inorganic hybrid materials. Angew Chem Int Ed 45:3216–3251
29. Salmio H, Bruhwiler D (2007) Distribution of amino groups on a mesoporous silica surface after submonolayer deposition of aminopropylsilanes from an anhydrous liquid phase. J Phys Chem C 111:923–929
30. Lim MH, Stein A (1999) Comparative studies of grafting and direct syntheses of inorganic–organic hybrid mesoporous materials. Chem Mater 11:3285–3295
31. Acosta EJ, Carr CS, Simanek EE, Shantz DF (2004) Engineering nanospaces: iterative synthesis of melamine-based dendrimers on amine-functionalized SBA-15 leading to complex hybrids with controllable chemistry and porosity. Adv Mater 16:985–989
32. Fukuoka A, Fujishima K, Chiba M, Yamagishi A, Inagaki S, Fukushima Y, Ichikawa M (2000) Photooxidation of cyclohexene and benzene with oxygen by fullerenes grafted on mesoporous FSM-16. Catal Lett 68:241–244
33. Burkett SL, Sims SD, Mann S (1996) Synthesis of hybrid inorganic–organic mesoporous silica by co-condensation of siloxane and organosiloxane precursors. Chem Commun 11:1367–1368
34. Macquarrie DJ (1996) Direct preparation of organically modified MCM-type materials. Preparation and characterisation of aminopropyl-MCM and 2-cyanoethyl-MCM. Chem Commun 16:1961–1962
35. Mercier L, Pinnavaia TJ (2000) Direct synthesis of hybrid organic-inorganic nanoporous silica by a neutral amine assembly route: structure-function control by stoichiometric incorporation of organosiloxane molecules. Chem Mater 12:188–196
36. Huh S, Wiench JW, Yoo J-C, Pruski M, Lin VS-Y (2003) Organic functionalization and morphology control of mesoporous silicas via a co-condensation synthesis method. Chem Mater 15:4247–4256
37. Fowler CE, Burkett SL, Mann S (1997) Synthesis and characterization of ordered organo-silica-surfactant mesophases with functionalized MCM-41-type architecture. Chem Mater 18:1769–1770
38. Cagnol F, Grosso D, Sanchez C (2004) A general one-pot process leading to highly functionalised ordered mesoporous silica films. Chem Commun 10:1742–1743
39. Inagaki S, Guan S, Fukushima Y, Ohsuna T, Terasaki O (1999) Novel mesoporous materials with a uniform distribution of organic groups and inorganic oxide in their frameworks. J Am Chem Soc 121:9611–9614
40. Melde BJ, Holland BT, Blanford CF, Stein A (1999) Mesoporous sieves with unified hybrid inorganic/organic frameworks. Chem Mater 11:3302–3308
41. Asefa T, MacLachlan MJ, Coombs N, Ozin GA (1999) Periodic mesoporous organosilicas with organic groups inside the channel walls. Nature 402:867–871
42. Yoshina-Ishii C, Asefa T, Coombs N, MacLachlan MJ, Ozin GA (1999) Periodic mesoporous organosilicas, PMOs: fusion of organic and inorganic chemistry 'inside' the channel walls of hexagonal mesoporous silica. Chem Commun 24:2539–2540
43. Kapoor MP, Yang Q, Inagaki S (2002) Self-assembly of biphenylene-bridged hybrid mesoporous solid with molecular-scale periodicity in the pore walls. J Am Chem Soc 124:15176–15177
44. Kim D-J, Chung J-S, Ahn W-S, Kang G-W, Cheong W-J (2004) Morphology control of organic-inorganic hybrid mesoporous silica by microwave heating. Chem Lett 33:422–423
45. Fukuoka A, Sakamoto Y, Guan S, Inagaki S, Sugimoto N, Fukushima Y, Hirahara K, Iijima S, Ichikawa M (2001) Novel templating synthesis of necklace-shaped mono- and bimetallic nanowires in hybrid organic-inorganic mesoporous material. J Am Chem Soc 123:3373–3374
46. Boltz DF, Howell JA (1978) Colorimetric determination of nonmetals, vol 8, 2nd edn. Wiley, New York
47. Chang F-Y, Chao K-J, Cheng H-H, Tan C-S (2009) Adsorption of CO_2 onto amine-grafted mesoporous silicas. Sep Purif Technol 70:87–95
48. Seçkin T, Gültek A, Kartaca S (2003) The grafting of Rhodamine B onto sol–gel derived mesoporous silicas. Dyes Pigments 56:51–57
49. Rosenholm JM, Czuryszkiewicz T, Kleitz F, Rosenholm JB, Lindén M (2007) On the nature of the Brønsted acidic groups on native and functionalized mesoporous siliceous SBA-15 as studied by benzylamine adsorption from solution. Langmuir 23:4315–4323

Journal of Physics and Chemistry of Solids 85 (2015) 56–61

Contents lists available at ScienceDirect

Journal of Physics and Chemistry of Solids

journal homepage: www.elsevier.com/locate/jpcs

Fluorescence properties of riboflavin-functionalized mesoporous silica SBA-15 and riboflavin solutions in presence of different metal and organic cations

Dawid Lewandowski [a,*], Grzegorz Schroeder [a], Mirosław Sawczak [b], Tadeusz Ossowski [c]

[a] Adam Mickiewicz University, Department of Chemistry, Umultowska 89b, 61-614 Poznań, Poland
[b] Department of Photophysics, IFFM Polish Academy of Sciences, Fiszera 14, 80-231 Gdańsk, Poland
[c] Department of Chemistry, University of Gdańsk, Wita Stwosza 63, 80-308 Gdańsk, Poland

ARTICLE INFO

Article history:
Received 26 November 2014
Received in revised form
16 March 2015
Accepted 14 April 2015
Available online 15 April 2015

Keywords:
Surfaces
Infrared spectroscopy
Thermogravimetric analysis (TGA)
Luminescence

ABSTRACT

Riboflavin was covalently linked to mesoporous SBA-15 silica surface via grafting technique. Then fluorescence properties of the system obtained were analyzed in the presence of several metal and organic cations. Both quenching and strengthening of fluorescence as well as significant changes in the maximum fluorescence wavelength were observed. The results were compared with absorption and fluorescence data obtained for riboflavin water solutions.

1. Introduction

Riboflavin, also known as Vitamin B2, is a naturally occurring substance and an essential nutrient for humans. It is only slightly soluble in water (from 0.05 to 0.33 g L^{-1} depending on its internal crystalline structure [1]). Aqueous solution of riboflavin shows the maxima of radiation absorption at λ_{abs}=223, 266, 373 and 445 nm and strong green-yellow fluorescence with a maximum at λ_{em}=520–530 nm [2]. Riboflavin in water solutions is easily degraded by UV and visible light of which that from the range of 420–560 nm causes the greatest destruction [3]. The degradation process is intensified with increasing temperature and pH. While in solution most of the riboflavin content is destroyed within a few hours of exposure to bright sunlight [4], dry (solid) preparations are much more stable, especially when kept away from sunlight [4]. Riboflavin is known for its ability to form stable complexes with metal ions [5–7], i.e. zinc, iron and cadmium complexes with riboflavin have their $\log_\beta$ equal to: 5.58, 7.12 and 4.72, respectively [8]. Only a few papers on the fluorescence activity of riboflavin in the presence of metal ions [9] have been published and, according to our knowledge, no studies on covalently grafted solid riboflavin preparations have been reported.

SBA-15 mesoporous silica was discovered in 1998 by Zhao et al. [10]. It has relatively large pores, with diameters within the range of 5–30 nm, and a system of micropores/small mesopores providing connectivity between larger, hexagonally ordered, pores [11]. Pore diameter allows sizable molecules to be encapsulated inside or numerous organic functional groups to be grafted on the surface. Recent advances on the SBA-15 silica functionalization include grafting of organic moieties (small ones like amino [12,13], sulfonic [14], folate [15] or others [16,17] as well as polymers like hyaluronic acid [18] or poly(methacrylic acid) [19]) to use their binding or catalytic properties and control the cargo (e.g. drugs) release. Attempts have been made to permanently immobilize inorganic or hybrid organic–inorganic additives, containing aluminum [20], copper(II) [21, 22] or molybdenum(VI) [23], for the same purposes.

The aim of this work was to graft riboflavin on SBA-15 mesoporous silica, study its fluorescence properties in the presence of selected metal ions and compare the results with those obtained for riboflavin solutions.

2. Experimental details

2.1. Reagents

Riboflavin, (3-isocyanatopropyl)triethoxysilane, metal perchlorates, silver nitrate, ethylamine hydrochloride, L-alanine

* Corresponding author.
E-mail address: dawid_le@amu.edu.pl (D. Lewandowski).

http://dx.doi.org/10.1016/j.jpcs.2015.04.007
0022-3697/

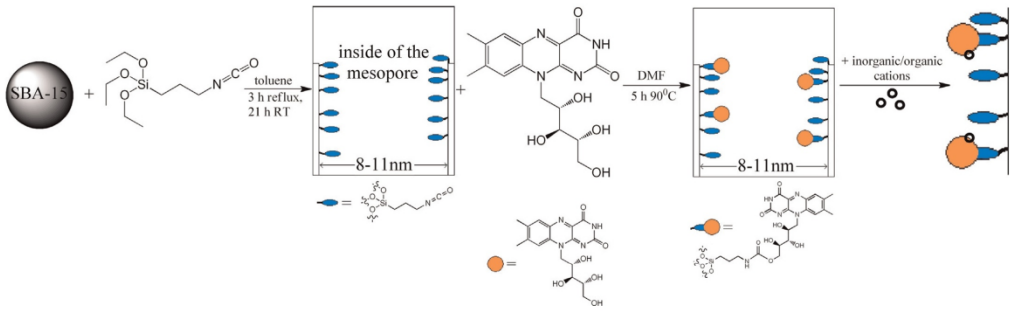

Fig. 1. Schematic route of SBA-15 mesoporous silica modification with riboflavin molecules.

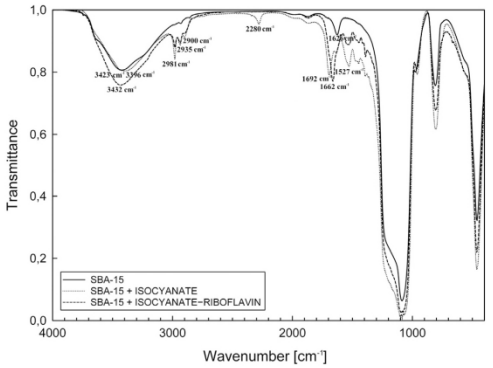

Fig. 2. FT-IR spectra of the initial SBA-15 mesoporous silica and the products of each modification.

methyl ester hydrochloride, L-lysine monohydrochloride, benzocaine and D-(+)-glucosamine hydrochloride were all purchased from Sigma-Aldrich, SBA-15 mesoporous silica (8–11 nm pore diameter, 600 $m^2 g^{-1}$ surface area and 1–2 μm particle size) was purchased from ACS Material and L-leucine hydrochloride from Alfa Aesar. Water solutions and suspensions were prepared using deionized water. Benzocaine hydrochloride was prepared by purging benzocaine solution in chloroform (Sigma-Aldrich, ≥99.8% purity) with gas hydrogen chloride and filtering off the precipitated crystals. The compound purity was confirmed by the determination of its melting point (207 °C).

2.2. Silica preparation

A portion of 0.4 g of SBA-15 mesoporous silica was suspended in toluene solution containing 1.48 g (6 mmol) (3-isocyanatopropyl)triethoxysilane and refluxed for 3 h and then stirred for 21 h at room temperature. White solid obtained was filtered off, washed with toluene and dried for several hours. In the second step 100.0 mg (0.266 mmol) of riboflavin was dissolved in 70 ml of hot (90 °C) dimethylformamide (DMF) and dry solid from the first step was added. The suspension was stirred for 5 h and then hot filtered and washed with hot DMF to remove physically adsorbed riboflavin. The solid was then dried and became pale yellow (Fig. 1) (photographs available in the Supplementary materials).

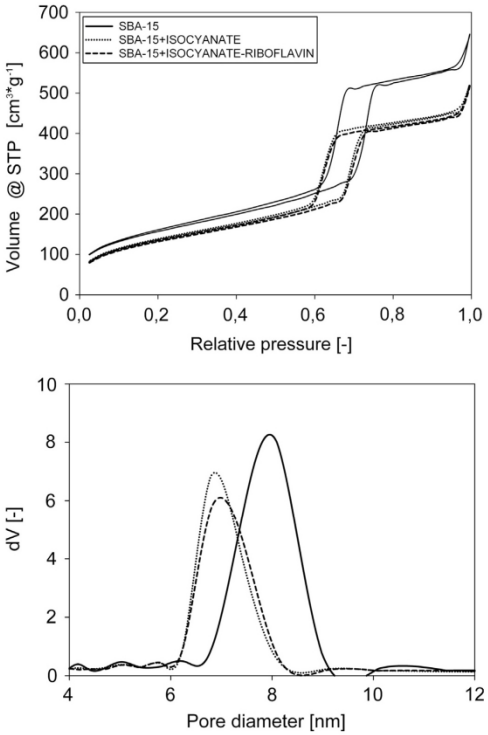

Fig. 3. Nitrogen adsorption analysis results indicating surface functionalization.

Modified silica was characterized using FT-IR spectrometer (IFS 66/s, Bruker) with 1.0 mg of the silica mixed with 200 mg of KBr and formed into a pellet; elemental analysis was carried on an elemental analyzer (EL III, Vario); thermogravimetric analysis was performed on a TGA Q50 (TA Instruments) apparatus and nitrogen adsorption was analyzed using Quantachrome Autosorb iQ apparatus. Deterioration of riboflavin solutions used in the preparation of riboflavin-functionalized silica was proved using electrospray mass spectrometry (ESI MS) and the spectra were obtained on a

mass spectrometer (Micromass ZQ, Waters) using 10^{-5} M methanol solutions.

2.3. Solutions preparation

Riboflavin solution was prepared from 5.0 mg (0.0133 mmol) of riboflavin dissolved in 100 ml of deionized water by sonication. The solutions of metal ions and hydrochlorides were prepared by dissolution of appropriate amount of a given metal perchlorate (or its hydrate or, in case of Ag^+ ions, nitrate) or organic hydrochloride in 1 ml of deionized water to obtain 0.05 M solution. The following perchlorates: sodium, magnesium, calcium, cadmium, nickel(II), mercury(II), lead(II), manganese(II), cobalt(II), chromium (III), aluminum and strontium were used in the study.

2.4. Spectrophotometric analysis

Riboflavin solutions with the addition of metal or organic cations were spectrophotometrically analyzed on a UV–vis spectrophotometer (8453, Agilent) to verify possible changes in the absorption spectra. Before the analysis, each solution was diluted 10 times using deionized water.

2.5. Fluorescence analysis

Fluorescence analysis for riboflavin solutions was conducted as follows: appropriate amount of given metal perchlorate or organic hydrochloride was dissolved in 1 ml of riboflavin solution to obtain 0.05 M cation concentration and kept in darkness for 24 h. Then the solutions were diluted 20 times and the fluorescence

Table 3
Fluorescence analysis results obtained for riboflavin solutions in the presence of different cations.

Ion	Fluorescence maximum value (AU)[a]	Relative fluorescence maximum value (%)	Emission maximum wavelength (nm)	Emission maximum shift (nm)
–(Water solution)	9048	100.0	514.6	0.0
Ag^+	868	9.6	512.9	−1.7
Al^{3+}	7835	86.6	513.5	−1.1
Ca^{2+}	8637	95.5	512.4	−2.2
Cd^{2+}	8606	95.1	514.2	−0.4
Co^{2+}	8970	99.1	514.5	−0.1
Cr^{3+}	7968	88.1	512.5	−2.1
Hg^{2+}	2952	32.6	513.6	−1.0
Mg^{2+}	8817	97.4	513.4	−1.2
Mn^{2+}	8604	95.1	513.6	−1.0
Na^+	8634	95.4	513.5	−1.1
Ni^{2+}	8769	96.9	513.6	−1.0
Pb^{2+}	8476	93.7	514.5	−0.1
Sr^{2+}	9118	100.8	514.5	−0.1
Ethylamine hydrochloride	8969	99.1	513.5	−1.1
L-alanine methyl ester hydrochloride	8345	92.2	513.5	−1.1
L-leucine hydrochloride	8720	96.4	513.5	−1.1
L-lysine hydrochloride	8969	99.1	514.5	−0.1
D-(+)-glucosamine Hydrochloride	8958	99.0	513.5	−1.1
Benzocaine Hydrochloride	5795	64.0	513.4	−1.2

[a] AU – arbitrary units.

Table 4
Fluorescence analysis results obtained for solid samples of riboflavin covalently grafted on SBA-15 surface after 24 h contact with solutions of different cations.

Ion	Fluorescence maximum value (AU)[a]	Relative fluorescence maximum value (%)	Emission maximum wavelength (nm)	Emission maximum shift (nm)
–(Water suspension)	14,320,000	100.0	517.8	0.0
Unmodified SBA-15	451,000	3.1	444.2	−73.6
Ag^+	2,937,000	20.5	538.1	+20.3
Al^{3+}	15,370,000	107.3	509.2	−8.6
Ca^{2+}	8,242,000	57.6	509.2	−8.6
Cd^{2+}	26,210,000	183.0	535.2	+17.4
Co^{2+}	1,550,000	10.8	509.6	−8.2
Cr^{3+}	1,758,000	12.3	500.2	−17.6
Hg^{2+}	2,340,000	16.3	499.3	−18.5
Mg^{2+}	21,480,000	150.0	509.0	−8.8
Mn^{2+}	11,360,000	79.3	512.0	−5.8
Na^+	15,150,000	105.8	512.2	−5.6
Ni^{2+}	2,113,000	14.8	510.8	−7.0
Pb^{2+}	6,672,000	46.6	507.7	−10.1
Sr^{2+}	19,840,000	138.5	522.9	+5.1
Ethylamine hydrochloride	15,140,000	105.7	487.2	−30.6
L-alanine methyl ester hydrochloride	26,250,000	183.3	505.7	−12.1
L-leucine hydrochloride	26,480,000	184.9	507.1	−10.7
L-lysine hydrochloride	15,260,000	106.6	499.7	−18.2
D-(+)-glucosamine hydrochloride	22,150,000	154.7	500.3	−17.6
Benzocaine hydrochloride	896,200	6.3	512.6	−5.2

[a] AU – arbitrary units.

spectra were obtained using FluoTime 300 spectrometer. Samples were excited with Xenon arc lamp (365 nm wavelength, 860 mW output power, 1 nm excitation bandpass) and the fluorescence signal was collected by Photomultiplier Tubes (PMT) with 1 nm detection bandpass.

Fluorescence analysis of riboflavin covalently grafted on SBA-15 silica was conducted as follows: 20.0 mg of previously prepared solid was suspended in 1 ml of given metal perchlorate or organic hydrochloride solution and kept in darkness at room temperature for 24 h. During that time the suspensions were agitated several times. Then the supernatant liquid was removed and the residual suspensions were dried at room temperature. The fluorescence measurements were carried on a laboratory setup consisting of a 0.3 m Czerny–Turner spectrograph (SR303i, Andor) equipped with ICCD camera (DH740, Andor). Samples in the form of powder were excited with UV LED (365 nm, 350 mW output power). The angle of incidence of the excitation radiation, focused by quartz lens, was 45°. Additionally the band-pass filter (UG11, Schott) was applied between the excitation source and the sample to block UV LED radiation above 380 nm. The fluorescence signal was collected perpendicularly to the sample surface using a microscope objective and focused on the entrance of an optical fiber. In the detection path, the band-pass filters (GG44, Schott) was used for blocking the excitation radiation.

Each sample was analyzed twice and the average result was calculated. Emission maxima values and wavelengths were calculated using bisquare fitting method with the parameters: sampling proportion – 0.1, polynomial degree – 1 and nearest neighbors as bandwidth method.

3. Results and discussion

3.1. Modified silica analysis

Elemental analysis for SBA-15 silica modified with (3-isocyanatopropyl)triethoxysilane showed 0.962% of nitrogen and 4.206% of carbon content coming from isocyanate groups and 1.099% of hydrogen from both organic moiety and silica surface. Carbon:nitrogen ratio suggests linking the isocyanate through two or three Si–O–Si bonds. Results obtained for riboflavin-functionalized silica indicated the presence of 1.163% of nitrogen and 4.943% of carbon from organic moieties anchored to the surface and 1.172% of hydrogen from both organic part and silica surface. The amount of riboflavin grafted on the silica surface was calculated from the nitrogen balance with the result of 3.46 mmol of riboflavin for each 100 g of unmodified silica used for the preparation. This result means that about 4–5% of isocyanate groups on the surface had been covered with riboflavin. Attempts to increase the coverage percentage by prolonging the stirring time (90 °C with overnight stirring) or increasing the reaction temperature (120 °C for 5 h) led to products with slightly increased riboflavin content – the solids obtained had more intensive yellow color. However, in these conditions the riboflavin solutions deteriorated and became dark yellow fading to brown probably because of the thermal degradation of riboflavin [24]. It was proved by ESI MS spectra in which the signals corresponding to riboflavin were not detectable. Riboflavin could be attached to the surface through a number of hydroxyl groups, but the most probable one is the last, 1° group, which is the least sterically hindered and has the highest electron density. Moreover, the size of riboflavin molecule makes it impossible to cover all of the –NCO groups on the material surface.

FT-IR results (Fig. 2) clearly indicate that SBA-15 silica was modified with isocyanate groups (–C=N=O stretching signal at 2280 cm^{-1}) and all of them reacted–some joined riboflavin molecules and some reacted with the solvent [25]. If so, the elemental analysis results would be disturbed and unreliable. However, the modification on isocyanate-functionalized SBA-15 with riboflavin in DMF led to considerable proportional increase in the O–H stretching signal strength as well as increase in the strength and shift of the signals from the range of 1700 to 1600 cm^{-1}. The resulting C=O carbamate bonds, C=N bonds (from the reaction between isocyanate and DMF) and C=O amide bonds from riboflavin give strong signals in the range 1690–1650 cm^{-1}. Other characteristic bands of riboflavin are difficult to be assigned because of its small content, however the deformation of the signal at 1550–1520 cm^{-1} can be a sign of riboflavin presence – pure riboflavin reveals very strong band at 1547 cm^{-1}.The signal at 1626 cm^{-1}, typical of O–H bending vibration is present in the spectrum of isocyanate-modified SBA-15, but in the spectrum of the final product it became a distortion of a stronger signal.

TG analysis also confirmed that isocyanate groups partially underwent a reaction with DMF that could lead to a decrease in the total amount of organic part on the silica surface (TG chart available in the Supplementary materials).

Nitrogen adsorption analysis (Fig. 3) proved that only small amount of riboflavin had been attached to the surface, which caused a slight decrease in the surface area and had no noticeable

Table 1
Summary of the nitrogen adsorption analysis.

Material	Surface area (BET) ($m^2 g^{-1}$)	Pore diameter (BJH) (nm)	Pore volume (BJH) ($cm^3 g^{-1}$)
SBA-15	555.9	8.1	0.902
SBA-15 + ISOCYANATE	482.2	6.8	0.720
SBA-15 + ISOCYANATE-RIBOFLAVIN	470.6	6.8	0.720

Table 2
Absorption analysis results obtained for riboflavin solutions ($1.3*10^{-5}$ M, which corresponds to 5.0 mg of riboflavin per 1000 mL of water) in the presence of different cations.

Ion	Absorption maxima wavelengths (nm)		Absorption maximum value for longer wavelength's maximum (–)	Relative absorption maximum value (%)
–(Water solution)	374	446	0.1475	100.0
Ag^+	377	470	0.0460	31.2
Al^{3+}	374	444	0.1469	99.6
Ca^{2+}	374	445	0.1490	101.0
Cd^{2+}	374	445	0.1524	103.4
Co^{2+}	374	446	0.1433	97.1
Cr^{3+}	377	442	0.1696	115.0
Hg^{2+}	374	448	0.1221	82.8
Mg^{2+}	374	446	0.1498	101.6
Mn^{2+}	375	444	0.1483	100.5
Na^+	374	447	0.1475	100.0
Ni^{2+}	375	446	0.1543	104.6
Pb^{2+}	374	445	0.1542	104.5
Sr^{2+}	374	444	0.1516	102.8
Ethylamine hydrochloride	375	444	0.1549	105.0
L-alanine methyl ester hydrochloride	374	446	0.1511	102.5
L-leucine hydrochloride	375	446	0.1475	100.0
L-lysine hydrochloride	375	446	0.1520	103.0
D-(+)-glucosamine Hydrochloride	375	446	0.1489	101.0
Benzocaine hydrochloride	374	446	0.1464	99.2

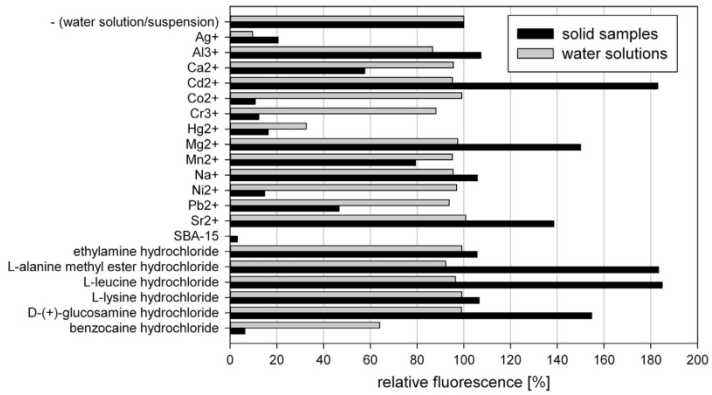

Fig. 4. Relative fluorescence maxima values for all samples analyzed. The results for riboflavin water solution and solid sample suspended in water are set to 100%.

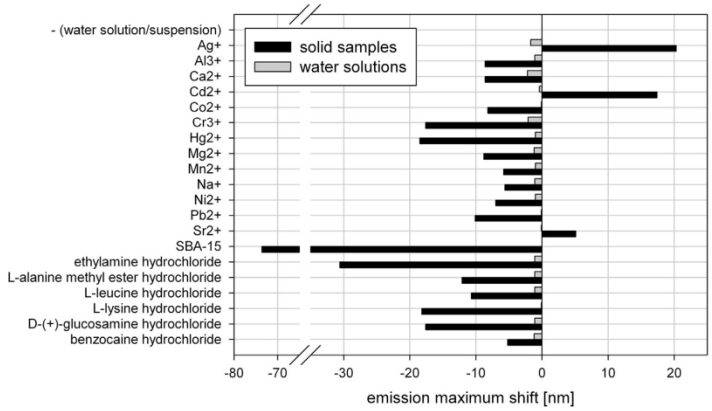

Fig. 5. Shifts of the fluorescence maxima wavelengths for all samples analyzed. The results for riboflavin water solution and solid sample suspended in water are set to 0.0 nm.

influence on both: mean pore diameter and pore volume (Table 1).

3.2. Spectrophotometric analysis

For spectrophotometric analysis riboflavin concentration was about $1.3*10^{-5}$ M and the metal cations concentration was 0.05 M, which is more than three orders of magnitude higher than the riboflavin concentration. Although the spectrum of riboflavin shows four absorption maxima, only two of them, those at 373 and 445 nm, could be measured reliably because of the innate absorption properties of nitrate anion, amide carbonyl group and aromatic benzocaine ring. The absorption maximum values shown in Table 2 refer to the maximum with longer wavelength. The absorption maxima wavelengths and absorption maximum intensities (Table 2) either do not change or change only slightly, except for silver and mercury(II) ions, which could be seen as the solution color turned from yellow to red and orange, respectively. Small shifts observed for chromium(III) ions are a result of its innate absorption. The absorption of other ions was negligible. Benzocaine solution was slightly darker changing to orange, but the absorption results were not reflected in the spectrum, that is in the changes in the maxima wavelengths. All spectra recorded (for both, solutions and solid samples) are available in the Supplementary materials.

3.3. Fluorescence analysis

Fluorescence spectra of riboflavin in water solutions in the presence of metal cations and organic cations (Table 3) were similar and showed only one peak. Significant changes in the intensity of riboflavin fluorescence were noted in the presence of silver and mercury(II) ions.

Worth mentioning are also the changes in the riboflavin fluorescence intensity caused by the presence of chromium(III), aluminum and benzocaine cations as well as the shifts of the maximum fluorescence induced by the presence of chromium(III) and calcium ions.

Results of fluorescence measurements for solid samples

(Table 4) were quite surprising. Both fluorescence maximum values and wavelengths varied within a wide range. Pure SBA-15 silica, as expected, revealed almost negligible fluorescence in comparison with modified systems. There is no reasonable pattern in the observed results. Nevertheless, the presence of all cations from the third period of *d* block resulted in high to very high decrease in the fluorescence intensity and negative shift of the emission maxima. The presence of most *s* block cations increased the intensity of riboflavin fluorescence. The presence of organic cations generally increased the fluorescence intensity except for benzocaine that suppressed it almost completely. Furthermore, their curves revealed the second modest maximum near 460 nm whose intensity was 50–75% of that of the primary peak.

General comparison of fluorescence results obtained from both solutions and solid samples analyzes is presented in Figs. 4 and 5.

The formation of self-assembled monolayer with trialkoxysilane on the surface of silica causes a drastic increase in the concentration of organosilane molecules on the material surface in comparison to their concentration in solution and therefore leads to formation of an area with densely packed terminal groups in the silane. Reaction of terminal substituents (–NCO) with riboflavin leads to a new material, which can be characterized as a molecular receptor reactive towards metal and organic cations. The riboflavin on the surface, conjugated with –NCO groups, shows different spectral properties than both riboflavin and its complexes with metal and organic cations in a solution.

The high concentration of the receptor on the surface and neighboring groups on a monolayer not occupied by riboflavin determine a drastic change in the fluorescence spectra in comparison with those of the solutions. Changes in fluorescence can be used for the analytical determination of selected cations.

4. Conclusions

SBA-15 mesoporous silica has been successfully modified with riboflavin. Although only 5% of isocyanate surface groups were covered with riboflavin it was enough to analyze the fluorescence properties of systems obtained. Attempts to increase the coverage percentage have failed because of riboflavin thermal instability. Absorption and fluorescence emission spectra revealed insignificant changes in the spectra of the solutions, except for silver, mercury(II), chromium(III), aluminum and benzocaine cations, for which both fluorescence maximum values and wavelengths shifts were observed. In contrast to riboflavin solutions, the riboflavin-functionalized silica showed significant changes in fluorescence emission spectra for all of the cations used. No consistent pattern of these changes was noticed.

Acknowledgements

The authors would like to thank Prof. Bohdan Skalski and Dr Tomasz Pędziński for providing access to a FluoTime 300 spectrofluorometer.

Appendix A. Supplementary material

Supplementary data associated with this article can be found in the online version at http://dx.doi.org/10.1016/j.jpcs.2015.04.007.

References

[1] A.C. Moffat, M.D. Osselton, B. Widdop, Clarke's Analysis of Drugs and Poisons, 4th ed., Pharmaceutical Press, London, Chicago, 2011.
[2] R.R. Eitenmiller, W.O. Landen Jr, L. Ye, Vitamin Analysis for the Health and Food Sciences, 2nd ed., CRC Press, London, New York, 2007.
[3] P.B. Ottaway, The Technology of Vitamins in Food, Chapman and Hall, London, 1993.
[4] G.F.M. Ball, Vitamins in Food: Analysis, Bioavailability and Stability, CRC Press, London New York, 2006.
[5] I.F. Baarda, D.E. Metzler, Biochim. Biophys. Acta 50 (1961) 463–471.
[6] J.T. Spence, E.R. Peterson, J. Inorg. Nucl. Chem. 24 (1962) 601–608.
[7] J. Masłowska, M. Malicka, J. Therm. Anal. 32 (1987) 1659–1665.
[8] H. Irving, R.J.P. Williams, J. Chem. Soc. (1953) 3192–3210, Resumed.
[9] A.W. Varnes, R.B. Dodson, E.L. Wehry, J. Am. Chem. Soc. 94 (1972) 946–950.
[10] D. Zhao, J. Feng, Q. Huo, N. Melosh, G.H. Fredrickson, B.F. Chmelka, G.D. Stucky, Science 279 (1998) 548–552.
[11] M. Kruk, M. Jaroniec, C.H. Ko, R. Ryoo, Chem. Mater. 12 (2000) 1961–1968.
[12] R. Sanz, G. Calleja, A. Arencibia, E.S. Sanz-Perez, Microporous Mesoporous Mater. 158 (2012) 309–317.
[13] M. Moritz, M. Łaniecki, Appl. Surf. Sci. 258 (2012) 7523–7529.
[14] D. Zuo, J. Lane, D. Culy, M. Schultz, A. Pullar, M. Waxman, Appl. Catal. B: Environ. 129 (2013) 342–350.
[15] J. Pang, L. Zhao, L. Zhang, Z. Li, Y. Luan, J. Colloid Interface Sci. 395 (2013) 31–39.
[16] W. Guo, R. Chen, M. Meng, X. Meng, Z. Hu, Z. Song, Colloids Surf. A: Physicochem. Eng. Asp. 436 (2013) 693–703.
[17] B. Motos-Pérez, J. Roeser, A. Thomas, P. Hesemann, Appl. Organomet. Chem. 27 (2013) 290–299.
[18] L. Medda, M.F. Casula, M. Monduzzi, A. Salis, Langmuir 30 (2014) 12996–13004.
[19] V. Vo, H.-J. Kim, H.-Y. Kim, Y. Kim, S.J. Kim, Bull. Korean Chem. Soc. 34 (2013) 3570–3576.
[20] M.M. Wan, W.J. Qian, W.G. Lin, Y. Zhou, J.H. Zhu, J. Mater. Chem. B 1 (2013) 3897–3905.
[21] A. Narani, R.K. Marella, P. Ramudu, K.S. Rama Rao, D.R. Burri, RSC Adv. 4 (2014) 3774–3781.
[22] J. Mondal, P. Borah, A. Modak, Y. Zhao, A. Bhaumik, Org. Process Res. Dev. 18 (2013) 257–265.
[23] A. Lazar, W.R. Thiel, A.P. Singh, RSC Adv. 4 (2014) 14063–14073.
[24] J. Masłowska, M. Malicka, J. Therm. Anal. 34 (1988) 3–9.
[25] M. Weiner, J. Org. Chem. 25 (1960) 2245–2246.

PLOS | ONE

RESEARCH ARTICLE

Immobilization of Zidovudine Derivatives on the SBA-15 Mesoporous Silica and Evaluation of Their Cytotoxic Activity

Dawid Lewandowski[1]*, Marta Lewandowska[1☯], Piotr Ruszkowski[2☯], Anita Pińska[2☯], Grzegorz Schroeder[1☯]

1 Faculty of Chemistry, Adam Mickiewicz University, Poznan, Poland, **2** Faculty of Pharmacy, Poznan University of Medical Sciences, Poznan, Poland

☯ These authors contributed equally to this work.
* dawid_le@amu.edu.pl

OPEN ACCESS

Citation: Lewandowski D, Lewandowska M, Ruszkowski P, Pińska A, Schroeder G (2015) Immobilization of Zidovudine Derivatives on the SBA-15 Mesoporous Silica and Evaluation of Their Cytotoxic Activity. PLoS ONE 10(5): e0126251. doi:10.1371/journal.pone.0126251

Academic Editor: Heidar-Ali Tajmir-Riahi, University of Quebect at Trois-Rivieres, CANADA

Received: February 12, 2015

Accepted: March 31, 2015

Published: May 5, 2015

Data Availability Statement: All relevant data are within the paper and its Supporting Information files.

Funding: Funding for this work came from the institution Narodowe Centrum Nauki (PL), www.ncn.gov.pl/, grant number: 2011/03/B/ST5/01573. The funding was received by author GS. The funders had no role in study design, data collection and analysis, decision to publish, or preparation of the manuscript.

Competing Interests: The authors have declared that no competing interests exist.

Abstract

Novel zidovudine derivatives, able to be covalently conjugated to silica surface, have been obtained and grafted to SBA-15 mesoporous silica. Cytotoxic activity of the hybrid organic-inorganic (zidovudine derivatives-silica) systems against HeLa and KB cell lines has been analyzed. Addition of folic acid had a positive influence on the cytotoxicity. Up to 69% of HeLa and 65% of KB tumor cells growth inhibition has been achieved at low silica concentration used (10 μg/mL).

Introduction

Mesoporous silicas discovered by Mobil researchers in the early 1990s gave rise to a family of materials that have found numerous applications. From among many morphologically different silicas, the two MCM-41 and SBA-15, have been the most often used. Both represent hexagonal order of mesopores but differ in pore diameters, which for MCM-41 is in the range of 2.0–6.5 nm [1] and for SBA-15–4.0–30.0 nm [2, 3]. MCM-41 is usually used as a carrier for smaller molecules that are packed inside its pores [4, 5], whilst SBA-15 is more suitable for larger ones like proteins [3, 6]. Both can undergo useful surface functionalization, wherein for the SBA-15 a wider variety of molecules is applicable.

Application of mesoporous silicas in the preparation of controlled drug release systems is well known, especially for transportation of anticancer and anti-inflammatory drugs. However, a vast majority of these systems rely on the adsorption properties of anticancer drugs and gate-like structures located on the pore entrances [7] or on surface modifications [8]. Only in very few systems a covalent conjugation of the drug to the silica surface takes place [9].

Physically adsorbed anticancer drugs need to be transported, using mesoporous silica carriers, to the vicinity of target tumor cells and protected from premature release by different stimuli-sensitive moieties. Covalently bound drugs require endocytosis of silica particles by the tumor cells, which already has been reported [10]. The addition of covalently conjugated folic acid enhances particles uptake [10, 11].

Nucleoside analogues, especially 2',3'-dideoxynucleosides, have found broad application as antiviral [12] and anticancer therapeutics [13–16], designed to mimic natural nucleosides. One of these molecules, which play an important role in anticancer therapeutics is 3'-azido-3'-deoxythymidine (AZT, zidovudine).

AZT has been developed as an antitumor drug, but later it was found to reveal antiretroviral activity and proved to be a proper drug for the treatment of acquired immunodeficiency syndrome (AIDS) [12]. There are also examples of application of AZT as an anticancer agent in therapy of colon cancer, especially in combination with cisplatin, methotrexate and 5-fluorouracil [17, 18].

The mechanism of antiviral or anticancer action of AZT involves its intracellular conversion to its active, 5'-triphosphate form, which is controlled by the cellular enzymes called kinases. The compound 5'-triphosphate is a competitive inhibitor of enzymes involved in the replication process (HIV reverse transcriptase or DNA polymerase) and after incorporation to DNA strand it becomes a chain terminator of the nascent DNA strand due to the lack of 3'-hydroxyl group [19, 20].

In 2001, Sharpless and his co-workers described the concept and criteria for the so-called 'click' reactions: versatility, high yield, modularity, readily available starting materials as well as simple reaction conditions. In 2002, Meldal and Sharpless [21, 22] independently, established that the Huisgen 1,3-dipolar cycloaddition reaction between organic azides and terminal alkynes can be efficiently catalyzed by copper(I) ions and can take place at room temperature. As a result, the 1,4-regioisomers of 1,2,3-triazole are formed. 'Click' chemistry has been recognized as a valuable synthetic tool in the field of nucleosides and nucleotides since azido and alkyne derivatives are readily accessible [23]. 1,4-Disubstituted 1,2,3-triazole ring is a stable element of the conjugate structure and it is considered as a mimic of *Z*-amide bond. Moreover, it can serve as an additional pharmacophore [24].

To the best of our knowledge, there is no report on zidovudine (AZT) having been successfully grafted onto the silica surface. The aim of this study was to covalently conjugate zidovudine to SBA-15 mesoporous silica surface and analyze the cytotoxic activity of hybrid organic-inorganic systems obtained. All intended aims had been successfully achieved.

Materials and Methods

Materials

All reagents and solvents used in the study were purchased from Sigma-Aldrich and used without further purification. SBA-15 mesoporous silica (8–11 nm pore diameter, 600 $m^{2*}g^{-1}$ surface area and 1–2 μm particle size) was purchased from ACS Material.

Synthesis of zidovudine derivatives

One molar equivalent of (3-isocyanatopropyl)triethoxysilane in THF was placed in an ice bath and an appropriate amount of propargyl compound (1.1 eq. for propargylamine and 5.0 eq. for propargyl alcohol) in the presence of small amounts of triethylamine (0.6 eq. for propargylamine and 0.25 eq. for propargyl alcohol, respectively) was added through a dropping funnel and the mixtures were stirred for 3 h. The amount of propargyl alcohol was much higher due to its weaker nucleophilic properties. While using lower propargyl alcohol:isocyanate ratios, the products of side reactions were detected, especially those of isocyanate self—addition reaction. The next step was to reflux the mixtures for 3 h, allow them to cool to the room temperature and stir overnight. Solvents were evaporated and residues were purified using column chromatography (ethyl acetate:*n*-hexane 3:1) resulting in colorless, viscous liquid and pale yellow solid for 'oxy'-AZT and 'aza'-AZT intermediates, respectively (Fig 1). TLC detection was

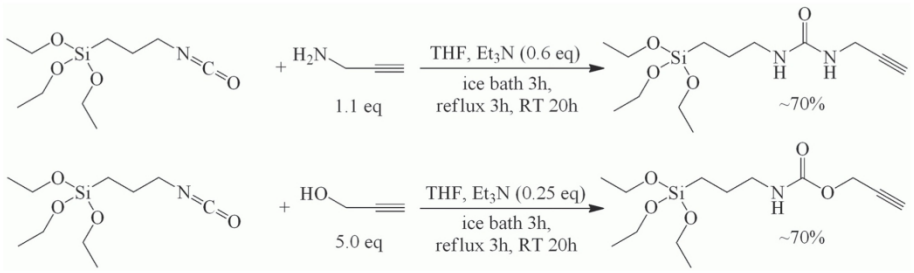

Fig 1. The reaction of synthesis of 'aza' and 'oxy' intermediates products.

doi:10.1371/journal.pone.0126251.g001

performed using ethyl acetate:*n*-hexane 1:2 as a mobile phase. In both cases the yield was about 70% and the compounds were characterized by electrospray mass spectrometry (Micromass ZQ spectrometer, Waters), melting point measurement (Mel-Temp 1002D), infrared spectroscopy (FT-IR Bruker IFS 66v/S) and ^{1}H and ^{13}C NMR spectroscopy (VARIAN Mercury 300).

In the second step, both intermediates were conjugated with AZT by the1,3-dipolar Huisgen cycloaddition in anhydrous conditions using copper(I) acetate as a catalyst and acetonitrile as a solvent. Exact conditions in both cases were adjusted to achieve the best purity and yield. After the synthesis, both products were purified using column chromatography (methanol:chloroform gradient), which gave pale green (Cu^{+} remnants) and pale orange solids for 'oxy'-AZT and 'aza'-AZT (Fig 2). TLC detection was performed using methanol:chloroform 1:10 as a mobile phase. The compounds were characterized by electrospray mass spectrometry (Micromass ZQ spectrometer, Waters), melting point measurement (Mel-Temp 1002D), infrared spectroscopy (FT-IR Bruker IFS 66v/S) and ^{1}H and ^{13}C NMR spectroscopy (VARIAN Mercury 300).

Immobilization of zidovudine derivatives on SBA-15 mesoporous silica surface

Both derivatives were immobilized on the surface by themselves or together with folic acid. To anchor 'aza'-AZT and 'oxy'-AZT on the surface, 70 mg of each of the compounds were

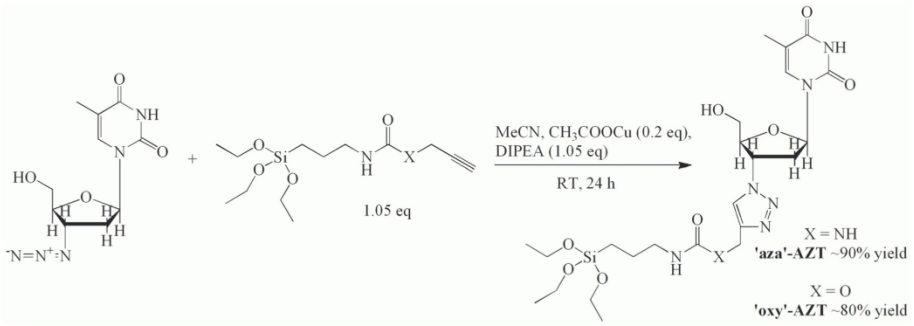

Fig 2. Synthesis reaction of the 'aza'- and 'oxy'-AZT derivatives.

doi:10.1371/journal.pone.0126251.g002

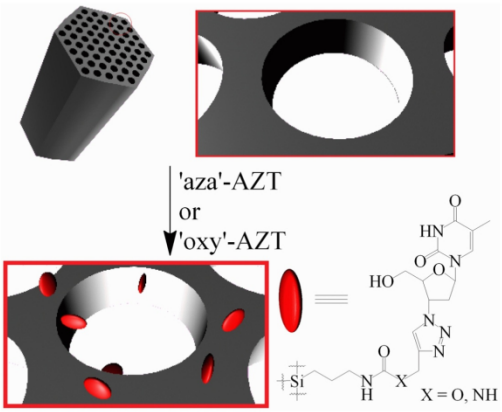

Fig 3. The immobilization of zidovudine derivatives on SBA-15 mesoporous silica surface.

doi:10.1371/journal.pone.0126251.g003

dissolved in 10 ml of DMF in separate flasks and 100 mg of SBA-15 silica was added to each flask. Suspensions were stirred at 80°C for 1 h and then allowed to cool to the room temperature and stirred overnight. Modified silica was filtered off, washed thoroughly with DMF and dried. SBA-15+'aza'-AZT and SBA-15+'oxy'-AZT were obtained as white solids (Fig 3). The accurate amounts of both derivatives anchored to the surface were calculated using elemental analysis (elemental analyzer EL III, Vario). The presence of AZT derivatives on the silica surface was additionally confirmed by the IR spectroscopy for 1.0 mg of the silica mixed with 200 mg of KBr and formed into a pellet.

In the second approach 300 mg of SBA-15 silica was suspended in 10 ml of toluene and 30 mg of (3-aminopropyl)trimethoxysilane (APTMS) was added. The mixture was refluxed for 3 h and then allowed to cool to the room temperature and stirred overnight. After that the silica was filtered off, washed with toluene and dried. SBA-15+APTMS as a white solid was obtained. In the next step 50 mg of folic acid (FA) was dissolved in 30 ml of DMF at slightly elevated temperature (40–45°C), an excess of diisopropylcarbodiimide (DIC) (30 mg) was added and, after 15 min, SBA-15+APTMS was suspended. The mixture was stirred for 24 h and then filtered off, washed thoroughly with DMF and dried. SBA-15+APTMS+FA as a pale yellow solid was obtained. In the final step 70 mg of both derivatives, 'aza'-AZT and 'oxy'-AZT, were dissolved in 10 ml of chloroform in separate flasks and 150 mg of SBA-15+APTMS+FA was added to each of them. Mixtures were refluxed for 20 min and then allowed to cool and stirred overnight. Both solids were filtered off, washed with chloroform and dried, yielding SBA-15 +APTMS+FA+'aza'-AZT and SBA-15+APTMS+FA+'oxy'-AZT (Fig 4). Both products were analyzed using elemental analysis and IR spectroscopy.

The cytotoxic activity of hybrid materials

Human cancer cells HeLa (cervical cancer cell line) and KB (*carcinoma nasopharynx*) were cultured in RPMI 1640 medium. Each medium was supplemented with 10% fetal bovine serum, 1% L-glutamine and 1% penicillin/streptomycin solution. The cell lines were kept in the incubator at 37°C. The optimal plating density of cell lines was determined to be 5×10^4. All the cell

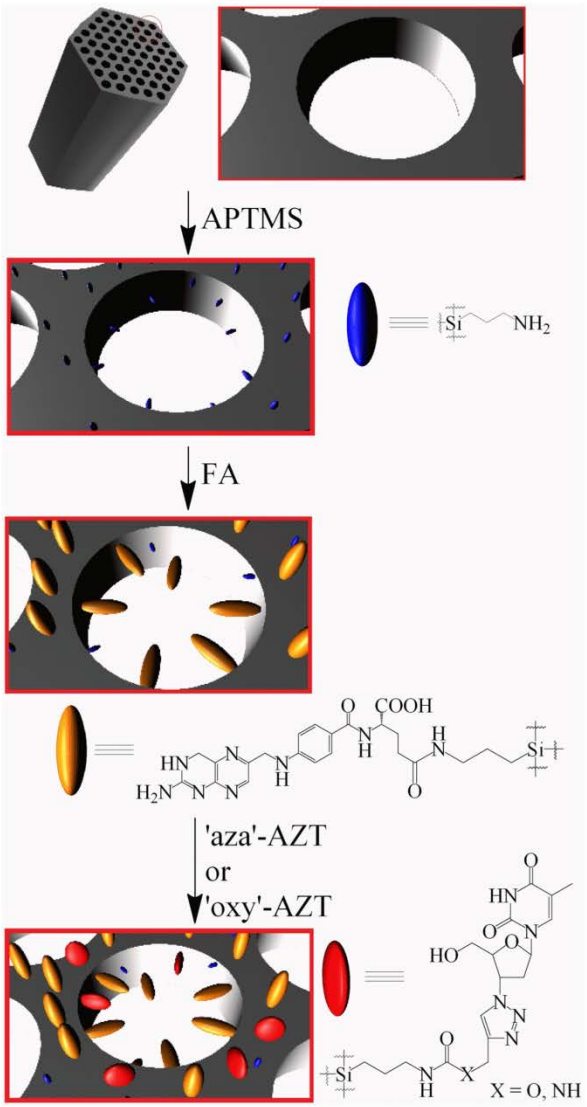

Fig 4. Immobilization of folic acid and both zidovudine derivatives on SBA-15 mesoporous silica surface.

doi:10.1371/journal.pone.0126251.g004

lines were obtained from The European Collection of Cell Cultures (ECACC) supplied by Sigma-Aldrich (catalogue numbers: HeLa cell line-93021013, KB cell line-94050408).

The protein-staining sulforhodamine B (SRB, Sigma-Aldrich) microculture colorimetric assay, developed by the National Cancer Institute (USA) for in vitro antitumor screening was used in this study, to estimate the cell number by providing a sensitive index of total cellular protein content, which is in a linear relationship to the cell density [25]. The monolayer cell culture was trypsinized and the cell count was adjusted to 5 x 10^4 cells. In each well of the 96 well microtiter plate, 0.1mL of the diluted cell suspension (approximately 10,000 cells) was placed. After 24 hours, when a partial monolayer was formed, the supernatant was washed out and 100 μL of six different silica suspension concentrations were added to the cells in microtiter plates. The tested silicas were suspended in DMSO (20 μM) and the content of DMSO did not exceed 0.1% as this concentration was found to be nontoxic to the cell lines. The cells were exposed to silicas for 72 hours. After that, 25 μL of 50% trichloroacetic acid were added to the wells and the plates were incubated for 1 hour at 4°C. The plates were then washed out with distilled water to remove traces of medium and next dried by air. The air-dried plates were stained with 100 μL SRB and kept for 30 minutes at room temperature. The unbound dye was removed by rapidly washing with 1% acetic acid and then air dried overnight. The optical density was read at 490 nm. All cytotoxicity experiments were performed three times. Cell survival was measured as the percentage absorbance compared to the control (non-treated cells). Zidovudine (Sigma-Aldrich) was used as the internal standard.

Results and Discussion

Characterization of synthesized compounds

Both propargyl-containing intermediates were obtained in high purity (full spectra available in the supplementary material):

'aza'-AZT intermediate—melting point: 35–38°C, ^{1}H NMR (300 MHz, CD_3CN) δ: 0.62–0.67 (2H, m), 1.21–1.25 (9H, t, J = 7.0 Hz), 1.58–1.66 (2H, m), 2.22 (1H, t, J = 2.5 Hz), 3.15–3.21 (2H, dt, J = 6.9 Hz, J = 5.9 Hz), 3.80–3.85 (6H, q, J = 7.0 Hz), 3.97–4.00 (2H, dd, J = 2.5 Hz, J = 5.5 Hz), 5.08–5.15 (2H, m), ^{13}C NMR (75 MHz, $CDCl_3$) δ: 7.5, 18.2, 23.5, 30.0, 42.8, 58.4, 70.9, 80.8, 157.9, FT-IR: 3330 cm^{-1} (N-H ν_{st}), 3250 cm^{-1} (≡C-H ν_{st}), 2975, 2925 and 2885 cm^{-1} (aliphatic C-H ν_{st}), 2115 cm^{-1} (C≡C ν_w), 1625 cm^{-1} (urea C = O ν_{st}), 1570 cm^{-1} (N-H δ_{st}), 1080 cm^{-1} (Si-O ν_{vs}), ESI MS *m/z* $[M\text{-}C_2H_5O]^+$ 257.3, $[M+Na]^+$ 325.3, $[M+K]^+$ 341.3.

'oxy'-AZT intermediate—melting point: below -25°C, ^{1}H NMR and ^{13}C NMR data can be found in literature [26], FT-IR: 3340 cm^{-1} (N-H ν_{st}), 3315 cm^{-1} (≡C-H ν_{st}), 2975, 2930 and 2890 cm^{-1} (aliphatic C-H ν_{st}), 2130 cm^{-1} (C≡C ν_w), 1715 cm^{-1} (carbamate C = O ν_{st}), 1535 cm^{-1} (N-H δ_{st}), 1235 cm^{-1} (C-O ν_{st}), 1080 cm^{-1} (Si-O ν_{vs}), ESI MS *m/z* $[M\text{-}C_2H_5O]^+$258.2, $[M+Na]^+$ 326.3, $[M+K]^+$ 342.3.

'aza'-AZT final product—melting point: 85–88°C, ^{1}H NMR (300 MHz, CD_3CN) δ: 0.53–0.58 (2H, m), 1.14–1.19 (9H, t, J = 7.0 Hz), 1.44–1.53 (2H, m), 1.85–1.86 (3H, d, J = 1.2 Hz), 2.60–2.68 (1H, m), 2.76–2,83 (1H, m), 3.02–3.08 (2H, dt, J = 6.9 Hz, J = 6.0 Hz), 3.47–3.51 (1H, t), 3.66–3.72 (1H, m), 3.74–3.84 (7H, m), 4.27–4.31 (1H, dt, J = 3.1 Hz, J = 5.4 Hz), 4.31–4.33 (2H, d, J = 5.8 Hz), 5.11–5.15 (1H, t, J = 5.7 Hz), 5.26–5.31 (1H, dt, J = 5.4 Hz, J = 8.5 Hz), 5.36–5.41 (1H, t, J = 5.7 Hz), 6.38–6.42 (1H, t, J = 6.6 Hz), 7.65–7.66 (1H, q, J = 1.2 Hz), 7.75 (1H, s), 9.10 (1H, s), ^{13}C NMR (75 MHz, $CDCl_3$) δ: 7.6, 12.4, 18.2, 23.6, 35.5, 37.9, 43.0, 58.4, 59.4, 61.3, 85.2, 86.4, 110.9, 122.7, 137.1, 146.5, 150.8, 158.9, 164.6, FT-IR: 3320 cm^{-1} (N-H ν_m), 3065 cm^{-1} (= C-H ν_m), 2975, 2925 and 2890 cm^{-1} (aliphatic C-H ν_{st}), 1700 cm^{-1} (pyrimidine C = O ν_{st} and urea C = O ν_{st} as a distortion of this signal), 1560 cm^{-1} (N-H δ_{st}), 1275 cm^{-1} (sugar C-O ν_m), 1080 cm^{-1} (Si-O ν_{vs}), ESI MS *m/z* $[M+Na]^+$ 592.4, $[2M+Na]^+$1161.7.

'oxy'-AZT final product—melting point: 56–59°C, ^{1}H NMR (300 MHz, CD_3CN) δ: 0.53–0.59 (2H, m), 1.14–1.19 (9H, t, J = 7.0 Hz), 1.47–1.56 (2H, m), 1.85–1.86 (3H, d, J = 1.2 Hz), 2.61–2.69 (1H, m), 2.77–2.84 (1H, m), 3.03–3.09 (2H, q, J = 6.8 Hz), 3.31 (1H, s), 3.68–3.73 (1H, dd, J = 3.1 Hz, J = 12.3 Hz), 3.74–3.84 (7H, m), 4.29–4.33 (1H, dt, J = 3.1 Hz, J = 5.4 Hz), 5.10 (2H, s), 5.29–5.34 (1H, dt, J = 5.3, J = 8.5 Hz), 5.61–5.67 (1H, t, broad signal), 6.38–6.43 (1H, t, J = 6.6 Hz), 7.64–7.65 (1H, q, J = 1.2 Hz), 7.88 (1H, s), 9.01 (1H, s), ^{13}C NMR (75 MHz, $CDCl_3$) δ: 7.5, 12.4, 18.2, 23.1, 37.6, 43.4, 57.6, 58.4, 59.1, 61.2, 85.2, 87.6, 111.0, 124.2, 137.5, 143.8, 150.5, 156.2, 164.2, FT-IR: 3330 cm^{-1} (N-H ν_m), 3065 cm^{-1} (= C-H ν_m), 2975, 2930 and 2890 cm^{-1} (aliphatic C-H ν_{st}), 2105 cm^{-1} (very weak—probably unreacted AZT), 1700 cm^{-1} (pyrimidine C = O ν_{st} and carbamate C = O ν_{st}), 1535 cm^{-1} (N-H δ_{st}), 1275 cm^{-1} (sugar C-O ν_m), 1080 cm^{-1} (Si-O ν_{vs}), ESI MS *m/z* $[M+Na]^+$ 593.3, $[2M+Na]^+$ 1163.5.

Characterization of modified silica obtained

Mean amounts of nitrogen and carbon in SBA-15+'aza'-AZT equal to, respectively, 0.471% and 1.379% permitted calculation of the total amount of 'aza'-AZT on the silica surface. As the content of carbon is slightly dependent on the number of Si-O-Si links between 'aza'-AZT and silica surface, the nitrogen percentage is more reliable and gives 2.735±0.185% mass percentage of 'aza'-AZT, that is 48.1±3.3 μmol of 'aza'-AZT per 1g of modified silica. Similar calculations for SBA-15+'oxy'-AZT, with 0.374% of nitrogen and 1.247% of carbon content, lead to 2.538 ±0.058% mass percentage or 44.5±1.0 μmol of 'oxy'-AZT per 1 g of modified silica. The IR

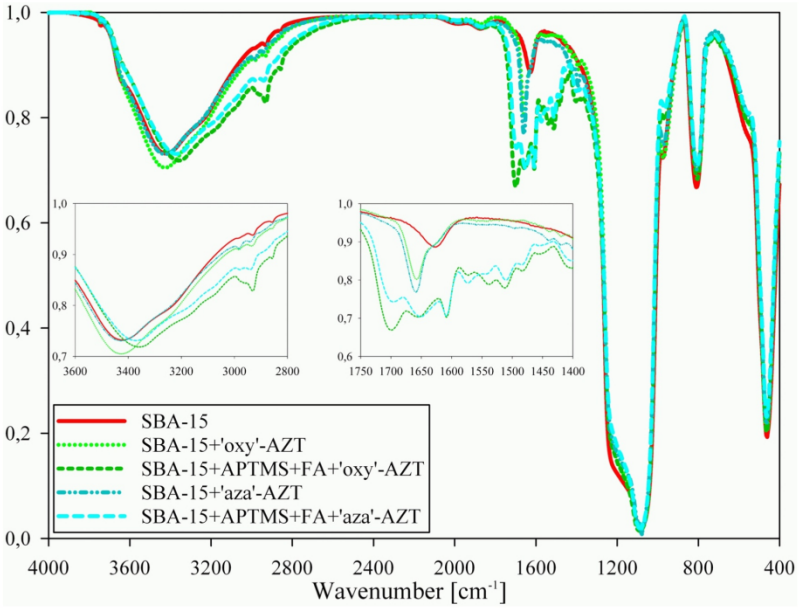

Fig 5. IR spectra of all hybrid systems obtained and pure SBA-15 mesoporous silica for comparison.

doi:10.1371/journal.pone.0126251.g005

spectra (Fig 5) indicate the presence of both zidovudine derivatives, which can be proved by the presence of C = O amide stretching signal at 1659 cm^{-1}, other signals are invisible, because of the low derivative content. The shift of the signal assigned to the C = O bond can be connected with the immobilisation process. Moreover, this signal in the spectra of zidovudine, according to the literature [27–31], can be found between 1700 and 1650 cm^{-1}.

IR spectra of the systems containing folic acid are more complicated. However, the main signals can still be assigned, the signal at1654 cm^{-1} is assigned to the stretching of C = O amide from zidovudine, the signals at 1698 and 1609 cm^{-1} come from C = O carboxyl and C = O amide groups of folic acid respectively. The shift of the peak assigned to the stretching of O-H from 3425–3420 cm^{-1} for the silicas without folic acid to 3370–3360 cm^{-1} for both systems with folic acid is thus also related to the presence of folic acid. Elemental analysis results for both modified silicas are 3.428% of nitrogen and 9.019% of carbon for SBA-15+APTMS+FA+'oxy'-AZT and 3.703% of nitrogen and 9.237% of carbon for SBA-15+APTMS+FA+'aza'-AZT. They are difficult to interpret because of the number of steps in the synthesis. Nevertheless, the mass increase correlates well with the elemental analysis results for simple SBA-15+'aza'-AZT and SBA-15+'oxy'-AZT systems and following this line of reasoning it can be calculated that in SBA-15+APTMS+FA+'aza'-AZT and SBA-15+APTMS+FA+'oxy'-AZT systems the amounts of zidovudine derivatives are slightly above 100 μmol per 1 g of modified silica, which is about twice as much as for simple SBA-15+'aza'-AZT and SBA-15+'oxy'-AZT systems. Small amounts of APTMS used in the first step of the synthesis left enough free space on the surface

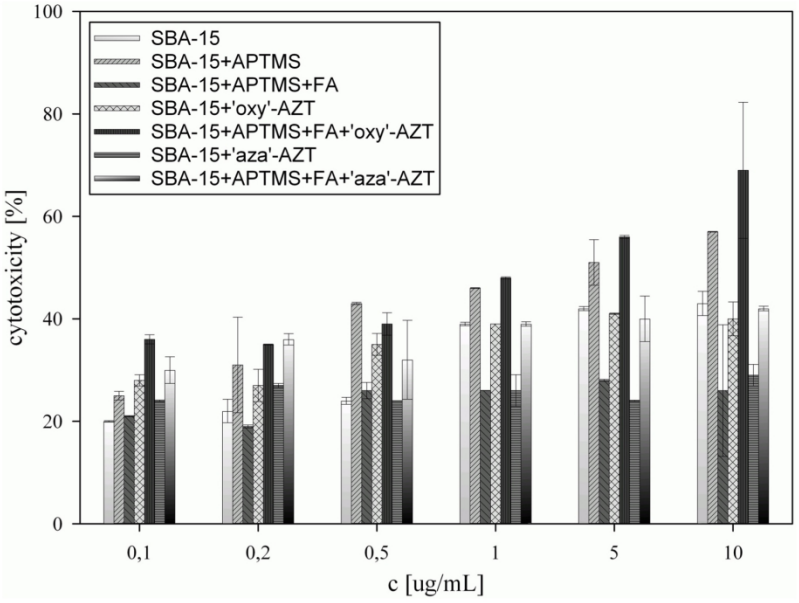

Fig 6. Cytotoxic activity against HeLa cell line, calculated for all samples tested.

doi:10.1371/journal.pone.0126251.g006

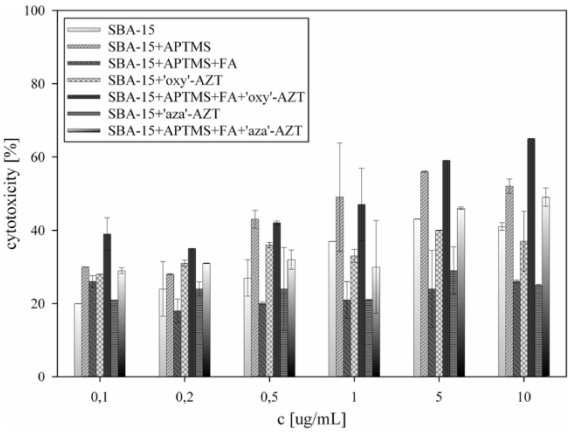

Fig 7. Cytotoxic activity against KB cell line, calculated for all samples tested.

doi:10.1371/journal.pone.0126251.g007

to anchor both derivatives, moreover the use of another solvent (of a lower dielectric constant to facilitate its penetration into the silica [32]) brought a positive effect on their total amounts.

The cytotoxic activity

All analyzed solids showed concentration-dependent cytotoxic activity against HeLa and KB cell lines (Fig 6 and Fig 7). Introduction of amino groups on the silica surface greatly increased its activity, which is in agreement with the results observed for pure, organic compounds [33–35].

Covering the surface with folic acid had ambivalent influence. On the one hand, modification of the amino groups with folic acid causes a decrease in the activity of SBA-15+APTMS +FA, because the access to primary amino groups is blocked with folic acid molecules. On the other hand, the addition of folic acid molecules to both systems containing zidovudine derivatives, significantly increases their activity, promoting the interactions between silica particles and cell membrane, as KB and HeLa cell lines are known to be FR-positive [36]. Higher cell growth inhibition observed for SBA-15+APTMS+FA+'oxy'-AZT in comparison with the result for SBA-15+APTMS+FA+'aza'-AZT may be due to the fact that carbamate group in the 'oxy' derivative is more susceptible to hydrolysis than the urea-like one in the 'aza' derivative, that means it can release more zidovudine molecules from the surface. Cytotoxic activities obtained, especially that of SBA-15+APTMS+FA+'oxy'-AZT, are comparable to those of pure zidovudine(IC_{50} = 3.12 μg/mL for KB and 2.28 μg/mL for HeLa cell line), but at much lower zidovudine concentration. High deviations of the results obtained for some of the samples are a result of sedimentation in silica suspensions.

Conclusions

Two novel zidovudine derivatives have been obtained and characterized. Both of them have been easily introduced onto the SBA-15 mesoporous silica surface using the grafting technique. Cytotoxic activity against HeLa and KB cell lines of all solids obtained has been evaluated. The

addition of folic acid on the silica surface enhances the activity of the derivatives studied due to the interaction with folate receptors. The values of cell growth inhibition obtained for SBA-15 +APTMS+FA+'oxy'-AZT are relatively high and equal to 69% and 65% for HeLa and KB tumor cells. The results of this study can be a basis for further attempts at covalent conjugation of cytotoxic compounds to the silica surface.

Supporting Information

S1 Spectrum. Full ESI MS spectra of 'aza'- and 'oxy'-AZT intermediates.
(TIF)

S2 Spectrum. Full FT-IR spectra of 'aza'- and 'oxy'-AZT intermediates.
(TIF)

S3 Spectrum. ^{1}H NMR spectrum of 'aza'-AZT intermediate.
(TIF)

S4 Spectrum. ^{13}C NMR spectrum of 'aza'-AZT intermediate.
(TIF)

S5 Spectrum. Full ESI MS spectra of 'aza'- and 'oxy'-AZT final products.
(TIF)

S6 Spectrum. Full FT-IR spectra of 'aza'- and 'oxy'-AZT final products.
(TIF)

S7 Spectrum. ^{1}H NMR spectrum of 'aza'-AZT final product.
(TIF)

S8 Spectrum. ^{13}C NMR spectrum of 'aza'-AZT final product.
(TIF)

S9 Spectrum. ^{1}H NMR spectrum of 'oxy'-AZT final product.
(TIF)

S10 Spectrum. ^{13}C NMR spectrum of 'oxy'-AZT final product.
(TIF)

Author Contributions

Conceived and designed the experiments: DL GS. Performed the experiments: DL ML PR AP. Analyzed the data: DL GS. Contributed reagents/materials/analysis tools: PR GS. Wrote the paper: DL.

References

1. Silaghi M-C, Chizallet C, Raybaud P (2014) Challenges on molecular aspects of dealumination and desilication of zeolites. Micropor Mater 191: 82–96. doi: 10.1016/j.ijfoodmicro.2014.09.007 PMID: 25255308
2. Vinu A, Murugesan V, Tangermann O, Hartmann M (2004) Adsorption of Cytochrome c on Mesoporous Molecular Sieves: Influence of pH, Pore Diameter, and Aluminum Incorporation. Chem Mater 16: 3056–3065.
3. Katiyar A, Ji L, Smirniotis P, Pinto NG (2005) Protein adsorption on the mesoporous molecular sieve silicate SBA-15: Effects of pH and pore size. J Chromatogr A 1069: 119–126. PMID: 15844490
4. Bernardos A, Aznar E, Coll C, Martinez-Manez R, Barat JM, Marcos MD, et al. (2008) Controlled release of vitamin B_2 using mesoporous materials functionalized with amine-bearing gate-like scaffoldings. J Control Release 131: 181–189. doi: 10.1016/j.jconrel.2008.07.037 PMID: 18727946

5. Halamova D, Zelenak V (2012) NSAID naproxen in mesoporous matrix MCM-41: drug uptake and release properties. J Incl Phenom Macrocycl Chem 72: 15–23.
6. Miyahira M, Vinu A, Hossain KZ, Nakanishi T, Ariga K (2006) Adsorption study of heme proteins on SBA-15 mesoporous silica with pore-filling models. Thin Solid Films 1–2: 13–18.
7. Meng H, Xue M, Xia T, Zhao Y- L, Tamanoi F, Stoddart JF, et al. (2010) Autonomous in Vitro Anticancer Drug Release from Mesoporous Silica Nanoparticles by pH-Sensitive Nanovalves. J Am Chem Soc 132: 12690–12697. doi: 10.1021/ja104501a PMID: 20718462
8. Bahrami Z, Badiel A, Atyabi F (2014) Surface functionalization of SBA-15 nanorods for anticancer drug delivery. Chem Eng Res Des 92: 1296–1303.
9. Wani A, Muthsuwamy B, Savithra GHL, Mao G, Brock S, Oupicky D (2012) Surface Functionalization of Mesoporous Silica Nanoparticles Controls Loading and Release Behavior of Mitoxantrone. Pharm Res 29: 2407–2418. doi: 10.1007/s11095-012-0766-9 PMID: 22555380
10. Slowing I, Trewyn BG, Lin VS-Y (2006) Effect of surface functionalization of MCM-41-type mesoporous silica nanoparticles on the endocytosis by human cancer cells. J Am Chem Soc 128: 14792–14793. PMID: 17105274
11. Fan J, Fang G, Wang X, Zeng F, Xiang Y, Wu S (2011) Targeted anticancer prodrug with mesoporous silica nanoparticles as vehicles. Nanotechnology 22: 1–11.
12. De Clercq E (2004) Antiviral drugs in current clinical use. J Clin Virol 30: 115–133. PMID: 15125867
13. Brunton LL, Lazo JS, Parker KL (2006) Goodman and Gilman's the pharmacological basis of therapeutics. New York: McGraw-Hill.
14. Galmarini CM, Popowycz F, Joseph B (2008) Cytotoxic Nucleoside Analogies: Different Strategies to Improve their Clinical Efficacy. Curr Med Chem 15: 1072–1082. PMID: 18473803
15. Longley DB, Harkin DP, Johnston PG (2003) 5-Fluorouracil: mechanisms of action and clinical strategies. Nat Rev Cancer 3: 330–338. PMID: 12724731
16. Périgaud C, Gosselin G, Imbach JL (1992) Nucleoside Analogues as Chemotherapeutic Agents: A Review. Nucleosides Nucleotides 11: 903–945. PMID: 1494543
17. Brunetti I, Falcone A, Calabresi P, Goulette FA, Darnowski JW (1990) 5-Fluorouracil enhances azidothymidine cytotoxicity: In vitro, in vito, and biochemical studies. Cancer Res 50: 4026–4031. PMID: 2354452
18. Darnowski JW, Goulette FA (1994) 3′-azido-3′-deoxythymidine cytotoxicity and metabolism in the human colon tumor cell line HCT-8. Biochem Pharmacol 48: 1797–1805. PMID: 7980649
19. Iyer VV, Griesgraber GW, Radmer MR, McIntee EJ, Wagner CR (2000) Synthesis, in Vitro Anti-Breast Cancer Activity, and Intracellular Decomposition of Amino Acid Methyl Ester and Alkyl Amide Phosphoramidate Monoesters of 3'-Azido-3'-deoxythymidine (AZT). J Med Chem 43: 2266–2274. PMID: 10841805
20. Wagner CR, Iyer VV, McIntee EJ (2000) Pronucleotides: Toward the in vivo delivery of antiviral and anticancer nucleotides. Med Res Rev 20: 417–451. PMID: 11058891
21. Tornøe CW, Christensen C, Meldal M (2002) Peptidotriazoles on Solid Phase: [1,2,3]-Triazoles by Regiospecific Copper(I)-Catalyzed 1,3-Dipolar Cycloadditions of Terminal Alkynes to Azides. J Org Chem 67: 3057–3064. PMID: 11975567
22. Rostovtsev VV, Green LG, Fokin VV, Sharpless KB (2002) A Stepwise Huisgen Cycloaddition Process: Copper(I)-Catalyzed Regioselective "Ligation" of Azides and Terminal Alkynes. Angew Chem Int Ed Engl 41: 2596–2599. PMID: 12203546
23. Amblard F, Cho JH, Schinazi RF (2009) Cu(I)-Catalyzed Huisgen Azide—Alkyne 1,3-Dipolar Cycloaddition Reaction in Nucleoside, Nucleotide, and Oligonucleotide Chemistry. Chem Rev 109: 4207–4220. doi: 10.1021/cr9001462 PMID: 19737023
24. Meldal M, Tornøe CW (2008) Cu-Catalyzed Azide—Alkyne Cycloaddition. Chem Rev 108: 2952–3015. doi: 10.1021/cr0783479 PMID: 18698735
25. Skehan P, Storeng R, Scudiero D, Monks A, McMahon J, Vistica D, et al. (1990) New Colorimetric Cytotoxicity Assay for Anticancer-Drug Screening. J Natl Cancer Inst 82: 1107–1112. PMID: 2359136
26. Chen M, Huang C, He C, Zhu W, Xu Y, Lu Y (2012) A glucose-responsive controlled release system using glucose oxidase-gated mesoporous silica nanocontainers. Chem Commun (Camb) 48: 9522–9524. doi: 10.1039/c2cc34290a PMID: 22903226
27. Wannachaiyasit S, Chanvorachote P, Nimmannit U (2008) A Novel Anti-HIV Dextrin—Zidovudine Conjugate Improving the Pharmacokinetics of Zidovudine in Rats. AAPS PharmSciTech 9: 840–850. doi: 10.1208/s12249-008-9122-0 PMID: 18626772
28. Jain N, Prabhakar S, Singh RA (2013) Fourier transform infrared spectra and normal mode analysis of drug molecules: Zidovudine. J Mol Struct 1036: 414–421.

29. Panda S, Pattnaik S, Maharana L, Babu Botta G, Mohapatra P (2013) Formulation and evaluation of zidovudine loaded olibanum resin microcapsules: Exploring the use of natural resins as biodegradable polymeric materials for controlled release. Asian J Pharm Clin Res 6: 191–196.

30. Raghavendra Rao NG, Ghurghure SM, Munde M, Hadi A (2011) Design and characterization of gas powered system of Zidovudine using synthetic polymers. Int J Pharma Bio Sci 2: 269–280.

31. Rama K, Senapati P, Das MK (2005) Formulation and in vitro evaluation of ethyl cellulose microspheres containing zidovudine. J Microencapsul 22: 863–876. PMID: 16423758

32. Sharma KK, Anan A, Buckley RP, Ouellette W, Asefa T (2008) Toward efficient nanoporous catalysts: Controlling site-isolation and concentration of grafted catalytic sites on nanoporous materials with solvents and colorimetric elucidation of their site-isolation. J Am Chem Soc 130: 218–228. PMID: 18076164

33. Dauzonne D, Folléas B, Martinez L, Chabot GG (1997) Synthesis and in vitro cytotoxicity of a series of 3-aminoflavones. Eur J Med Chem 32: 71–82.

34. Xia Y, Yang Z-Y, Xia P, Bastow KF, Nakanishi Y, Lee K-H (2000) Antitumor agents. Part 202: Novel 2′-amino chalcones: design, synthesis and biological evaluation. Bioorg Med Chem Lett 10: 699–701. PMID: 10782667

35. Ma C-M, Cai S-Q, Cui J-R, Wang R-Q, Tu P-F, Hattori M, et al. (2005) The cytotoxic activity of ursolic acid derivatives. Eur J Med Chem 40: 582–589. PMID: 15922841

36. Weber CJ, Müller S, Safley SA, Gordon KB, Amancha P, Villinger F, et al. (2013) Expression of functional folate receptors by human parathyroid cells. Surgery 154: 1385–1393. doi: 10.1016/j.surg.2013.06.045 PMID: 24206618

PLOS | ONE

RESEARCH ARTICLE

SBA-15 Mesoporous Silica Modified with Gallic Acid and Evaluation of Its Cytotoxic Activity

Dawid Lewandowski[1]*, Piotr Ruszkowski[2☯], Anita Pińska[2☯], Grzegorz Schroeder[1☯], Joanna Kurczewska[1☯]

1 Faculty of Chemistry, Adam Mickiewicz University, Poznan, Poland, **2** Faculty of Pharmacy, Poznan University of Medical Sciences, Poznan, Poland

☯ These authors contributed equally to this work.
* dawid_le@amu.edu.pl

Citation: Lewandowski D, Ruszkowski P, Pińska A, Schroeder G, Kurczewska J (2015) SBA-15 Mesoporous Silica Modified with Gallic Acid and Evaluation of Its Cytotoxic Activity. PLoS ONE 10(7): e0132541. doi:10.1371/journal.pone.0132541

Editor: Heidar-Ali Tajmir-Riahi, University of Quebect at Trois-Rivieres, CANADA

Received: May 4, 2015

Accepted: June 17, 2015

Published: July 7, 2015

Data Availability Statement: All relevant data are within the paper and its Supporting Information files.

Funding: This work was supported by the Polish National Science Center (NCN: www.ncn.gov.pl; grant no. 2011/03/B/ST5/01573). GS received the funding. The funders had no role in study design, data collection and analysis, decision to publish, or preparation of the manuscript.

Competing Interests: The authors have declared that no competing interests exist.

Abstract

Gallic acid has been covalently conjugated to SBA-15 mesoporous silica surface through different linkers. Cytotoxic activity of the hybrid organic-inorganic systems against HeLa and KB cell lines has been analyzed. Up to 67% of HeLa or KB tumor cells growth inhibition has been achieved at low silica concentration used (10 μg mL^{-1}).

Introduction

Mesoporous silicas discovered in the early 1990s have found numerous applications in science and industry because of their versatility, high surface area, thermal resistance and ease of surface functionalization. The last feature can be used for the enhancement of adsorption properties [1,2], ion exchange [3], catalytic properties [4,5] or cargo delivery [6,7]. SBA-15 mesoporous silica, with pore diameter ranging between 4.0 and 30.0 nm [8,9] and hexagonal pore order, can be utilized in each of these fields.

The use of SBA-15 mesoporous silica in the preparation of controlled drug release systems is well known [10] and anticancer drugs, besides the anti-inflammatory drugs, have been most intensively delivered in such systems. Most of these systems rely on the adsorption properties of anticancer drugs and gate-like structures located at the pore entrances [11] or on surface modifications [12] affecting the adsorption process. Covalent conjugation of the drug to the silica surface has been seldom reported [13]. The probable reason is that physically adsorbed anticancer drugs need only to be transported, using mesoporous silica carriers, to the vicinity of target tumor cells and protected from premature release by different stimuli-sensitive moieties. Covalently bound drugs require endocytosis of the silica particles by the tumor cells as already been reported in literature[14]. The addition of covalently conjugated folic acid enhances the particles uptake[14,15].

Polyphenolic compounds occur commonly in nature and play an important role in natural processes and ecology of plants. Less frequently they can also be found in animals. Polyphenols have been proved to show anticancer activity via many mechanisms of action [16]. Gallic acid

is a triphenol derivative of benzoic acid and has been studied intensively towards anticancer properties either solely [17,18] as well as a part of more sophisticated systems, like magnetic nanoparticles [19,20]. The mechanisms of anticancer behavior of polyphenols have not been definitely solved yet. Some authors have suggested mobilization of chromatin-bound copper and prooxidation leading to cell death [21], while others point out cell stress damaging cellular integrity and functionality [22] or high structure dependence on polyphenol compound activity [23].

To the best of our knowledge, gallic acid in any form has not been successfully grafted onto the mesoporous silica nanoparticles surface. The aim of this study was to covalently conjugate gallic acid to SBA-15 mesoporous silica and analyze cytotoxic activity of these complex systems.

Materials and Methods

Materials

Gallic acid (GA, ≥98.0%) and 3-(2-aminoethylamino)propyltrimethoxysilane (AMETAM, ≥98.0%) were purchased from Fluka, polyethylenimine (PEI, M_w~2000, 50% wt. solution in water), (3-aminopropyl)trimethoxysilane (APTMS, 97%), (3-chloropropyl)trimethoxysilane (CPTMS, 97+%), folic acid (FA, ≥97%), diisopropylcarbodiimide (DIC, ≥98.0%), N,N-diisopropylethylamine (DIPEA, ≥99.0%) and all solvents used in the study were purchased from Sigma-Aldrich and used without further purification. SBA-15 mesoporous silica (8–11 nm pore diameter, 600 $m^2 g^{-1}$ surface area and 1–2 μm particle size) was purchased from ACS Material.

Preparation of gallic acid derivatives

In the first step gallic acid was converted to its tri-O-acetyl derivative using the procedure adapted from Ye et al. [24]. A portion of 2.90 g of gallic acid was placed in a flask to which 10.0 ml (~6.2 eq) of acetic anhydride was added. The mixture was stirred while 15 μl of concentrated sulfuric acid was added. The temperature rose up to about 60°C and the mixture became a clear solution. It was allowed to cool to the room temperature and 60 ml of water was added. After stirring for 2 h, the white precipitate was filtered off, washed thoroughly with water and dried under reduced pressure. The amount of 4.29 g of acetyl-protected gallic acid was obtained, which is 86% of theoretical yield. The purity was confirmed by melting temperature determination (Mel-Temp melting point apparatus), electrospray mass spectrometry (Micromass ZQ spectrometer, Waters) and IR spectroscopy (FT-IR spectrometer IFS 66/s, Bruker).

Acetylated gallic acid was converted into its acyl chloride each time before the immobilization on the surface. The procedure was as follows: tri-O-acetylgallic acid was dissolved in a small amount (a few ml) of dichloromethane and then large excess of thionyl chloride (~40 eq) was added, followed by catalytic amounts of dimethylformamide. The mixture was refluxed for 2 h and then volatiles were evacuated *in vacuo* (Fig 1). Residual amounts of unreacted thionyl chloride were removed by co-evaporation with toluene. Remaining solid was dissolved in toluene and all toluene-insoluble impurities were eliminated by filtration.The final product was obtained as white, crystalline solid with almost (>95%) quantitative yield.

Immobilization of gallic acid derivatives on the SBA-15 mesoporous silica surface

All gallic acid derivatives were immobilized on the silica surface through amine containing groups: APTMS, AMETAM and PEI.

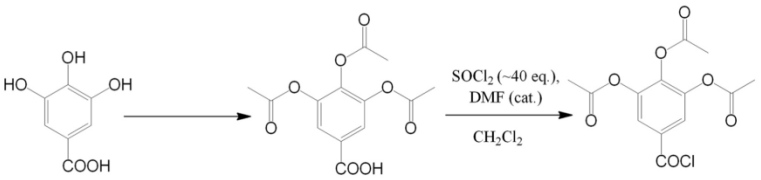

Fig 1. Modifications of gallic acid enabling its introduction onto the silica surface.

doi:10.1371/journal.pone.0132541.g001

The preparation of SBA-15 mesoporous silica covered with APTMS and GA (named SBA-15+APTMS+GA) was conducted as follows: 0.300 g of SBA-15 mesoporous silica was suspended in 10 ml of toluene and an excess (1.000 g) of APTMS was added. The mixture was refluxed for 3 h and then stirred overnight at room temperature, filtered off, washed with toluene and dried. The amount of 0.362 g of APTMS-modified SBA-15 silica was obtained. In the second step 0.360 g of SBA-15+APTMS was suspended in 5 ml of THF and a small excess of DIPEA was added, followed by the addition of 0.425 g of tri-O-acetylgalloyl chloride dissolved in 5 ml of THF (that is 2–3 times higher with respect to the amount of NH_2 groups on the surface). The mixture was stirred overnight at room temperature and then filtered off. The solid was washed carefully with THF, methanol and water to remove all soluble impurities, and dried. The amount of 0.427 g of SBA-15+APTMS+GA as a white solid was obtained and analyzed using elemental analysis and IR spectroscopy.

The procedure applied for SBA-15+AMETAM+GA was similar to that described above; 0.200 g of SBA-15 was suspended in toluene and an excess of AMETAM was added. The mixture was refluxed for 3 h and then stirred overnight at room temperature, filtered off, washed with toluene and dried. The amount of 0.274 g of SBA-15+AMETAM was obtained. A portion of 0.270 g of SBA-15+AMETAM was suspended in THF and DIPEA, followed by tri-O-acetylgalloyl chloride addition in a small excess with respect to the stoichiometric amount (that is 2 chloride molecules per each AMETAM group on the surface). The mixture was stirred at room temperature overnight and filtered off. The solid was washed carefully with THF, methanol and water and dried. The amount of 0.322 g of SBA-15+AMETAM+GA as a white solid was obtained.

The immobilization through PEI was carried out by a different method. A portion of 0.254 g of SBA-15 was suspended in toluene and 0.425 g of CPTMS in toluene was added. The mixture was refluxed for 5 h, stirred overnight at room temperature and filtered off. The solid was washed with toluene and dried. The amount of 0.267 g of SBA-15+CPTMS was obtained as a white solid. In the second step, 0.260 g of SBA-15+CPTMS was suspended in methanol and 0.565 g of PEI (50% water solution) along with small excess of DIPEA was added, the reagents were refluxed for 5 h, stirred overnight at room temperature and filtered off. The solid was washed with water and methanol and dried. The amount of 0.300 g of SBA-15+CPTMS +PEI as a white solid was obtained. Finally, 0.291 g of SBA-15+CPTMS+PEI was suspended in THF and tri-O-acetylgalloyl chloride along with DIPEA (in a small excess with respect to the chloride) were added. The mixture was stirred overnight at room temperature and filtered off. The solid was washed with water and methanol, then dried. The amount of 0.369 g of SBA-15+CPTMS+PEI+GA as a pale yellow solid was obtained.

In all procedures, the last step was the deprotection of acetyl groups. The procedure was adapted from Corey et al. [25] and carried out as follows: the modified silica sample was suspended in a saturated methanolic solution of K_2CO_3 and stirred at room temperature for

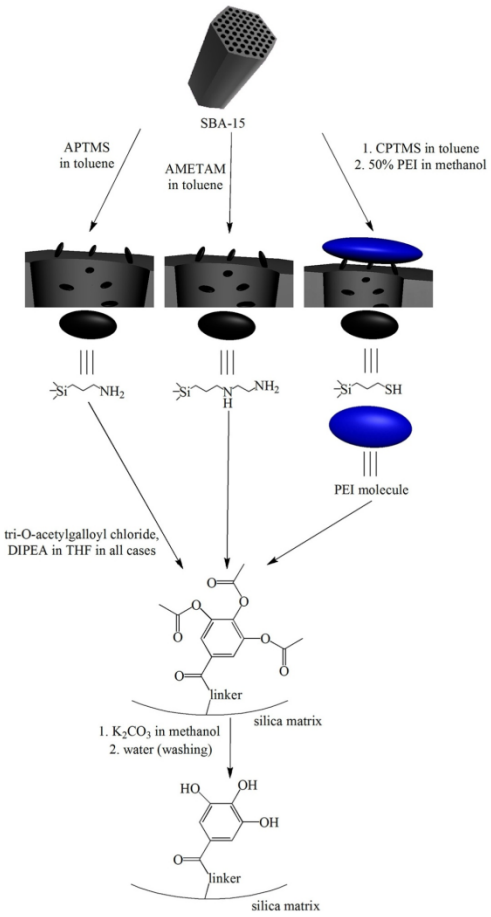

Fig 2. Schematic representation of the procedure used for the synthesis of gallic acid modified SBA-15 mesoporous silica.

doi:10.1371/journal.pone.0132541.g002

15 min (Fig 2). All final products changed colour during this step, starting with white, through pale pink ending with light brown. The solids were then filtered off, washed carefully with methanol and water, and dried. The presence of free phenol–OH groups could be quickly confirmed by suspending particles in a Fe^{3+} solution (which is slightly acidic). Deprotected products immediately formed dark violet complexes with Fe^{3+} ions, while the silica with acetyl-blocked phenol groups became violet after at least 5–10 min.

All systems obtained were characterized using elemental analysis and IR spectroscopy. Modified silica samples were also tested to check for uncontrolled gallic acid detachment. It

was carried out by suspending samples of 20 mg of the composite materialsin water at different pH values (buffer solutions with integer pH values between 2 and 8) and stirring for 24 h. Then the suspensions were filtered and the filtrates' absorbances were measured on an UV-VIS spectrophotometer (Agilent 8453). No detachment was observed.

Evaluation of the cytotoxic activity of the systems obtained

Human cancer cells HeLa (cervical cancer cell line) and KB (*carcinoma nasopharynx*) were cultured in RPMI 1640 medium. Each medium was supplemented with 10% fetal bovine serum, 1% L-glutamine and 1% penicillin/streptomycin solution. The cell lines were kept in the incubator at 37°C. The optimal plating density of cell lines was determined to be 5 x 10^4. All the cell lines were obtained from The European Collection of Cell Cultures (ECACC) supplied by Sigma-Aldrich (catalogue numbers: HeLa cell line – 93021013, KB cell line – 94050408).

The protein-staining sulforhodamine B (SRB, Sigma-Aldrich) microculture colorimetric assay, developed by the National Cancer Institute (USA) for in vitro antitumor screening was used in this study, to estimate the cell number by providing a sensitive index of total cellular protein content, which is in a linear relationship to the cell density [26]. The monolayer cell culture was trypsinized and the cell count was adjusted to 5 x 10^4 cells. In each well of the 96 well microtiter plate, 0.1 mL of the diluted cell suspension (approximately 10,000 cells) was placed. After 24 hours, when a partial monolayer was formed, the supernatant was washed out and 100 μL of six different silica suspension concentrations were added to the cells in microtiter plates. The tested silicas were suspended in DMSO (20 μM) and the content of DMSO did not exceed 0.1% as this concentration was found to be nontoxic to the cell lines. The cells were exposed to silicas for 72 h. After that, 25 μL of 50% trichloroacetic acid were added to the wells and the plates were incubated for 1 hour at 4°C. The plates were then washed out with distilled water to remove traces of medium and next dried by air. The air-dried plates were stained with 100 μL SRB and kept for 30 minutes at room temperature. The unbound dye was removed by rapidly washing with 1% acetic acid and then air dried overnight. The optical density was read at 490 nm. All cytotoxicity experiments were performed three times. Cell survival was measured as the percentage absorbance compared to the control (non-treated cells). Zidovudine (Sigma-Aldrich) was used as the internal standard.

Results and Discussion

Characterization of synthesized compounds

Melting point of acetylated gallic acid was found at 168–171°C, which is in agreement with literature data [27]. IR characterization (full spectrum available in the supplementary material) of acetylated gallic acid confirmed the presence of essential moieties. Comparatively low intensities observed in the range between 3100 and 2500 cm^{-1} suggest complete substitution of phenol–OH groups with acetyl ones. The signal at 1700 cm^{1} relates to the untouched carboxyl group (C = O stretching) and those at 1790 and 1770 cm^{-1} come from acetoxy groups (C = O stretching).

ESI MS analysis (full spectra available in the supplementary material) also unambiguously proves the presence of the desired product. ES- part represents loss of H^+, carboxyl group and consecutive detachment of acetyl groups. ES+ part shows signals related to product's complexes with sodium and potassium ions.

Characterization of modified silica obtained

IR spectra (full spectra available in the supplementary material) of all obtained solids confirmed the presence of secondary amide bonds in the samples. The most characteristic signals, related to the C = O stretching can be found at 1640 cm^{-1}, 1630 cm^{-1} and 1610 cm^{-1} for SBA-15+AMETAM+GA, SBA-15+APTMS+GA and SBA-15+CPTMS+PEI+GA, respectively. The differences between all these samples are a result of the formation of different types of amides that is to say secondary and tertiary ones. SBA-15+APTMS+GA may contain only secondary amide bonding, SBA-15+AMETAM+GA, secondary (mostly) and tertiary and SBA-15 +CPTMS+PEI+GA—tertiary with a small addition of secondary one. The positions of signals from the stretching vibrations of the C = O group from SBA-15+APTMS+GA and SBA-15+AMETAM+GA differ only by 10 cm^{-1} (or even less, because precise location of both peaks is problematic as they are not sharp enough), which is a negligible difference and the position of the signal from SBA-15+CPTMS+PEI+GA differs more, because of the fact explained above. Numerous examples found in literature confirm that for amides, a descending order occurs that is the wavenumbers of amide C = O stretching signals of primary, secondary and tertiary amides decrease in that order. The spectra of all samples showed a signal at 1500 cm^{-1}, which corresponds to the N-H deformation band (for SBA-15+APTMS+GA this signal is only a distortion of a stronger one). There is also no signal from acetyl groups (near 1800 cm^{-1}) which proves that the deprotection process has occurred. Other signals, which can normally be assigned in the spectra of pure compounds, are lost because of the abundance of mesoporous silica or are not decisive ones.

As in SBA-15+APTMS+GA and SBA-15+AMETAM+GA samples the only sources of nitrogen were APTMS and AMETAM and there were two sources of carbon (nitrogen-containing linkers and the attached gallic acid), the elemental analyses allowed the calculation showing that SBA-15+APTMS+GA (10.11% C, 1.709% N and 2.275% H in total) contained 0.51 mmol of gallic acid per gram of the modified silica, which gave about 40% of nitrogen atoms covered with gallic acid. The same calculations conducted for the SBA-15+AMETAM+GA (14.31% C, 3.806% N and 3.380% H) led to 0.64 mmol of gallic acid per gram of the modified silica and 23% of nitrogen atoms coverage. The calculations for the SBA-15+CPTMS+PEI+GA (13.56% C, 3.313% N and 3.073% H) required additional analyses (three carbon-containing sources) and finally led to the result of 0.59 mmol of gallic acid per gram of the modified silica and averaged 25% of nitrogen atoms coverage. The coverage differs in all samples because of the spatial issues (acetylated GA occupies a lot of space) and nitrogen atoms order. APTMS contains only primary amino groups—easily accessible and reactive. AMETAM introduced more than twice as many nitrogen atoms as APTMS, equally primary and secondary ones. Probably most of the primary and some part of secondary nitrogen atoms reacted, but the total coverage (due to high total amount of nitrogen) is lower than that of the APTMS. PEI introduced less nitrogen (as primary, secondary and tertiary atoms) and allowed to anchor less GA than AMETAM, mainly due to its steric properties. Low accessibility of nitrogen atoms resulted in low coverage.

Evaluation of cytotoxic activity

All prepared and analyzed solids showed concentration-dependent cytotoxic activity against HeLa and KB cell lines (Fig 3 **and** Fig 4) which are used very often in such studies.

The sample modified with APTMS and gallic acid was not as active as the unmodified silica, though it contained 0.51 mmol of gallic acid per gram of the solid, which is about 8% in weight. That minor difference can be explained by the fact that the surface coverage drastically reduced the accessibility of acidic silanol groups (which are the active agents in bare silica particles)

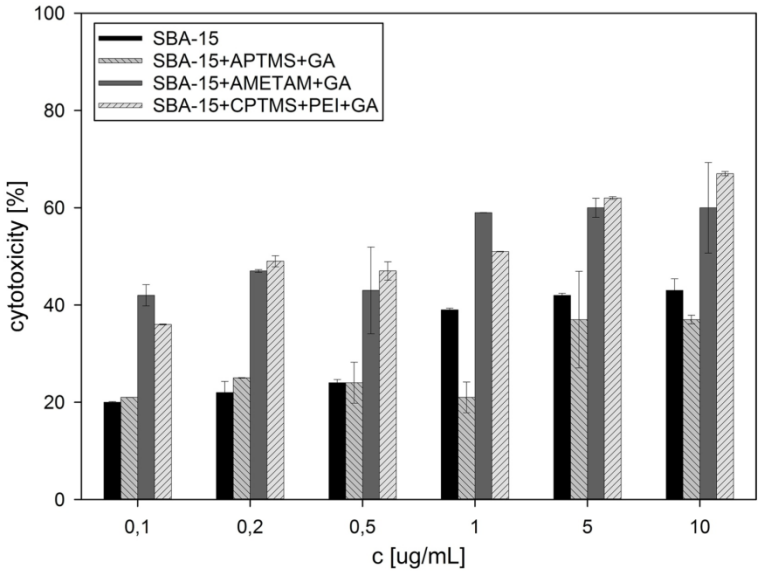

Fig 3. Cytotoxic activity against HeLa cell line, calculated for all samples tested.

doi:10.1371/journal.pone.0132541.g003

and, in exchange, introduced a combination of primary amino groups (potentially increasing the activity and enhancing the uptake) and phenolic hydroxyl groups (much less numerous in comparison to silanol ones), which proved to be less active. Two other samples, with gallic acid anchored to the surface through AMETAM and a combination of CPTMS and PEI, showed much higher activity, equalling or even surpassing that of pure Zidovudine (IC_{50} = 3.12 μgmL^{-1} for KB and 2.28 μgmL^{-1} for HeLa cell line). The activity of SBA-15+AMETAM+GA increased slowly at concentrations up to 1 $\mu g\ mL^{-1}$ and then remained at the same level, even at the concentration ten times higher. The activity of SBA-15+CPTMS+PEI+GA increased steadily as the concentration rose up to 10 $\mu g\ mL^{-1}$, and surpassed that of SBA-15+AMETAM+GA between 1 and 5 $\mu g\ mL^{-1}$. This might be a result of differences in the non-specific interactions with cell membrane that influenced the cellular uptake. In these samples the amount of gallic acid on the surface was noticeably higher and the percentage of nitrogen atoms covered with gallic acid was lower than in SBA-15+APTMS+GA. These two features can be related to the observed increase in activity (in standard organic compounds, introduction of the amino group generally increases their biological activity [28,29,30]) and, what is also worth noticing, free amino groups in SBA-15+AMETAM+GA and SBA-15+CPTMS+PEI+GA are mainly secondary and tertiary ones. High deviations of the results obtained for some of the samples are a result of sedimentation in silica suspensions (statistical data available in the supplementary material).

Conclusions

Gallic acid was successfully introduced onto the SBA-15 mesoporous silica surface using different linkers. Cytotoxic activity against HeLa and KB cell lines of all solids obtained has been

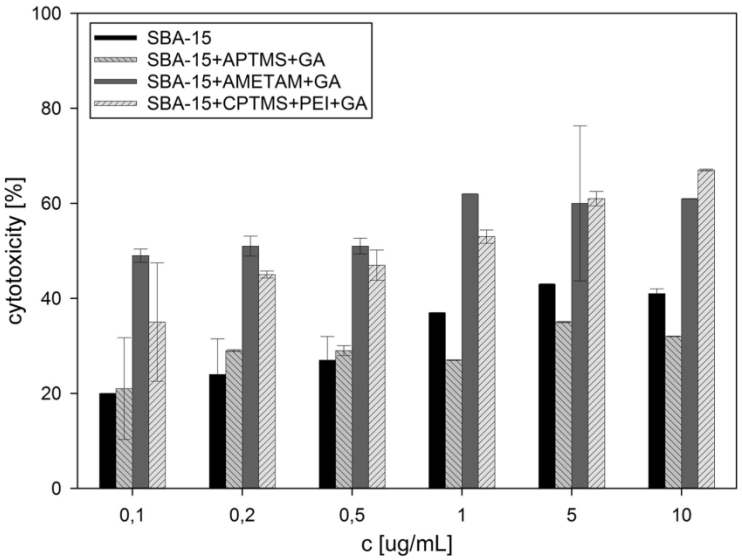

Fig 4. Cytotoxic activity against KB cell line, calculated for all samples tested.

doi:10.1371/journal.pone.0132541.g004

evaluated. The values of cell growth inhibition obtained for the samples are relatively high and equal up to 67% for HeLa and KB tumor cells at low silica suspension concentration. The results of this study can be a basis for further attempts at covalent conjugation of gallic acid and other polyphenols to the silica surface.

Supporting Information

S1 Spectrum. Full FT-IR spectrum of acetylated gallic acid.
(TIF)

S2 Spectrum. ESI MS negative and positive spectra of acetylated gallic acid.
(TIF)

S3 Spectrum. IR spectra of SBA-15 mesoporous silica modified with gallic acid.
(TIF)

S1 Table. Statistical data from the cytotoxicity assay.
(DOCX)

Author Contributions

Conceived and designed the experiments: DL. Performed the experiments: DL PR AP. Analyzed the data: DL. Contributed reagents/materials/analysis tools: PR GS JK. Wrote the paper: DL.

References

1. Hiyoshi N, Yogo K, Yashima T (2005) Adsorption characteristics of carbon dioxide on organically functionalized SBA-15. Microporous Mesoporous Mater 84: 357–365.
2. Perez-Quintanilla D, del Hierro I, Fajardo M, Sierra I (2006) Adsorption of cadmium(ii) from aqueous media onto a mesoporous silica chemically modified with 2-mercaptopyrimidine. J Mater Chem 16: 1757–1764.
3. Ganesan V, Walcarius A (2004) Surfactant Templated Sulfonic Acid Functionalized Silica Microspheres as New Efficient Ion Exchangers and Electrode Modifiers. Langmuir 20: 3632–3640. PMID: 15875393
4. Johnson BJS, Stein A (2001) Surface Modification of Mesoporous, Macroporous, and Amorphous Silica with Catalytically Active Polyoxometalate Clusters. Inorg Chem 40: 801–808. PMID: 11225126
5. Díaz I, Mohino F, Pérez-Pariente Jn, Sastre E (2001) Synthesis, characterization and catalytic activity of MCM-41-type mesoporous silicas functionalized with sulfonic acid. Appl Catal A Gen 205: 19–30.
6. Bhattarai S, Muthuswamy E, Wani A, Brichacek M, Castañeda A, Brock S, et al. (2010) Enhanced Gene and siRNA Delivery by Polycation-Modified Mesoporous Silica Nanoparticles Loaded with Chloroquine. Pharm Res 27: 2556–2568. doi: 10.1007/s11095-010-0245-0 PMID: 20730557
7. Szegedi A, Popova M, Goshev I, Mihály J (2011) Effect of amine functionalization of spherical MCM-41 and SBA-15 on controlled drug release. J Solid State Chem 184: 1201–1207.
8. Vinu A, Murugesan V, Tangermann O, Hartmann M (2004) Adsorption of Cytochrome c on Mesoporous Molecular Sieves: Influence of pH, Pore Diameter, and Aluminum Incorporation. Chem Mater 16: 3056–3065.
9. Katiyar A, Ji L, Smirniotis P, Pinto NG (2005) Protein adsorption on the mesoporous molecular sieve silicate SBA-15: Effects of pH and pore size. J Chromatogr A 1069: 119–126. PMID: 15844490
10. Song S- W, Hidajat K, Kawi S (2005) Functionalized SBA-15 Materials as Carriers for Controlled Drug Delivery: Influence of Surface Properties on Matrix-Drug Interactions. Langmuir 21: 9568–9575. PMID: 16207037
11. Meng H, Xue M, Xia T, Zhao Y-L, Tamanoi F, Stoddart JF, et al. (2010) Autonomous in Vitro Anticancer Drug Release from Mesoporous Silica Nanoparticles by pH-Sensitive Nanovalves. J Am Chem Soc 132: 12690–12697. doi: 10.1021/ja104501a PMID: 20718462
12. Bahrami Z, Badiel A, Atyabi F (2014) Surface functionalization of SBA-15 nanorods for anticancer drug delivery. Chem Eng Res Des 92: 1296–1303.
13. Wani A, Muthsuwamy B, Savithra GHL, Mao G, Brock S, Oupicky D (2012) Surface Functionalization of Mesoporous Silica Nanoparticles Controls Loading and Release Behavior of Mitoxantrone. Pharm Res 29: 2407–2418. doi: 10.1007/s11095-012-0766-9 PMID: 22555380
14. Slowing I, Trewyn BG, Lin VS-Y (2006) Effect of surface functionalization of MCM-41-type mesoporous silica nanoparticles on the endocytosis by human cancer cells. J Am Chem Soc 128: 14792–14793. PMID: 17105274
15. Fan J, Fang G, Wang X, Zeng F, Xiang Y, Wu S (2011) Targeted anticancer prodrug with mesoporous silica nanoparticles as vehicles. Nanotechnology 22: 1–11.
16. Fresco P, Borges F, Diniz C, Marques MPM (2006) New insights on the anticancer properties of dietary polyphenols. Med Res Rev 26: 747–766. PMID: 16710860
17. Subramanian V, Venkatesan B, Tumala A, Vellaichamy E (2014) Topical application of Gallic acid suppresses the 7,12-DMBA/Croton oil induced two-step skin carcinogenesis by modulating anti-oxidants and MMP-2/MMP-9 in Swiss albino mice. Food Chem Toxicol 66: 44–55. doi: 10.1016/j.fct.2014.01.017 PMID: 24444547
18. Locatelli C, Filippin-Monteiro FB, Creczynski-Pasa TB (2013) Alkyl esters of gallic acid as anticancer agents: A review. Eur J Med Chem 60: 233–239. doi: 10.1016/j.ejmech.2012.10.056 PMID: 23291333
19. Dorniani D, Kura AU, Hussein-Al-Ali SH, Bin Hussein MZ, Fakurazi S, et al. (2014) In Vitro Sustained Release Study of Gallic Acid Coated with Magnetite-PEG and Magnetite-PVA for Drug Delivery System. ScientificWorldJournal 2014: 11.
20. Dorniani D, Bin Hussein MZ, Kura AU, Fakurazi S, Shaari AH, Ahmad Z (2012) Preparation of Fe_3O_4 magnetic nanoparticles coated with gallic acid for drug delivery. Int J Nanomedicine 7: 5745–5756. doi: 10.2147/IJN.S35746 PMID: 23166439
21. Khan HY, Zubair H, Ullah MF, Ahmad A, Hadi SM (2012) A Prooxidant Mechanism for the Anticancer and Chemopreventive Properties of Plant Polyphenols. Curr Drug Targets 13: 1738–1749. PMID: 23140285

22. Kim H-S, Quon MJ, Kim J-a (2014) New insights into the mechanisms of polyphenols beyond antioxidant properties; lessons from the green tea polyphenol, epigallocatechin 3-gallate. Redox Biol 2: 187–195. doi: 10.1016/j.redox.2013.12.022 PMID: 24494192

23. Mitsuhashi S, Saito A, Nakajima N, Shima H, Ubukata M (2008) Pyrogallol Structure in Polyphenols is Involved in Apoptosis-induction on HEK293T and K562 Cells. Molecules 13: 2998. doi: 10.3390/molecules13122998 PMID: 19052524

24. Ye J, Abiman P, Crossley A, Jones JH, Wildgoose GG, Compton RG (2009) Building Block Syntheses of Gallic Acid Monomers and Tris-(O-gallyl)-gallic Acid Dendrimers Chemically Attached to Graphite Powder: A Comparative Study of Their Uptake of Al(III) Ions. Langmuir 26: 1776–1785.

25. Corey EJ, Weinshenker NM, Schaaf TK, Huber W (1969) Stereo-controlled synthesis of dl-prostaglandins F2.alpha. and E2. J Am Chem Soc 91: 5675–5677. PMID: 5808505

26. Skehan P, Storeng R, Scudiero D, Monks A, McMahon J, Vistica D, et al. (1990) New Colorimetric Cytotoxicity Assay for Anticancer-Drug Screening. J Natl Cancer Inst 82: 1107–1112. PMID: 2359136

27. Bian X, Fan X, Ke C, Luan Y, Zhao G, Zeng A (2013) Synthesis and α-glucosidase inhibitory activity evaluation of N-substituted aminomethyl-β-d-glucopyranosides. Bioorg Med Chem 21: 5442–5450. doi: 10.1016/j.bmc.2013.06.002 PMID: 23810673

28. Dauzonne D, Folléas B, Martinez L, Chabot GG (1997) Synthesis and in vitro cytotoxicity of a series of 3-aminoflavones. Eur J Med Chem 32: 71–82.

29. Xia Y, Yang Z-Y, Xia P, Bastow KF, Nakanishi Y, Lee K-H (2000) Antitumor agents. Part 202: Novel 2′-amino chalcones: design, synthesis and biological evaluation. Bioorganic & Medicinal Chemistry Letters 10: 699–701.

30. Ma C-M, Cai S-Q, Cui J-R, Wang R-Q, Tu P-F, Hattori M, et al. (2005) The cytotoxic activity of ursolic acid derivatives. Eur J Med Chem 40: 582–589. PMID: 15922841

„From molecules to functional architecture. Supramolecular interactions"
Edited by V.I. Rybachenko
Donetsk 2012, East Publisher House, ISBN 978-966-317-155-5

Chapter 11

Mesoporous silicas as carriers in controlled release systems in biomedicine and cosmetics industry

Dawid Lewandowski and Grzegorz Schroeder
Adam Mickiewicz University in Poznań, Department of Chemistry, Umultowska 89b, 61-614 Poznań

1. Introduction

Porous materials have attracted more attention since the 1960s because of their numerous scientific and technological applications. Generally, the term 'pore' means any tiny hole (unoccupied space) admitting passage of a liquid (fluid or gas) and according to the International Union of Pure and Applied Chemistry, three main pores categories may be distinguished: micropores (<2 nm), mesopores (2-50 nm), and macropores (>50 nm). In view of a wide variety of materials that can be classified as porous an additional classifications are required[1], i.e. between regular and irregular porous materials (distribution of the pores in silica particles), uniformly-sized and non-uniformly-sized materials (when speaking of pores or particles size distribution), highly ordered and amorphous (internal structure), spherical, fibrous and irregular (particles shape).

The breakthrough in porous materials chemistry occurred in 1992, when researchers from Mobil Oil Corporation discovered a group of mesoporous silica oxides known as M41S family[2] with MCM-41 as the most important from among them. However, some sources mention that the discovery of such materials had taken place over 20 years earlier, when as described 'low-bulk density silica' had been obtained[3].

Until now many new silica families have been discovered - as mentioned in the literature:

- MCM-41 (space group *p6mm*), MCM-50 (space group *p*2), MCM-48 (space group $Ia\bar{3}d$) and other from M41S silicas family (**M**obil **C**omposition of **M**atter) – ordered mesoporous silicas templated by cationic surfactants with pore diameter of about 2-10 nm[2]
- SBA-1, SBA-12, SBA-15 (University of California at **S**anta **Ba**rbara) –

ordered mesoporous silicas templated by neutral copolymers (triblock copoloymers), usually larger pores

- KIT-1 (**K**orea Advanced **I**nstitute of Science and **T**echnology 1) or MSU-X (**M**ichigan **S**tate **U**niversity) - disordered mesoporous silicas[4]
- IBN (**I**nstitute of **B**ioengineering and **N**anotechnology)[5]
- FDU-n (**Fu**dan **U**niversity)[6]
- KSW silicas - orthorhombic structure with rectangular arrangements of semi-squared one-dimensional channels[7,8]
- FSM (**F**olded **S**heet **M**aterial) - hexagonal array of uniform channels[9]
- HMS (**H**exagonal **M**esoporous **S**ilica)[10]

Amongst numerous advantages of mesoporous silicas some most important may be distinguished: good thermal stability, high surface area (650 – >1000m^2/g) and surface/volume relationship[1], narrow pores size distribution[11], tunable pores size and volume[12].

Another advantage of mesoporous silicas is that their channels, which serve as cargo reservoirs, can be opened or closed by different systems, i. e. nanocrystals[13], polymers[14], photosensitive derivatives[15] and other organic or inorganic moieties. Triggers such as pH[16], chemicals (dithiothreitol[13], carboxylates[16], pseudorotaxanes[17], cucurbit[6]uril[18], cucurbit[7]uril[19], α-cyclodextrins[20]), light[15], ultrasound[14], heat[21,22], redox reactions[23], enzymes[24], magnetism[12,25] or a combination of two or more of them[12] can be applied to control the cargo delivery.

Each of these families have been used in different applications including supports for catalysis, adsorption, enzyme adsorption and immobilization[26], separation, filtration[11], low-k-materials[27], detection and sensing[28-30].

Mesoporous silicas have also been studied in the context of biomedical use – drug delivery[14,16,31-33] and protein delivery[34] with complete cargo release in the matter of minutes, hours or days[31,35], drug targeting[36,37], tissue engineering[38,39], gene transfection[40] and cell tracking[41].

However, there are several hurdles to make mesoporous silica particles competitive with other drug formulations (microcapsules, micelles, vesicles, dendrimers, polymeric matrices[42], nanocristals or cyclodextrins[43]): first of them is to develop nanocarriers that can encapsulate enough therapeutic agents with activated release. Second one is to deliver these nanoparticles through all the *in vivo* barriers to targeted location. Third is the toxicity, which is still an important issue, and the fourth are costs of fabrication that are still too high for industrial application[44].

2. Preparation and properties

2.1. General mechanism

There are two different mechanisms involved: first, so called true liquid-crystal template mechanism, mentions about the formation of lyotropic liquid-crystalline phase under high surfactant concentration and prevailing conditions, even without a presence of silica source. Second one concerns lower surfactant concentrations, when silica source is needed for directed (hexagonal, cubic or laminar) self-assembly of structure directing agent. This process is known as cooperative crystal template mechanism[45].

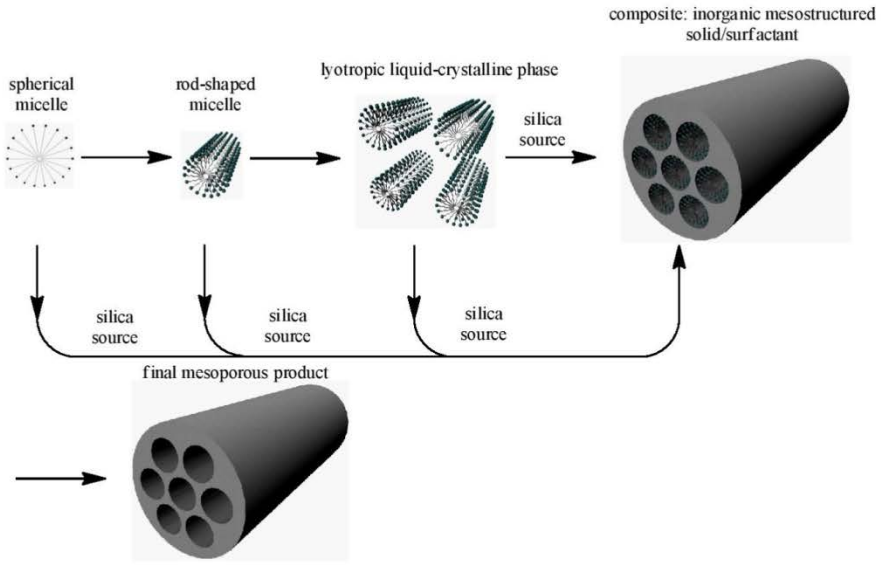

Figure 1. General mechanism of mesoporous silica formation.

2.2. Simple (unmodified) silica particles

Generally, the easiest way of obtaining mesoporous silicas is a solution synthesis, similar to Stöber method for preparation of silica particles[46], which is carried out under basic conditions, but there are many other methods in both, acidic and basic, conditions; with use of anionic, cationic or neutral surfactants, and sometimes mediator ions are required to enhance interactions between silica source and structure directing agent[45].

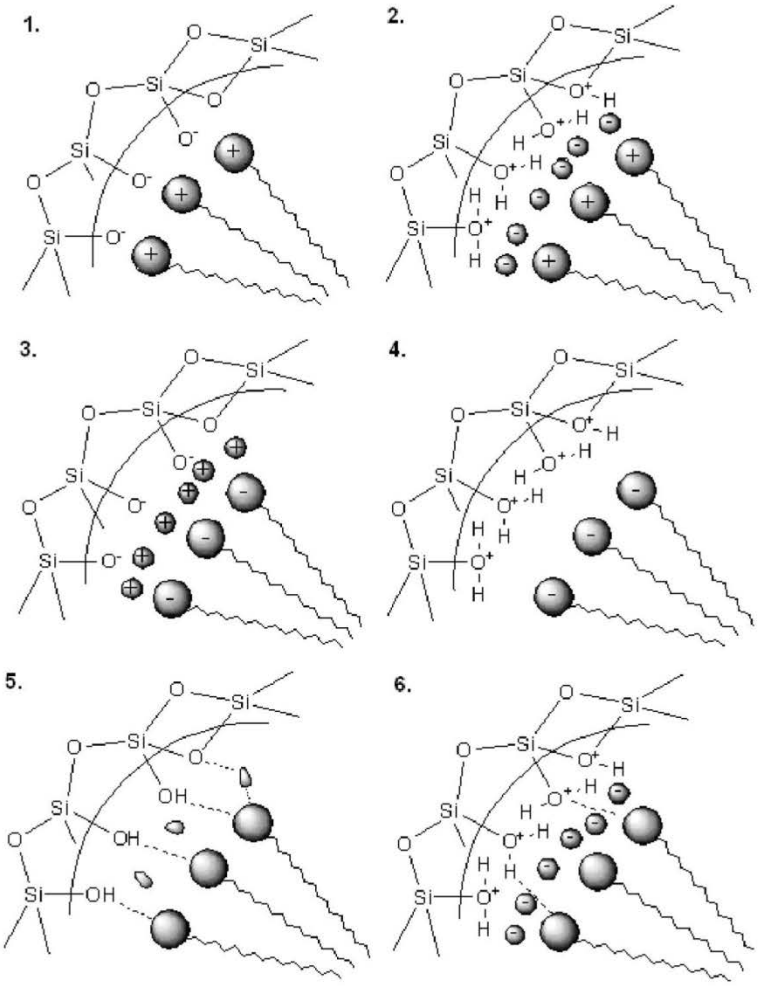

Figure 2. Interactions between the particles during silica matrix formation.

Following Vallet-Regi's *et al.* procedure a water solution of surfactant is mixed with a solution of silica source in a basic solvent (i. e. tetramethylammonium hydroxide - TMAOH, where hydrolysis of silica source takes place) by slow addition of silica source to avoid its condensation, and stirred until silica source hydrolysis is completed[31].

Obtained gel is dried and the surfactant is removed by extraction with a

mixture of concentrated hydrochloric acid and ethanol (1:10 ratio) and kept at reflux for 24 hours. Final material is filtered, washed with water and ethanol, and dried[31]. Other possibility to remove surfactant is to calcinate condensated gel at 500°C for a few hours, while all organic content is burned out.

Under basic conditions most of existing silanol groups is deprotonated and to match this negative charge, cationic surfactants are normally used. Moreover, the hydrolysis and condensation rates of the silica source (tetramethoxysilane – TMOS, tetraethoxysilane – TEOS and others) is highly dependent on several factors such as pH, type of silica source, additives and temperature[47].

The influence of pH value is vital. Hydrolysis rate of silica source generally increases with the pH increase and reaches its maximum at 8,4 for TEOS. Still, there is no evidence, that pH value has a direct influence on size of the obtained particles[48,49]. However, condensation rate, rather than the hydrolysis rate, is the most important factor affecting the particles size. Chiang *et al.* demonstrated that pH is more significant than the amount of silica source used and the reaction time[50].

Only very few trials have been made to prepare mesoporous silicas under acidic conditions. Amongst the advantages of applying these conditions is the capability to use other structure directing agents (SDAs), i. e. block copolymers, allowing to achieve larger pores diameter, but at the cost of uniformity of particles size and shape[51].

There have been also reports indicating that silica source has an influence on particles size. For example, using TMOS as silica source and hexadecyltrimethylammonium bromide (C_{16}TMABr) as a SDA gave particles smaller than 20 nm in size, while TEOS gave *ca.* 30 nm particles. Differences were explained as a result of different hydrolysis rates for both silica sources[52].

The particles size can also be modified by addition of organic (e. g. co-solvents) organosilane compounds, which disturb the interactions between silica source and surfactant[53].

In a suspension of synthesized mesoporous silica, nanoparticles collide and aggregate, attaching to each other *via* van der Waals forces. Aggregation usually occurs during the removal of surfactant and reduces the quality of obtained product[47]. However, when applying different removal procedures[52] or external surface functionalization[54], uniform dispersity may be achieved.

Particles morphology can also be determined by the catalyst (base) type used: TMAOH and NaOH form sphere-shaped particles of MCM-41, NH_4OH may also be used and it leads to rod-like particles[55].

Moreover, for other silica families: Nazar *et al.* presented a synthesis of SBA-15 rods with smaller, than normal, length (300-600 nm) and large pores

(~6 nm) using very dilute solution of P123[56] and Kim *et al.* prepared SBA-15-type nanospheres with pluronic P104 as a template and TMOS as a silica source[57]. More difficult than the production of spherical-shaped particles is the preparation of fibers. Under specific conditions, the formation of hollow tubules[58] or fibers consisting of agglomerated particles has already been reported[59-61].

Han *et al.* obtained IBN-type mesoporous cubic-structured silica by using cationic fluorocarbon surfactants with a higher surface activity and lipophobic nature and pore sizes up to 20 nm[5].

Pore size depends mainly on the surfactant used in the synthesis but also on other parameters of the synthesis[2,62] such as addition of auxiliary organic molecules solubilized in the hydrophobic part of the micelles, increasing their size[62], or *via* hydrothermal treatment of product to restructure it[63]. Functionalization and silica precursor type[44] can also modify the pores size.

However, pore size doesn't affect wall thickness, which is mainly connected with the head group of the surfactant[4]. Walls thickness can be modulated by pH value - it increases when pH decreases[4].

External walls surface of the pores consist mainly of silanol groups and siloxane bridges that could be used to attach many chemical species and serve as a matrix, even without functionalization[31]. Siloxane bridges may be irreversibly hydrolyzed, which is well documented[64].

Pores order may be influenced by the surfactant used - the longer alkyl chain used the higher is the order degree. This is explained by higher hydrophobicity of those longer chains, which create well-defined cylindrical micelles. Moreover, magnetic field may also be used to alter the orientation of silica-surfactant liquid crystal before the final product is formed[65,66]. Heat is an another factor influencing on pore structure, i. e. poorly condensed MCM-41, formed in less than 2 hours undergoes phase transformation upon thermal treatment and, depending on experimental conditions, it can be transformed either into a lamellar phase or into cubic MCM-48[67]

The nature and concentration of inorganic or organic anions existing in reaction mixture influences many properties of the final product, such as wall thickness, overall stability and its long range order[65]. This can be associated with changing the total amount of dissociated silanol groups required to balance the surfactant electrical charge and amount of water stabilized in organic-inorganic interface[4].

Methods described in this section are classified as endotemplate methods ("soft-matter templating"). In exotemplate methods ordered mesoporous silicas are used as templates in place of the surfactant and, after whole synthesis process,

cured, leaving "negative image" of mesoporous structure[68,69]. However, this strategy is complex, time-consuming and labor-intensive.

2.3. Modified mesoporous silica particles

2.3.1 Hollow sphere silica particles

Hollow sphere mesoporous particles have already been synthesized by using different techniques: gas bubbles[70], silica or latex beads[71], emulsions[72] and vesicles[73]. Making small (<200 nm) and uniformly sized particles was developed using two co-templates – polyvinylpyrrolidone (PVP-10) and dodecylamine (DDA)[74].

Until now, many different synthesis methods have been developed for the preparation of hollow silica spheres: soft templating, hard templating, layer-by-layer method[75], Kirkendall effect[76], Ostwald ripening[77] and galvanic replacement[78].

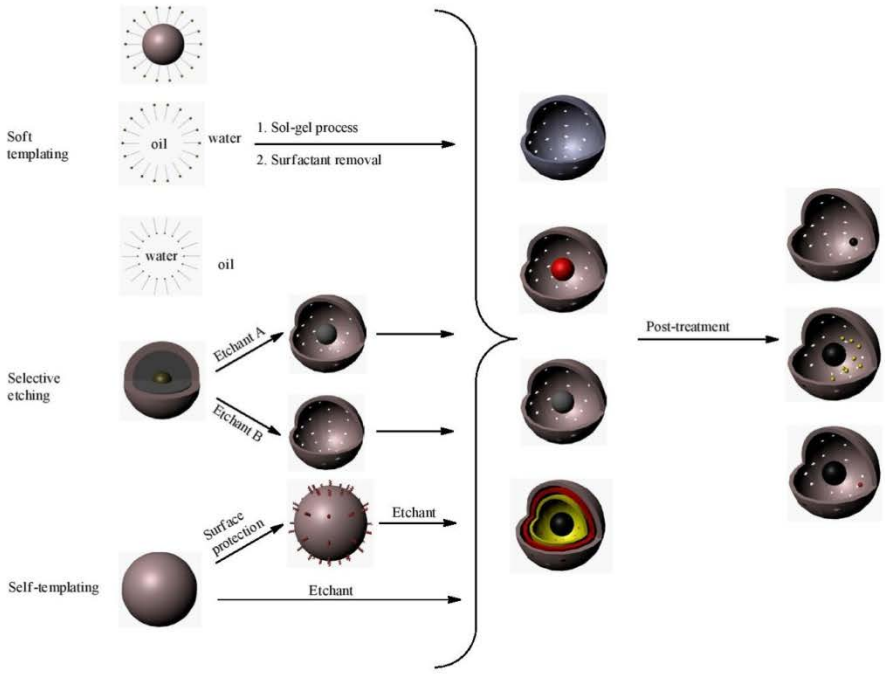

Figure 3. Routes of hollow mesoporous silica partciles preparation.

Soft-templating method allows to synthesize different types of hollow

sphere silica, i. e. yolk-shell particles prepared by Xu *et al.* by dispersing SiO_2 or Au nanoparticles into aqueous mixtures of a zwitterionic surfactant, lauryl sulfonate betaine (LSB) and an anionic surfactant, sodium dodecyl benzenosulfonate (SDBS), to induce formation of vesicles with movable, solid nanoparticle cores. Then they attached 3-aminopropyltriethoxysilane on both surfaces of the vesicles, which served as an additional SDA. After removing the surfactant final product may be obtained[79]. This method can also be used for the synthesis of multilayered shells and hollow spheres with tunable wall thickness[80]. Mesoporous silica shells with hollow interior may also be prepared by other soft-template methods with addition of co-template[73], oil-in-water[81] or water-in-oil[82] microemulsions, water/oil/water emulsion[83] and micelle polymer aggregate[84]. Advantages of soft-template methods are simplicity and effectiveness for the synthesis of hollow- and rattle-type nanomaterials. Unfortunately, there are some disadvantages too. i. e. it is difficult to obtain good dispersity of particles, their size and shell thickness over a broad range. Another one is that large amounts of surfactants are needed, which greatly increases the total cost of industrial synthesis, also complete removal of surfactants is very difficult, and surfactant residues may cause undesirable consequences in biomedical applications[44].

Selective etching method uses structure and composition differences between pure silica framework and hybrid organic-inorganic networks and their behavior against different etching agents or under exceptional temperature or pH conditions. It allows to easily prepare multilayer core/shell nanoparticles and nanoreactors[44].

So called self-template method, that doesn't require any additional template was firstly reported in 2005, when the alkaline treatment of cationic polyelectrolyte (poly-(dimethyldiallylammonium chloride) (PDDA)) pre-coated mesoporous silica spheres could transfer the nanoparticles to hollow structure[85]. It was found that hydroxyl groups permeate through PDDA layer to generate dissolved negatively charged silicate oligomers, which then immigrate and deposit onto the positively charged PDDA layer and cross-link forming the final silica-PDDA complex shell.

2.3.2. Mesostructured silica thin films

Mesostructured silica thin films can be prepared from a solution at room temperature by a process named "evaporation-induced self-assembly", in which one-pot sol, comprising of a silica source and a templating surfactant in aqueous ethanol, is needed[86]. A substrate (glass or silicon) is dipped into the solution and a thin film of liquid is pulled along with the substrate as it is

retracted. Preferential evaporation of the ethanol during the film deposition leads to the formation of surfactant micelles, that further assemble into crystalline mesophase. Condensation of the silica source around the formed micelles finally produces desired mesostructured silica films[87].

Mesostructured silica films may be used as a matrix for quantum dots[88].

2.3.3. Mesoporous silica particles with incorporated metals

Mesoporous silica spheres can be formed around the metal nanocrystals by mixing the silica precursor with an aqueous solution of surfactant-coated nanocrystal[89]. The electrostatic interactions between the surfactant-coated nanocrystals, free surfactant molecules and hydrolyzed silicate molecules lead to base-catalyzed silica condensation and form the mesostructure. This procedure has been used to embed iron oxide, gold and silver nanocrystals. Such functionalized mesoporous nanoparticles may be used for imaging, as well as for the delivery of biologically active molecules[90].

Also simple impregnation of mesoporous silica can be useful – Pt/MCM-41 is far more active catalyst than amorphous silica[91]. Basic catalysts using MCM-41 as the matrix can also be prepared by impregnating it with caesium and lanthanum[92].

2.3.4. Surface-functionalized mesoporous materials

Surface functionalization for mesoporous silica can be applied by different methods, i. e. co-condensation, by preparing periodically mesoporous organosilicas (PMOs) or by post-synthetic modification called "grafting".

Co-condensation is an example of direct synthesis route for surface-modified mesoporous materials. In this method SDA is stirred together with a silica source, which is a mixture of standard tetraalkoxysilanes (TMOS and TEOS) and organotrialkoxysilica compounds of the type $(R'O)_3SiR$. The reaction leads to materials with organic residues anchored covalently to pore walls. This synthetic route has some advantages in compare with other ways: organic groups introduced into silica matrix don't block pore opening as it happens in post-synthetic modification and are more homogenously distributed over material's surface. However, co-condensation has also some disadvantages. Increasing concentration of organic residues within the mesostructure influences negatively its order, which can lead to totally disordered products. Maximal reasonable content of organic groups incorporated by co-condensation method cannot exceed 40 mol %. Also, the amount of organic functionalities inside the matrix is generally lower than it corresponds to the starting mixture. This is

caused by the differences in hydrolysis and condensation rates, which leads to favorable homocondensation of organotrialkoxysilanes rather than cross-linking. Moreover, increased content of loading of the incorporated groups causes reduction of pore diameter, pore volume and specific surface areas[45]. Another inconvenience of this method is that only extraction, as for removing of residual surfactant, may be used, calcination is not suitable.

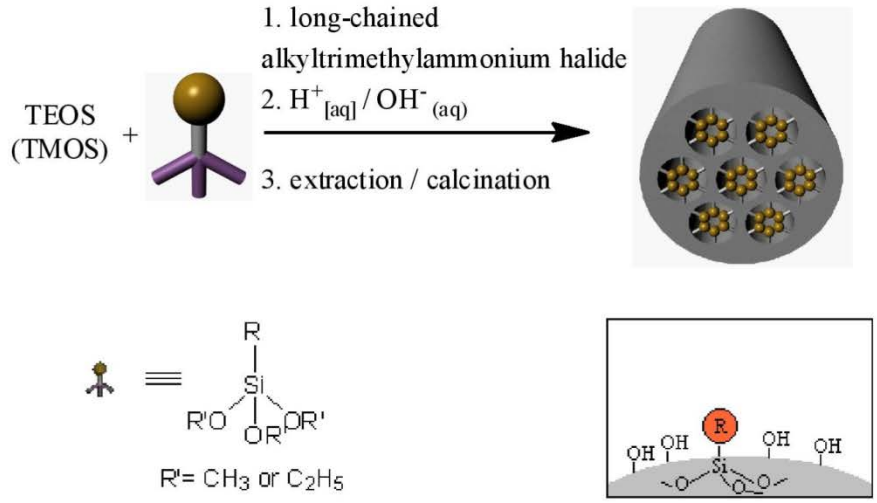

Figure 4. Functionalization through direct synthesis – general scheme for co-condensation method.

The chemical nature of condensing reagents influences the final shape of particles – hydrophilic agents lead to preparation of small, round particles while hydrophobic ones give rod shaped particles[26].

Also mutual orientation of 2D hexagonal channels in mesoporous silicas may be altered by an addition of chemicals, i. e. some urea-organosilane in different amounts changes alignment of mesoporous channels from straight, helical to radial[93].

After pioneering articles of the groups of Mann[94], MacQuarrie[95] and Stein[96] many other organically modified mesoporous silicas have been prepared by co-condensation, including alkyl, thiol, vinyl/allyl[97], amino, cyano/isocyano[98], alkoxy[99], organophosphine and aromatic groups[100]. Mesoporous materials, obtained by following direct synthesis route exhibit interesting catalytic and adsorption properties[101-107]. It is possible to modify mesoporous silica with even

more complex groups, such as cyclam molecules[108], large chelate ligands[109], cyclodextrins[110], calyx[8]arenes[111] and pH-sensitive dyes[112].

Some different mesoporous materials prepared by co-condensation method have been reported. Corriu *et al.* synthesized in 1998 a new hybrid xerogels with pores diameter less than 3,5 to 4 nm[113]. For the preparation they used dendrimer-like organosilanes.

Preparation of periodic mesoporous organosilicas (PMOs) is another method of obtaining hybrid organic-inorganic materials.

It has been known for a long time in sol-gel chemistry as hydrolysis and condensation of bridged organosilica compounds of the type $(R'O)_3Si–R–Si(OR')_3$. In this case organic units are incorporated into three-dimensional silica network through two covalent bonds and thus distributed homogenously in the pore walls. Materials prepared in this way as aero- and xerogels can have up to 1800 $m^2 g^{-1}$ of surface area but with completely disordered pore systems and wide pore size distribution[45]. PMOs differ from these amorphous materials with periodically organized pore system and narrow pore size distribution. They were synthesized in 1999 by three groups working independently[114-116] (Inagaki's group – ethane-bridged, Ozin's and Stein's groups – ethene-bridged PMOs). PMO materials are considered as promising candidates for a series of technical applications, i. e. catalysis, chromatography, adsorption, nanoelectronics or cargo releasing systems[45].

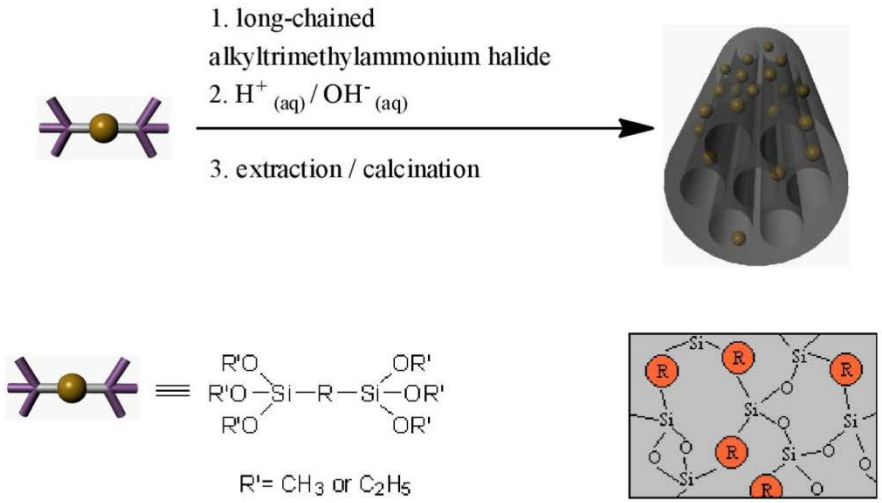

Figure 5. Functionalization through direct synthesis – general scheme for preparation of PMOs.

In a general review of already prepared PMOs, some more interesting may be distinguished:

- aromatic PMOs – benzene[117], 2,5-dimethylbenzene and 2,5-dimethoxybenzene[118] bridged with high degree of structural order and pore diameters of about 2 nm
- crystal-like benzene-, bisphenyl-bridged PMOs with long range ordered walls[119,120]
- ethane-bridged PMOs with use of gemini surfactants and some swelling agents to obtain products with 11 nm pores and without long range order[121]
- PMOs made with the use of nonionic polymers, with large pores of a diameter up to 20 nm[122,123], further researches increased their walls order by an addition of inorganic salts[124] or, without them, by changing the silica precursor and surfactant ratios[125]; aromatic and unsaturated PMOs with large pores have also been prepared[126,127]; PMOs based on nonionic surfactants but with smaller pores have also been presented[128]
- PMOs from tri- and multisilylated precursors[129,130]
- PMAs (periodic mesoporous aminosilicas) with amino groups anchored in the matrix[131]
- carbon/silica nanoparticles prepared from benzene-bridged PMOs[132]
- PMOs from different mixtures of silica precursors.

There have been some studies to adapt PMOs, their morphology, pore size and wall order to different applications: chromatography – monodispersed, spherical, with a particle size of about a few μm[133], adsorbents – with large surface area[134], low-k materials – PMO films[135], nanowires and catalysis – defined pore geometry, large inner surface area[136].

Grafting method refers to subsequent modification of the inner surfaces of mesoporous silica phases with organic groups. It's usually carried out by reaction of organosilanes of the type $(R'O)_3SiR$ or chlorosilanes $ClSiR_3$ or silazanes $HN(SiR_3)_3$ with the free silanol groups on the pore surfaces.

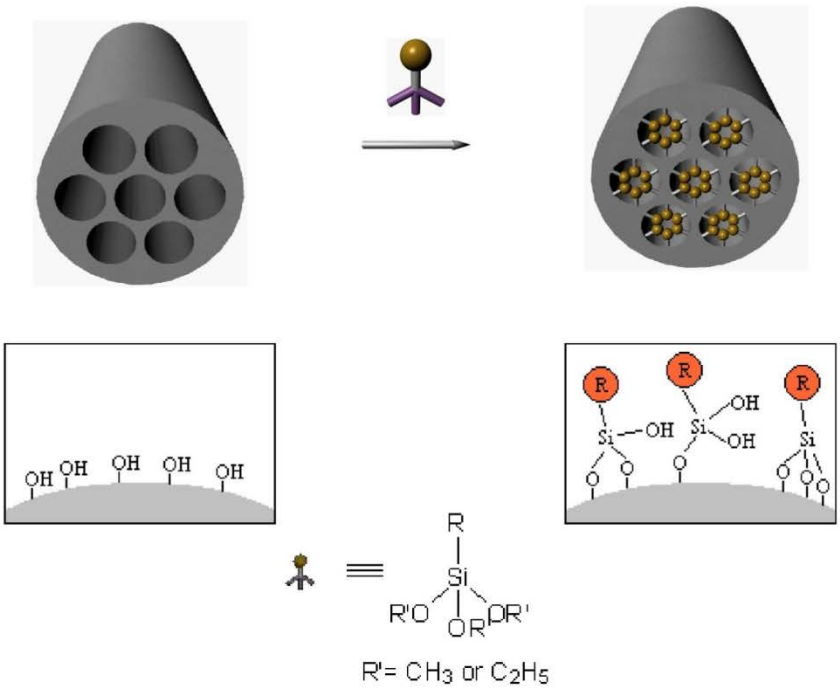

Figure 6. Post-synthetic functionalization – general scheme for grafting.

It is considered, that the reaction of anchoring silanes in presence of water consists of four steps, which can go simultaneously after the first hydrolysis step

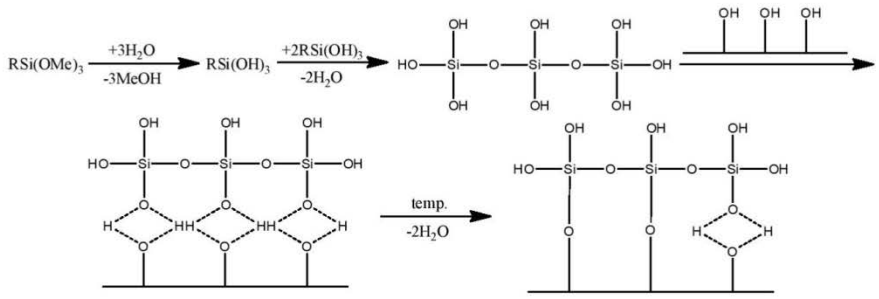

Figure 7. Mechanism of post-synthetic modification through the grafting process in presence of water.

Presence of water in the reacting mixture and its influence on grafting reaction has also been studied. Modifying with 3-aminopropyltrimethoxysilane (APTMS) in presence of water leads to clustering of APTMS and preferential grafting at the pore entrances, reducing uniformity of distribution[137]. However, for the preparing of the monolayer comprised with 3-mercaptopropyltrimethoxysilane, water is crucial for the formation of respecting hydroxysilane[138] so there is no one certain answer to the water presence in the reaction mixture.

Anhydrous conditions leads to one-step reaction

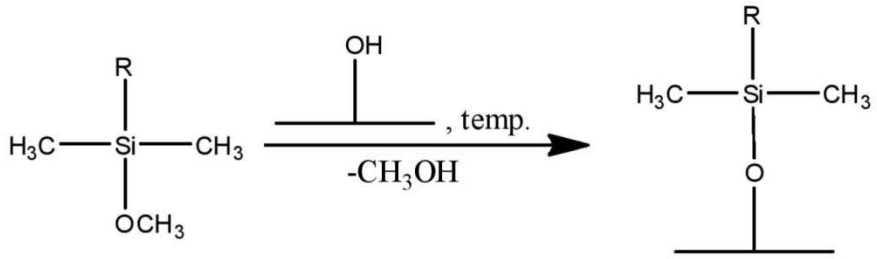

Figure 8. Mechanism of post-synthetic modification through the grafting process in absence of water.

Usually, only one bond between the surface and silane is formed, other two substituents undergo condensation or remain free[139].

This method has an advantage that the mesostructure of the starting silica phase is usually retained. If the organosilanes react with silanol groups at the pore entrances, the diffusion of other molecules can be impaired or even stopped (pore blockade)[45,140]. Also solvents used affect the distribution of functional groups on the surface, i. e. toluene is not a proper choice, because it leads to anchoring organosilanes near pore entrances, while alcohols or THF produce higher degree of site isolation and more homogenous distribution[141,142].

Obtaining of site-isolated functionalization of silica's surface has also been performed. McKittrick and Jones used tritylimine patterning agent to control the minimum distance between the amino- groups anchored to the surface, and after grafting the tritylimine to the surface and capping remaining silanol groups with hexamethyldisilazane, they hydrolyzed patterning agent to get the final product[143]. The use of smaller protecting group leads to higher grafting density. Also imprinting method can be used to get site-isolated functionalization of the surface. Circle molecules can be grafted onto internal surface, leaving some part of the surface free. Then, another functionality can be introduced, but only on

the unoccupied part of the surface. In the last step, circle molecules are removed, leaving site-isolated modified surface.

Selective grafting of the external surface can be done, while SDA is still inside the pores of as-synthesized silica[144].

It is also possible to graft thin silica films for an additional functionality – Tanaka *et al.* prepared such films modified by a new vapor-infiltration technique, where the samples were exposed to the vapor of organosilica functionalization reagents at high temperature for several hours in an autoclave[145].

Grafting can also be done for larger organic groups like dendrimers[146], chlorophyll[147] and fullerenes[148], for making acid[149], base[150], oxidative[151] and chiral[152] catalysts. Thiol functionalized MCM-41 has been used as an adsorptive for heavy metals from solution[153].

3. Application of mesoporous silicas in biomedicine and cosmetics industry

3.1. Biocompatibility and toxicity

An ideal delivery system used in biomedicine should be able do deliver cargo to a targeted site in a controlled manner and be characterized by:

- biocompatibility and biodegradability
- controlled release of cargo
- controlled loading and targeted release of therapeutics
- zero premature release
- stimuli responsiveness[26].

Mesoporous silica MCM-41 compared to solid silica spheres was found to be less toxic[154]. Surface functionalization has drastic effect on the toxicity of mesoporous silicas[155].

Positively charged silicas induces more immune response and cytotoxicity than neutral or negatively charged ones but they are better for transvascular transport in tumor[156]. Silanol groups can react with biological molecules such as lipids and proteins destroying their structures[157]. Unmodified silica with negative zeta potential is rapidly associated with serum opsonin in blood and cleared from circulating system. The most effective coating, increasing biocompatibility and half-time of mesoporous silica particles is PEGylation, approved by FDA, which creates a protective, hydrophilic layer around them[158]. PEGylation also improves silica's properties in the hemolytic activity and cytotoxicity, and decreases the endocytosis of modified silica particles[155]. *In vitro* studies have shown how mesoporous silica interacts with different cell lines, i. e. 3T3 endothelial cells[159], human colon carcinoma (Caco-2)[160], glioma cells[161], human mesenchymal stem cells[162] and HeLa cells[163]. *In vivo* biodistribution and excretion can be regulated by adding the functional groups like amino, carboxyl,

phenyl and methyl phosphonate with different zeta potentials, i. e. nitrogen-modified (different functional groups) manipulates the particle endocytosis of HeLa cells[164]. Coating silica with lipid layer improves its biocompatibility and performance, gives better suspensibility and much lower nonspecific binding in vitro in compare to unmodified silica[165]. Cellular uptake studies may be performed and visualized by attaching a fluorescent dye to the silica surface by co-condensation method[41].

Influence of particles shape on the endocytosis rate is also significant – there is a model with a concept of "wrapping time" which explains, why the spherical particles undergo faster endocytosis than the cylindrical ones[166] for both *in vitro* and *in vivo* (human fibroblast cells[167]) studies.

Size of the mesoporous silica particles has an uncertain status of being important for their toxicity – although some sources mention that the smaller particles used the less cytotoxic they are[168]. Particles with a diameter less than 500 nm are easily taken up by the cell through endocytosis and can be localised in lysosomes of the cell.

Structure and high surface area of mesoporous silica partcles may also be an important factor influencing the total toxicity – large amount of free silanol groups generate reactive oxygen species that are the cause of nanomaterial-caused injuries[169]. It is also a cause of cellular and mitochondrial respiration inhibition[170] and oxidative stress[171].

He *et al.* found that the synthesis method plays also some role in the overall toxicity – different MCM-41 particles using Triton, CTAB and SDBS as surfactants were prepared and their toxicity was tested. CTAB-based MCM-41 was more toxic than SDBS one and the least was Triton-based MCM-41[172].

Also the influence of size, porosity, particles coating and dosage of mesoporous materials on the activity of hemolytic cells was tested and the results were that the smaller particles the higher is their hemolytic activity[173]. However, *in vivo* studies have shown that mesoporous silica nanoparticles reveal size-independent toxicity but highly dependent on the administration route[174].

Mesoporous particles are eliminated from the human body by hepatobiliary excretion, which was proved by Souris *et al*[175]. Elimination rate is size and surface modification dependent as well as the way of synthesis – mesoporous silicas prepared by extraction are much faster eliminated than calcinated and amorphous ones[176].

3.2. Adsorption and release studies

Until now, a wide variety of drugs (or dyes) have been loaded and released in a controlled manner using unmodified or modified mesoporous silicas[26]:

- MCM-41 – ibuprofen, vancomycin, gentamycin, aspirin, alendronate, camptothecin, atenolol, BSA, cytochrome C, paclitaxel, DNA, vitamine B_2, calcein, safranine O,
- SBA-15 – gentamycin, amoxicillin, erythromycin, alendronate, L-tryptophan, BSA,
- hollow mesoporous silicas – fluorescein isothiocyanate,
- MSN – Orange II, rhodamine-B, DNA, ibuprofen, alendronate,
- MSN II – DNA into plant cells,
- MCM-48 – erythromycin,
- FSM – Taxol,

There are many physicochemical parameters, that can affect adsorption and release of cargo from mesoporous silicas:

- particle size and morphology – Monzano *et al.* studied the release of ibuprofen from spherical MCM-41 particles with a size between 490-770 nm and they concluded that better release control was achieved with smaller particles. However, it was much slower than while using irregularly shaped particles. They summarized, that spherical particles are better in controlled delivery of ibuprofen[177]. Qu *et al.* showed that adsorption of captopril was higher in rod shaped particles than in spherical ones[178]; hollow structured mesoporous silicas show higher loading capacities than typical ones, except of pore blocking molecules (effective pore volume decreases rapidly for hollow particles[179]),
- pore size – Hata *et al.* first reported the effect of pore size and influence of solvent on the loading and release of Taxol[180] and Vallet-Regi *et al.* – release rate of ibuprofen[31]. Large pores are required for adsorption and separation of proteins[181,182] and adsorption of DNA or RNA[183]; pore size affects also loading kinetics, which has been proved for captopril[178],
- pore structure – it is demonstrated that pore connectivity, geometry and matrix degradation have an influence on adsorption and release properties of mesoporous silica, i. e. Linden *et al.*[184] showed that SBA-1 mesoporous silica with interconnected pores system revealed similar loading capacity and slightly faster release rate of ibuprofen than SBA-3 mesoporous silica without internal interconnection,
- pore volume – it is considered as a critical factor for drug loading and release because of drug-drug interactions which may be even more important than drug-silica surface ones, it has been reported that consecutive loadings of drug in ordered mesoporous materials leads to larger filling of the mesopores[185],

- surface area – increased number of active adsorption sites increases amount of cargo adsorbed, which has been verified for alendronate[186],
- surface functionalization – carried out by co-condensation, grafting and PMO synthesis methods, i. e. creating different coatings made of PEI (polyethylineimine) increases amount of DNA and siRNA adsorbed or improves the delivery of paclitaxel[187]; Tourne-Peteilh *et al.* prepared transport system for ibuprofen by simple anchoring it to the surface through ester bond, where release was achieved after its cleavage[188],
- pH at which the adsorption is carried out – for proteins the highest amount of cargo loaded was observed near the isoelectric point[189],
- molecule's polarity – since silica surface is polar (silanol groups) or negatively charged (pK_a ~2,5) at higher pH values, polarity is an important factor affecting the amount and distribution of molecules adsorbed – Okazaki and Toriyama have studied the diffusion of isopropanol and cyclohexane in contact with MCM-41 and they have found that alcohol preferred to occupy the regions at and near the external surface while the cyclohexane deposited deeper within the nanochannels[190],
- surface polarity – silica may be functionalized with hydrophobic species, in this case cargo-surface interactions don't play any significant role, but the cargo transport out of the matrix is seriously impeded as the polar solvents don't easily penetrate it[186]; hydrophobization of silica surface makes it more resistant to hydrolysis[191].

Amount of drug needed is a very important issue, because even with achieving high loading capacities, large amounts of mesoporous matrix is needed to create a drug formulation, which can be digested by i. e. oral route (tablets usually). As an examples of daily drug dose/matrix needed: gentamicin:SBA-15 150-300mg:2g, erythromycin:SBA-15 1,5-3g:3,4g, ibuprofen:MCM-41 0,9-1,2g:7g[186].

Liu *et al.* synthesized multi-shelled hollow spheres, which can be utilized to load different chemicals in each shell and release them controllably by changing the walls thickness[192].

Release of the cargo can be activated by different stimuli such as:

- pH – it is one of the most important factor triggering release of trapped molecules, because of the facility to control it and that in human's body there are regions, organs, cells differing in the pH value, which can be used in targeted delivery; the most often pH sensitive systems use amine functionalization because of their ability to protonate/deprotonate at certain pH values[20]; some of the more interesting systems using pH triggering are: coating made of cyclodextrin and

PEI complexes releasing cargo upon breaking the polypseudorotaxane protection[17], molecular machines made of cucurbituril complexes with the silica, opening at lower pH values and closing at higher ones (so called molecular clock)[193] or the use of surface modifying individuals with bonds breaking at certain pH values (hydrazone[194], acetal[195] or orthoester[196]),

- enzymes – systems based on enzymes contain coatings sensitive to the treatment of specific enzymes, i. e. capping mesoporous silica with biotin-avidin complex makes it sensitive to proteases[24], β-CD coating is responsive to the α-amylase and lipase enzymes[197],
- chemicals – CdS capped nanoparticles sensitive to the reaction of amidation was reported by Lai *et al*[13]; gold nanoparticles associated with the surface by photocleavable linker, thioundecyltetraethyleneglycoester-*o*-nitrobenzylethyldimethyl ammonium bromide (TUNA) sensitive to UV irradiation reported by Lin *et al.*[198] and Amoros *et al*[199].; also some magnetic nanoparticles coated with supraparamagnetic iron oxide with anti-oxidants as triggering factor were prepared; glucose responsive delivery of insulin with a gluconic acid modified insulin proteins immobilized on mesoporous silica is an another example of chemical trigger for cargo release[163] and anion-driven gate-like system based on polyamines (sensitive to different organic and inorganic anions like chloride, acetate or ATP)[200],
- thermal responsive systems are based on sensitive polymers like poly-N-isopropylacrylamide (PNIPAm)[201]; moreover, it is possible to create a system based on PNIPAm, in which conformational changes of polymer induce structural changes in silica – it can give a possibility to release cargo at certain temperature[202],
- light – irradiation at certain wavelength can induce breaking bonds of pore blocking individuals, as presented by Mal *et al.* who grafted coumarin onto the outer surface of MCM-41 mesoporous silica and irradiated them with UV light at 310 nm. Coumarin undergoes dimerization then and closes pore openings, making cargo release impossible. Subsequent irradiation at 250 nm breaks the coumarin dimer and allows to release the cargo[15]; Sierocki *et al.* reported similar light responsiveness for azobenzene derivatives, that change their *cis-trans* geometry upon light irradiation[203].

There are also some sophisticated systems based on catenanes and rotaxanes (mechanically interlocked molecules) which use different interactions such as donor-acceptor[204], hydrogen bonding[205], metal-ligand[206] and hydrophobic[207]

interactions to release cargo in a controllable way.

Release profiles differ from each other, depending on the adsorption and functionalization methods: nonfunctionalized matrices (a) shows burst release at start and then slow release, diffusion or dissolution processes (b) presents first-order kinetics with respect to drug concentration, zero-order release kinetics (c) for some functionalized systems, profile (d) corresponds sophisticated stimulus-responsive system with release rate controlled by external changes[186].

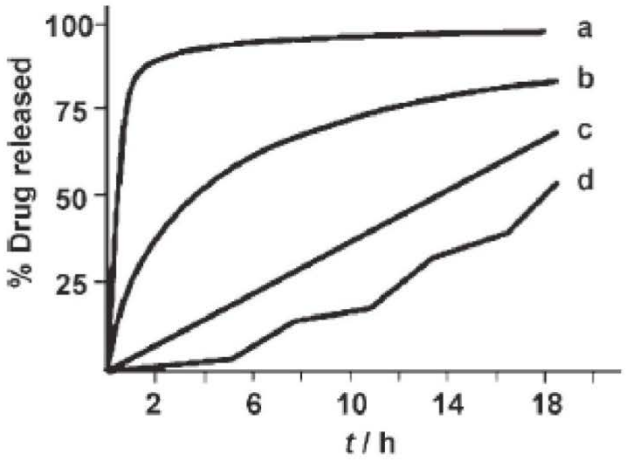

Figure 9. Release profiles from different mesoporous systems – adapted from [186].

3.3. Sensors and some other appplications

Functionalized mesoporous silicas may also have an important meaning as sensors.

Radu *et al.* synthesized by co-condensation method thiol-functionalized MCM-41 silica and attached epoxyhexyl groups to the outer surface before removal of the surfactant. Inner thiol groups were modified by *o*-phthalaldehyde and a layer of poly-L-lactic acid was polymerized onto the outer surface to eventually obtain a neurotransmitter sensor, which could differentiate between three different neurotransmitters: dopamine, tyrosine and glutamic acid. The outer, polymeric coating has different permeability for each of them and that caused the selectivity[208].

Descalzo *et al.* prepared an ATP sensor based on N-propylanthracene-10-amino functionalized MCM-41 silica. Presence of ATP was detected by the reduction of fluorescence signal[209].

Mesoporous silica-based may also be used in analytic chemistry, i. e. to quantitative determination of copper ions[210], binding mercury(II)[211], palladium(II) and platinum(II)[212] or borate[213] ions.

Iron oxide may be used in cancer treatment as superparamagnetic nanoparticles embedded in mesoporous silica, delivering heat under alternating magnetic fields, as a result of Brownian rotation and Neel relaxation[214].

Acknowledgements

This work was partially supported from the funds of National Science Centre (grant no. 2011/03/B/ST5/01573).

References

1. Hasanzadeh, M.; Shadjou, N.; Eskandani, M.; de la Guardia, M. Mesoporous silica-based materials for use in eletrochemical enzyme nanobiosensors. *Trends in Analytical Chemistry* **40**, 106-118 (2012).
2. Kresge, C. T.; Leonowicz, M. E.; Roth, W. J.; Vartuli, J. C.; Beck J. S. Ordered mesoporous sieves synthesized by a liquid crystal templating mechanism. *Nature* **359**, 710-712 (1992).
3. Di Renzo, F.; Cambon, H.; Dutarte R. A 28-year-old synthesis of micelle-templated mesoporous silica. *Micropor. Mater.* **10**, 283-286 (1997).
4. Davidson, A. Modyfying the walls of mesoporous silicas prepared by supramolecular-templating. *Colloid & Interface Science* **7**, 92-106 (2002).
5. Han, Y.; Ying, J. Y. Generalized Fluorocarbon-Surfactant-Mediated Synthesis of Nanoparticles with Various Mesoporous Structures. *Angew. Chem. Int. Ed.* **44**, 288-292 (2004).
6. Huo, Q.; Margolese, D. I.; Ciesla, U.; Feng, P.; Gier, T. E.; Sieger, P.; Leon, R.; Petroff, P. M.; Schuth, F.; Stucky, G. D. Generalized synthesis of periodic surfactant/inorganic composite materials. *Nature* **368**, 317-321 (1994).
7. Shigeno, T.; Nagao, M.; Kimura, T.; Kuroda, K. Direct Silylation of a Mesostructured Precursor for Novel Mesoporous Silica KSW-2. *Langmuir* **18**, 8102-8107 (2002).
8. Kimura, T.; Itoh, D.; Okazaki, N.; Kaneda, M.; Sakamoto, Y.; Terasaki, O.; Sugahara, Y.; Kuroda, K. Lamellar hexadecyltrimethylammonium silicates derived from kanemite. *Langmuir* **16**, 7624-7628 (2000).
9. Inagaki, S.; Fukushima, Y.; Kuroda, K. Synthesis of Highly Ordered

Mesoporous Materials from a Layered Polysilicates. *J. Chem. Soc., Chem. Commun.*, 680-682 (1993).
10. Zhang, W.; Pauly, T. R.; Pinnavaia, T. J. Tailoring the Framework and Textural Mesopores of HMS Sieves through an Electrically Neutral (S^oI^o) Assembly Pathway. *Chem. Mater.* **9**, 2491-2498 (1997).
11. Kadib, A. E.; Katir, N.; Bousmina, M.; Majoral, J. P. Dendrimer-silica hybrid mesoporous materials. *New J. Chem.* **36**, 241-255 (2012).
12. Ruiz-Hernandez, E.; Baeza, A.; Vallet-Regi, M. Smart Drug Delivery through DNA/Magnetic Nanoparticle Gates. *ACS Nano* **5**, 1259-1266 (2011).
13. Lai, C. Y.; Trewyn, B. G.; Jeftinija, D. M.; Jeftinija, K.; Xu, S.; Jeftinija, S. et al. A mesoporous silica nanosphere-based carrier system with chemically removable CdS nanoparticle caps for stimuli-responsive controlled release of neurotransmitters and drug molecules. *J. Am. Chem. Soc.* **125**, 4451-4459 (2003).
14. Kim, H. J.; Matsuda, H.; Zhou, H. S.; Honma, I. Ultrasound-triggered smart drug rlease from a poly(dimethylsiloxane)-mesoporous silica composite. *Adv. Mater.* **18**, 3083 (2006).
15. Mal, N. K.; Fujiwara, M.; Tanaka, Y. Photocontrolled reversible release of guest molecules from coumarin-modified mesoporous silica. *Nature* **421**, 350-353 (2003).
16. Yang, Q.; Wang, S. H.; Fan, P. W.; Wang, L. F.; Di, Y.; Lin, K. F. et al. pH-Responsive carrier system based on carboxylic acid modified mesoporous silica and polyelectrolyte for drug delivery. *Chem. Mater.* **17**, 5999-6003 (2005).
17. Park, C.; Oh, K.; Lee, S. C.; Kim, C. Controlled Release of Guest Molecules from Mesoporous Silica Particles Based on a pH-Responsive Polypseudorotaxane Motif. *Angew. Chem. Int. Ed.* **46**, 1455-1457 (2007).
18. Khashab, N. M.; Belowich, M. E.; Trabolsi, A.; Friedman, D. C.; Valente, C.; Lau, Y.; Khatib, H. A.; Zink, J. I.; Stoddart, J. F. pH-Responsive mechanised nanoparticles gated by semirotaxanes. *Chem. Commun.*, 5371-5373 (2009).
19. Khashab, N. M.; Trabolsi, A.; Lau, Y. A.; Ambrogio, M. W.; Friedman, D. C.; Khatib, H. A.; Zink, J. L.; Stoddart, J. F. Redox- and pH-controlled mechanized nanoparticles. *Eur. J. Org. Chem.*, 1669-1673 (2009).
20. Du, L.; Liao, S.; Khatib, H. A.; Stoddart, J. F.; Zink, J. I. Controlled-Access Hollow Mechanized Silica Nanocontainers. *J. Am. Chem. Soc.* **131**, 15136-15142 (2009).

21. Fu, Q.; Rao, G. V. R.; Ista, L. K.; Wu, Y.; Andrzejewski, B. P.; Sklar, L. A. et al. Control of molecular transport through stimuli-responsive ordered mesoporous materials. *Adv. Mater.* **15**, 1262-1266 (2003).
22. Aznar, E.; Mondragon, L.; Ros-Lis, J. V.; Sancenon, F.; Marcos, D.; Martinez-Manez, R.; Soto, J.; Perez-Paya E.; Amoros, P. Finely Tuned Temperature-Controlled Cargo Release Using Pararffin-Capped Mesoporous Silica Nanoparticles. *Angew. Chem. Int. Ed.* **50**, 11172-11175 (2011).
23. Hernandez, R.; Tseng, H.-R.; Wong, J. W.; Stoddart, J. F.; Zink, J. I. An Operational Supramolecular Nanovalve. *J. Am. Chem. Soc.* **126**, 3370-3371 (2004).
24. Patel, K.; Angelos, S.; Dichtel, W. R.; Coskun, A.; Yang, Y.-W.; Zink, J. I.; Stoddart, J. F. Enzyme-Responsive Snap-Top Covered Silica Nanocontainers. *J. Am. Chem. Soc.* **130**, 2382-2383 (2008).
25. Arruebo, M.; Galan, M.; Navascues, N.; Tellez, C.; Marquina, C.; Ibarra, M. R. et al. Development of magnetic nanostructured silica-based materials as potential vectors for drug-delivery applications. *Chem. Mater.* **18**, 1911-1919 (2006).
26. Popat, A.; Hartono, S. B.; Stahr, F.; Liu, J.; Qiao, S. Z.; Lu, G. Q. Mesoporous silica nanoparticles for bioadsorption, enzyme immobilisation, and delivery carriers. *Nanoscale* **3**, 2801-2818 (2011).
27. Theije, F. K. de; Balkenende, A. R.; Verheijen, M. A.; Baklanov, M. R.; Mogilnikov, K. P.; Furukawa, Y. Structural Characterization of Mesoporous Organosilica Films for Ultralow-*k* Dielectrics. *J. Phys. Chem.* **107**, 4280-4289 (2003).
28. Tao, S.; Li, G. Porphyrin-doped mesoporous silica films for rapid TNT detection. *Colloid Polym. Sci.* **285**, 721-728 (2007).
29. Hasanzadeh, M.; Shadjou, N.; Eskandani, M.; de la Guardia, M.; Sheikhzadeh, P. Mesoporous silica-based materials for use in biosensors. *Trends in Analytical Chemistry* **33**, 117-129 (2012).
30. Trewyn, B. G.; Giri, S.; Slowing, I. I.; Lin, V. S.-Y. Mesoporous silica nanoparticles based controlled release, drug delivery, and biosensor systems. *Chem. Commun.*, 3236-3245 (2007).
31. Vallet-Regi, M.; Ramila, A.; del Real, R. P.; Perez-Pariente, J. A New Property of MCM-41: Drug Delivery System. *Chem. Mater.* **13**, 308-311 (2001).
32. Barbe, C.; Bartlett, J.; Kong, L. G.; Finnie, K.; Lin, H. Q.; Larkin, M. et al. Silica particles: a novel drug-delivery system. *Adv. Mater.* **16**, 1959-1966 (2004).

33. Ambrogi, V.; Perioli, L.; Marmottini, F.; Giovagnoli, S.; Esposito, M.; Rossi, C. Improvement of dissolution rate of piroxicam by inclusion into MCM-41 mesoporous silicate. *Eur. J. Pharm. Sci.* **137**, 30-37 (2007).
34. Song, S.-W.; Hidajat, K.; Kawi, S. Functionalized SBA-15 Materials as Carriers for Controlled Drug Delivery: Influence of Surface Properties on Matrix-Drug Interactions. *Langmuir* **21**, 9568-9575 (2005).
35. Lopez, T.; Basaldella, E. I.; Ojeda, M. L.; Manjarrez, J.; Alexander-Katz, R. Encapsulation of valproic acid and sodic phenytoin in ordered mesoporous SiO_2 solids for the treatment of temporal lobe epilepsy. *Opt. Mater.* **29**, 75-81 (2006).
36. Pasqua, L.; Testa, F.; Aiello, R.; Cundari, S.; Nagy, J. B. Preparation of bifunctional hybrid mesoporous silica potentially useful for drug targeting. *Microporous and Mesoporous Materials* **103**, 166-173 (2007).
37. Gu, J.; Fan, W.; Shimojima, A.; Okubo, T. Organic-inorganic mesoporous nanocarriers, integrated with biogenic ligands. *Small* **3**, 1740-1744 (2007).
38. Izquierdo-Barba, I.; Ruiz-Gonzalez, L.; Doadrio, J. C.; Gonzalez-Calbet, J. M.; Vallet-Regi, M. Tissue regeneration: a new property of mesoporous materials. *Solid State Sci.* **7**, 983-989 (2005).
39. Li, X.; Shi, J. L.; Zhu, Y. F.; Shen, W. H.; Li, H.; Liang, J. et al. A template route to the preparation of mesoporous amorphous calcium silicate with high in vitro bone-forming bioactivity. *J. Biomed. Mater. Res. B.* **83B**, 431-439 (2007).
40. Radu, D. R.; Lai, C. Y.; Jeftinija, K.; Rowe. E. W., Jeftinija, S.; Lin, V. S. Y. A polyamidoamine dendrimer-capped mesoporous silica nanosphere-based gene transfection reagent. *J. Am. Chem. Soc.* **126**, 13216-13217 (2004).
41. Lin, Y. S.; Tsai, C. P.; Huang, H .Y.; Kuo, C. T.; Hung, Y.; Huang, D. M. et al. Well-ordered mesoporous silica nanoparticles as cell markers. *Chem. Mater.* **17**, 4570-4573 (2005).
42. Aznar, E.; Sancenon, F.; Marcos, M. D.; Martinez-Manez, R.; Stroeve, P.; Cano, J.; Amoros, P. Delivery Modulation in Silica Mesoporous Supports via Alkyl Chain Pore Outlet Decoration. *Langmuir* **28**, 2986-2996 (2011).
43. Marcato, P. D.; Duran, N. New Aspects of Nanopharmaceutical Delivery Systems. *J. Nanosci. Nanotechnol.* **8**, 1-14 (2008).
44. Tang, F.; Li, L.; Chen, D. Mesoporous Silica Nanoparticles: Synthesis,

Biocompatibility and Drug Delivery. *Adv. Mater.* **24**, 1504-1534 (2012).
45. Hoffmann, F.; Cornelius, M.; Morell, J.; Froba, M. Silica-Based Mesoporous Organic-Inorganic Hybrid Materials. *Angew. Chem. Int. Ed.* **45**, 3216-3251 (2006).
46. Stober, W.; Fink, A.; Bohn, E. Controlled growth of monodisperse silica spheres in the micron size range. *J. Colloid Interface Sci.* **26**, 62-69 (1968).
47. Wu, K. C.-W.; Yamauchi, Y. Controlling physical features of mesoporous silica nanoparticles (MSNs) for emerging applications. *Journal of Materials Chemistry* **22**, 1251-1256 (2012).
48. Lu, F.; Wu, S. H.; Hung, Y.; Mou, Y. N. Size effect on Cell Uptake in Well-Suspended, Uniform Mesoporous Silica Nanoparticles. *Small* **5**, 1408 (2009).
49. Qiao, Z. A.; Zhang, L.; Guo, M.; Liu, Y.; Huo, Q. Synthesis of Mesoporous Silica Nanoparticles via Controlled Hydrolysis and Condensation of Silicon Alkoxide. *Chem. Mater.* **21**, 3823-3829 (2009).
50. Chiang, Y.-D.; Lian, H.-Y.; Leo, S.-Y.; Wang, S.-G.; Yamauchi, Y.; Wu, K.C.-W. Controlling particle size and structural properties of mesoporous silica nanoparticles using the taguchi method. *J. Phys. Chem. C* **115**, 13158-13165 (2011).
51. Berggren, A.; Palmqvist, A.E.C. Particle size control of colloidal suspensions of mesostructured silica. *J. Phys. Chem. C* **112**, 732-737 (2008).
52. Urata, C.; Aoyama, Y.; Tonegawa, A.; Yamauchi, Y.; Kuroda, K. Dialysis process for the removal of surfactants to form colloidal mesoporous silica nanoparticles. *Chem. Commun.*, 5094-5096 (2009).
53. Anderson, M. T.; Martin, J. E.; Odinek, J. G.; Newcomer, P. P. Surfactant-Templated Silica Mesophases Formed in Water:Cosolvent Mixtures. *Chem. Mater.* **10**, 311-321 (1998).
54. Rosenholm, J. M.; Sahlgren, C.; Linden, M. Towards multifunctional, targeted drug delivery systems using mesoporous silica nanoparticles - Opportunities & challenges. *Nanoscale* **2**, 1870-1883 (2010).
55. Cai, Q.; Luo, Z.-S.; Pang, W.-Q.; Fan, Y.-W.; Chen, X.-H.; Cui, F.-Z. Dilute solution routes to various controllable morphologies of MCM-41 silica with a basic medium. *Chem. Mater.* **13**, 258-263 (2001).
56. Ji, X.; Lee, K. T.; Monjauze, M.; Nazar, L. F. Strategic sunthesis of SBA-15 nanorods. *Chem. Commun.*, 4288-4290 (2008).
57. Kim, T.-W.; Slowing, I. I.; Chung, P.-W.; Lin, V.S.-Y. Ordered mesoporous polymer-silica hybrid nanoparticles as vehicles for the

intracellular controlled release of macromolecules. *ACS Nano* **5**, 360-366 (2011).
58. Lin, H.-P.; Mou, C.-Y. 'Tubules-within-a-tubule' hierarchical order of mesoporous molecular sieves in MCM-41. *Science* **273**, 765-768 (1996).
59. Schacht, S.; Huo, Q.; Voigt-Martin, I. G.; Stucky, G. D.; Schuth, F. Oil-water interface templating of mesoporous macroscale structures. *Science* **273**, 768-771 (1996).
60. Huo, Q.; Zhao, D.; Feng, J.; Weston, K.; Buratto, S. K.; Stucky, G. D.; Schacht, S.; Schuth, F. Room temperature growth of mesoporous silica fibers: A new high-surface-area optical waveguide. *Adv. Mater.* **9**, 974-978 (1997).
61. Bruinsma, P. J.; Kim, A. Y.; Liu, J.; Baskaran, S. Mesoporous Silica Synthesized by Solvent Evaporation: Spun Fibers and Spray-Dried Hollow Spheres. *Chem. Mater.* **9**, 2507-2512 (1997).
62. Beck, J. S.; Vartuli, J. C.; Roth, W. J.; Leonowicz, M. E.; Kresge, C. T.; Schmitt, K. D.; Chu, C. T.-W.; Olson, D. H.; Sheppard, E. W.; McCullen, S. B.; Higgins, J. B.; Schlenker, J. L. A new family of mesoporous molecular sieves prepared with liquid crystal templates. *J. Am. Chem. Soc.* **114**, 10834-10843 (1992).
63. Khushalani, D.; Kuperman, A.; Ozin, G.A.; Tanaka, K.; Garces, J.; Olken, M. M.; Coombs, N. Metamorphic materials: Restructuring siliceous mesoporous materials. *Adv. Mater.* **7**, 842-846 (1995).
64. Zhao, X. S.; Audsley, F.; Lu, G. Q. Irreversible change of pore structure of MCM-41 upon hydration at room temperature. *J. Phys. Chem. B* **102**, 4143-4146 (1998).
65. Schulz-Ekloff, G.; Rathousky, J.; Zukal, A. Controlling of morphology and characterization of pore structure of ordered mesoporous silicas. *Microporous and Mesoporous Materials* **27**, 273-285 (1999).
66. Sierra, L.; Guth, J.-L. Synthesis of mesoporous silica with tunable pore size from sodium silicate solutions and a polyethylene oxide surfactant. *Microporous and Mesoporous Materials* **27**, 243-253 (1999).
67. Landry, C. C.; Tolbert, S. H.; Gallis, K. W.; Monnier, A.; Stucky, G. D.; Norby, P.; Hanson, J. C. Phase transformations in mesostructured silica/surfactant composites. Mechanisms for change and applications to materials synthesis. *Chem. Mater.* **13**, 1600-1608 (2001).
68. Ryoo, R.; Joo, S. H.; Jun, S. Synthesis of highly ordered carbon molecular sieves via template-mediated structural transformation. *J. Phys. Chem. B* **103**, 7745-7746 (1999).

69. Lee, J.; Yoon, S.; Hyeon, T.; Oh, S. M.; Kim, K. B. Synthesis of a new mesoporous carbon and its application to electrochemical double-layer capacitors. *Chem. Commun.*, 2177-2178 (1999).
70. Rana, R. K.; Mastai, Y.; Gedanken, A. Acoustic cavitation leading to the morphosynthesis of mesoporous silica vesicles. *Adv. Mater.* **14**, 1414-1418 (2002).
71. Blas, H.; Save, M.; Pasetto, P.; Boissiere, C.; Sanchez, C.; Charleux, B. Elaboration of monodisperse spherical particles with ordered mesoporous silica shells via dual latex/surfactant templating: Radial orientation of mesopore channels. *Langmuir* **24**, 13132-13137 (2008).
72. Sun, Q.; Kooyman, P. J.; Grossmann, J. G.; Bomans, P. H. H.; Frederik, P. M.; Magusin, P. C. M. M.; Beelen, T. P. M.; Van Santen, R. A.; Sommerdijk, N. A. J. M. The formation of well-defined hollow silica spheres with multilamellar shell structure. *Adv. Mater.* **15**, 1097-1100 (2003).
73. Yeh, Y.-Q.; Chen, B.-C.; Lin, H.-P.; Tang, C.-Y. Synthesis of hollow silica spheres with mesostructured shell using cationic-anionic-neutral block copolymer ternary surfactants. *Langmuir* **22**, 6-9 (2006).
74. Du, L. Song, H.; Liao, S. Tuning the morphology of mesoporous silica by using various template combinations. *Applied Surface Science* **255**, 9365-9370 (2009).
75. Javier, A. M.; Kreft, O.; Semmling, M.; Kempter, S.; Skirtach, A. G.; Bruns, O. T.; Del Pino, P.; Bedard, M. F.; Raedler, J.; Kas, J.; Plank, C.; Sukhorukov, G. B.; Parak, W. J. Uptake of colloidal polyelectrolyte-coated particles and polyelectrolyte multilayer capsules by living cells. *Adv. Mater.* **20**, 4281-4287 (2008).
76. Yin, Y.; Rioux, R. M.; Erdonmez, C. K.; Hughes, S.; Somorjal, G. A.; Alivisatos, A. P. Formation of Hollow Nanocrystals Through the Nanoscale Kirkendall Effect. *Science* **304**, 711-714 (2004).
77. Low, X. W.; Yuan, C.; Rhoades, E.; Zhang, Q.; Archer, L. A. Encapsulation and Ostwald ripening of Au and Au-Cl complex nanostructures in silica shells. *Adv. Funct. Mater.* **16**, 1679-1684 (2006).
78. Chen, J.; McLellan, J. M.; Siekkinen, A.; Xiong, Y.; Li, Z.-Y.; Xia, Y. Facile synthesis of gold-silver nanocages with controllable pores on the surface. *J. Am. Chem. Soc.* **128**, 14776-14777 (2006).
79. Wu, X.-J.; Xu, D. Formation of Yolk/Sio2 shell structures using surfactant mixtures as template. *J. Am. Chem. Soc.* **131**, 2774-2775 (2009).
80. Djojoputr, H.; Zhou, X. F.; Qiao, S. Z.; Wang, L. Z.; Yu, C. Z.; Lu, G.

Q. Periodic mesoporous organosilica hollow spheres with tunable wall thickness. *J. Am. Chem. Soc.* **128**, 6320-6321 (2006).
81. Li, J.; Liu, J.; Wang, D.; Guo, R.; Li, X.; Qi, W. Intefacially controlled synthesis of hollow mesoporous silica spheres with radially oriented pore structures. *Langmuir* **26**, 12267-12272 (2010).
82. Lin, Y.S.; Wu, S.-H.; Tseng, C.-T.; Hung, Y.; Chang, C.; Mou, C.-Y. Synthesis of hollow silica nanospheres with a microemulsion as the template. *Chem. Commun.*, 3542-3544 (2009).
83. Fujiwara, M.; Shiokawa, K.; Sakakura, I.; Nakahara, Y. Silica hollow spheres with nano-macroholes like diatomaceous earth. *Nano Lett.* **6**, 2925-2928 (2006).
84. Khanal, A.; Inoue, Y.; Yada, M.; Nakashima, K. Synthesis of silica hollow nanoparticles templated by polymeric micelle with core-shell-corona structure. *J. Am. Chem. Soc.* **129**, 1534-1535 (2007).
85. Ren, N.; Wang, B.; Yang, Y.-H.; Zhang, Y.-H.; Yang, W.-L.; Yue, Y.-H.; Gao, Z.; Tang, Y. General method for the fabrication of hollow microcapsules with adjustable shell compositions. *Chem. Mater.* **17**, 2582-2587 (2005).
86. Brinker, C. J.; Lu, Y.; Sellinger, A.; Fan, H. Evaporation-induced self-assembly: Nanostructures made easy. *Adv. Mater.* **11**, 579-585 (1999).
87. Coti, K. K.; Belowich, M. E.; Liong, M.; Ambrogio, M. W.; Lau, Y. A.; Khatib, H. A.; Zink, J. I.; Khashab, N .M.; Stoddart, J. F. Mechanised nanoparticles for drug delivery. *Nanoscale* **1**, 16-39 (2009).
88. Tang, Y. S.; Cai, S.; Jin, G.; Duan, J.; Wang, K. L.; Soyez, H. M.; Dunn, B. S. SiGe quantum dots prepared on an ordered mesoporous silica coated Si substrate. *Appl. Phys. Lett.* **71**, 2448-2450 (1997).
89. Fan, H.; Yang, K.; Boye, D. M.; Sigmon, T.; Malloy, K .J.; Xu, H.; Lopez, G. P.; Brinker, C .J. Self-Assembly of Ordered, Robust, Three-Dimensional Gold Nanocrystal/Silica Arrays. *Science* **304**, 567-571 (2004).
90. Liong, M.; France, B.; Bradley, K. A.; Zink, J. I. Antimicrobial activity of silver nanocrystals encapsulated in mesoporous silica nanoparticles. *Adv. Mater.* **21**, 1684-1689 (2009).
91. Corma, A.; Martinez, A.; Martinez-Soria, V. Hydrogenation of aromatics in diesel fuels on Pt/MCM-41 catalysts. *J. Catal.* **169**, 4880-4891 (1997).
92. Kloestra, K. R.; van Laren, M.; van Bekkum, H. Binary caseium-lanthanum ocide supported on MCM-41: a new stable heterogenous basic catalyst. *J. Chem. Soc. - Faraday Trans.* **93**, 1211-1220 (1997).

93. Wang, S.-G.; Wu, C.-W.; Chen, K.; Lin, V. S.-Y. Fine-tuning mesochannel of organically functionalized mesoporous silica nanoparticles. *Chem.-Asian J.* **4**, 658-661 (2009).
94. Burkett, S. L.; Sims, S. D.; Mann, S. Synthesis of hybrid inorganic-organic mesoporous silica by co-condensation of siloxane and organosiloxane precursors. *Chem. Commun.*, 1367-1368 (1996).
95. Macquarrie, D. J. Direct preparation of organically modified MCM-type materials. Preparation and characterisation of aminopropyl-MCM and 2-cyanoethyl-MCM. *Chem. Commun.*, 1961-1962 (1996).
96. Lim, M. H.; Blanford, C. F.; Stein, A. Synthesis and characterization of a reactive vinyl-functionalized MCM-41: Probing the internal pore structure by a bromination reaction. *J. Am. Chem. Soc.* **119**, 4090-4091 (1997).
97. Mercier, L.; Pinnavaia, T. J. Direct synthesis of hybrid organic-inorganic nanoporous silica by a neutral amine assembly route: Structure-function control by stoichiometric incorporation of organosiloxane molecules. *Chem. Mater.* **12**, 188-196 (2000).
98. Huh, S.; Wiench, J. W.; Yoo, J.-C.; Pruski, M.; Lin, V.S.-Y. Organic Functionalization and Morphology Control of Mesoporous Silicas via a Co-Condensation Synthesis Method. *Chem. Mater.* **15**, 4247-4256 (2003).
99. Fowler, C. E.; Burkett, S. L.; Mann, S. Synthesis and characterization of ordered organo-silica-surfactant mesophases with functionalized MCM-41-type architecure. *Chem. Mater.*, 1769-1770 (1997).
100. Cagnol, F.; Grosso, D.; Sanchez, C. A general one-pot process leading to highly functionalised ordered mesoporous silica films. *Chem. Commun.* **10**, 1742-1743 (2004).
101. Macquarrie, D. J., Jackson, D. B. Aminopropylated MCMs as base catalysts: A comparison ith aminopropylated silica. *Chem. Commun.*, 1781-1782 (1997).
102. Lim, M. H.; Blanford, C. F.; Stein, A. Synthesis of Ordered Microporous Silicates with Organosulfur Surface Groups and Their Applications as Solid Acid Catalysts. *Chem. Mater.* **10**, 467-470 (1998).
103. Margolese, D.; Melero, J. A.; Christiansen, S. C.; Chmelka, B. F.; Stucky, G. D. Direct syntheses of ordered SBA-15 mesoporous silica containing sulfonic acid groups. *Chem. Mater.* **12**, 2448-2459 (2000).
104. Yang, C.-M.; Zibrowius, B.; Schuth, F. A novel synthetic route for negatively charged ordered mesoporous silica SBA-15. *Chem. Commun.* **9**, 1772-1773 (2003).

105. Corriu, R. J. P.; Datas, L.; Guari, Y.; Mehdi, A.; Reye, C.; Thieuleux, C. Ordered SBA-15 mesoporous silica containing phosphonic acid groups prepared by a direct synthetic approach. *Chem. Commun.*, 763-764 (2001).
106. Nooney, R. I.; Kalyanaraman, M.; Kennedy, G.; Maginn, E. J. Heavy metal remediation using functionalized mesoporous silicas with controlled macrostructure. *Langmuir* **17**, 528-533 (2001).
107. Guari, Y.; Thieuleux, C.; Mehdi, A.; Reye, C.; Corriu, R. J. P.; Gomez-Gallardo, S.; Philippot, K.; Chaudret, R.; Dutartre, R. In situ formation of gold nanoparticles within functionalised ordered mesoporous silica via an organometallic "chimie douce" approach. *Chem. Commun.*, 1374-1375 (2001).
108. Corriu, R. J. P.; Mehdi, A.; Reye, C.; Thieuleux, C. Direct Synthesis of Functionalized Mesoporous Silica by Non-Ionic Assembly Routes, Quantitative Chemical Transformations within the Materials Leading to Strongly Chelated Transition Metal Ions. *Chem. Mater.* **16**, 159-166 (2004).
109. Jia, M.; Seifert, A.; Berger, M.; Giegengack, H.; Schulze, S.; Thiel, W. R. Hybrid Mesoporous Materials with a Unifom Ligand Distribution: Synthesis, Characterization, and Application in Epoxidation Catalysis. *Chem. Mater.* **16**, 877-882 (2004).
110. Huq, R.; Mercier, L.; Kooyman, P. J. Incorporation of cyclodextrin into mesostructured silica. *Chem. Mater.* **13**, 4512-4519 (2001).
111. Liu, C.; Naismith, N. Fu, L.; Economy, J. Ordered mesoporous organic-inorganic hybrid materials containing microporous functional calix[8] arene amides. *Chem. Commun.* **9**, 2472-2473 (2003).
112. Wirnsberger, G.; Scott, B. J.; Stucky, G. D. pH sensing with mesoporous thin films. *Chem. Commun.*, 119-120 (2001).
113. Boury, B.; Corriu, R. J. P.; Nunez, R. Hybrid Xerogels from Dendrimers and Arborols. *Chem. Mater.* **10**, 1795-1804 (1998).
114. Inagaki, S.; Guan, S.; Fukushima, Y.; Ohsuna, T.; Terasaki, O. Novel mesoporous materials with a uniform distribution of organic groups and inorganic oxide in their frameworks. *J. Am. Chem. Soc.* **121**, 9611-9614 (1999).
115. Melde, B. J.; Holland, B. T.; Blanford, C. F.; Stein, A. Mesoporous sieves with unified hybrid inorganic/organic frameworks. *Chem. Mater.* **11**, 3302-3308 (1999).
116. Asefa, T.; MacLachlan, M. J.; Coombs, N.; Ozin, G. A. Periodic mesoporous organosilicas with organic groups inside the channel walls.

Nature **402**, 867-871 (1999).
117. Yoshina-Ishii, C.; Asefa, T.; Coombs, N.; MacLachlan, M. J.; Ozin, G. A. Periodic mesoporous organosilicas, PMOs: Fusion of organic and inorganic chemistry 'inside' the channel walls of hexagonal mesoporous silica. *Chem. Commun.*, 2539-2540 (1999).
118. Temtsin, G.; Asefa, T.; Bittner, S.; Ozin, G. A. Aromatic PMOs: Tolyl, xylyl and dimethoxyphenyl groups integrated within the channel walls of hexagonal mesoporous silicas. *J. Mater. Chem.* **11**, 3202-3206 (2001).
119. Inagaki, S.; Guan, S.; Ohsuna, T.; Terasaki, O. An ordered mesoporous organosilica hybrid material with a crystal-like wall structure. *Nature* **416**, 304-307 (2002).
120. Kapoor, M. P.; Yang, Q.; Inagaki, S. Self-assembly of biphenylene-bridged hybrid mesoporous solid with molecular-scale periodicity in the pore walls. *J. Am. Chem. Soc.* **124**, 15176-15177 (2002).
121. Liang, Y.; Anwander, R. Synthesis of pore-enlarged mesoporous organosilicas under basic conditions. *Microporous and Mesoporous Materials* **72**, 153-165 (2004).
122. Muth, O.; Schellbach, C.; Froba, M. Triblock copolymer assisted synthesis of periodic mesoporous organosilicas (PMOs) with large pores. *Chem. Commun.*, 2032-2033 (2001).
123. Burleigh, M. C.; Markowitz, M. A.; Wong, E. M.; Lin, J.-S.; Gaber, B. P. Synthesis of periodic mesoporous organosilicas with block copolymer templates. *Chem. Mater.* **13**, 4411-4412 (2001).
124. Guo, W.; Park, J.-Y.; Oh, M.-O.; Jeong, H.-W.; Cho, W.-J.; Kim, I.; Ha, C.-S. Triblock copolymer synthesis of highly ordered large-pore periodic mesoporous organosilicas with the aid of inorganic salts. *Chem. Mater.* **15**, 2295-2298 (2003).
125. Bao, X.Y.; Zhao, X.S.; Li, X.; Chia, P. A.; Li, J. . A Novel Route toward the Synthesis of High-Quality Large-Pore Periodic Mesoporous Organosilicas. *J. Phys. Chem. B* **108**, 4684-4689 (2004).
126. Goto, Y.; Inagaki, S. Synthesis of large-pore phenylene-bridged mesoporous organosilica using triblock copolymer surfactant. *Chem. Commun.*, 2410-2411 (2002).
127. Wang, W.; Xie, S.; Zhou, W.; Sayari, A. Synthesis of Periodic Mesoporous Ethylenesilica under Acidic Conditions. *Chem. Mater.* **16**, 1756-1762 (2004).
128. Burleigh, M. C.; Markowitz, M. A.; Spector, M. S.; Gaber, B. P. Nanoporous organosilicas: Periodic materisl synthesized with surfactant templates in acidic media. *J. Phys. Chem. B* **106**, 9712-9716 (2002).

129. Kuroki, M.; Asefa, T.; Whitnal, W.; Kruk, M.; Yoshina-Ishii, C.; Jaroniec, M.; Ozin, G. A. Synthesis and properties of 1,3,5-benzene periodic mesporous organosilica (PMO): Novel aromatic PMO with three point attachments and unique thermal transformations. *J. Am. Chem. Soc.* **124**, 13886-13895 (2002).
130. Landskron, K.; Hatton, B. D.; Perovic, D. D.; Ozin, G. A. Periodic mesoporous organosilicas containing interconnected [Si(CH2)]3 rings. *Science* **302**, 266-269 (2003).
131. Asefa, T.; Kruk, M.; Coombs, N.; Grondey, H.; MacLachlan, M. J.; Jaroniec, M.; Ozin, G. A. Novel route to periodic mesoporous aminosilicas, PMAs: Ammonolysis of periodic mesoporous organosilicas. *J. Am. Chem. Soc.* **125**, 11662-11673 (2003).
132. Pang, J.; John, V. T.; Loy, D. A.; Yang, Z.; Lu, Y. Hierarchical mesoporous carbon/silica nanocomposites from phenyl-bridged organosilane. *Adv. Mater.* **17**, 704-707 (2005).
133. Kim, D.-J.; Chung, J.-S.; Ahn, W.-S.; Kang, G.-W.; Cheong, W.-J. Morphology control of organic-inorganic hybrid mesoporous silica by microwave heating. *Chem. Lett.* **33**, 422-423 (2004).
134. Zhang, L.; Zhang, W.; Shi, J.; Hua, Z.; Li, Y.; Yan, J.;. A new thioether functionalized organic-inorganic mesoporous composite as a highly selective and capacious Hg2+ adsorbent. *Chem. Commun.* **9**, 210-211 (2003).
135. Lu, Y.; Fan, H.; Doke, N.; Loy, D. A.; Assink, R. A.; LaVan, D. A.; Brinker, C. J. Evaporation-induced self-assembly of hybrid bridged silsesquioxane film and particulate mesophases with integral organic functionality. *J. Am. Chem. Soc.* **122**, 5258-5261 (2000).
136. Fukuoka, A.; Sakamoto, Y.; Guan, S.; Inagaki, S.; Sugimoto, N.; Fukushima, Y.; Hirahara, K., Iijima, S.; Ichikawa, M. Novel templating synthesis of necklace-shaped mono- and bimetallic nanowires in hybrid organic-inorganic mesoporous material [1]. *J. Am. Chem. Soc.* **123**, 3373-3374 (2001).
137. Gartmann, N.; Schutze, C.; Ritter, H.; Bruhwiler, D. The effect of water on the functionalization of mesoporous silica with 3-aminopropyltriethoxysilane. *J. Phys. Chem. Lett.* **1**, 379-382 (2010).
138. Liu, J.; Feng, X.; Fryxell, G. E.; Wang, L.-Q.; Kim, A. Y.; Gong, M. Hybrid mesoporous materials with functionalized monolayers. *Adv. Mater.* **10**, 161-165 (1998).
139. Gelest, Inc. Silane Coupling Agents: Connecting Across Boundaries. 2-20 (2006).

140. Lim, M. H.; Stein, A. Comparative studies of grafting and direct syntheses of inorganic-organic hybrid mesoporous materials. *Chem. Mater.* **11**, 3285-3295 (1999).
141. Sharma, K. K.; Anan, A.; Buckley, R. P.; Ouellette, W.; Asefa, T. Toward efficient nanoporous catalysts: Controlling site-isolation and concentration of grafted catalytic sites on nanoporous materials with solvents and colorimetric elucidation of their site-isolation. *J. Am. Chem. Soc.* **130**, 218-228 (2008).
142. Salmio, H.; Bruhwiler, D. Distribution of amino groups on a mesoporous silica surface after submonolayer deposition of aminopropylsilanes from an anhydrous liquid phase. *J. Phys. Chem. C* **111**, 923-929 (2007).
143. McKittrick, M. W.; Jones, C. W. Toward single-site functional materials - Preparation of amine-functionalized surfaces exhibiting site-isolated behavior. *Chem. Mater.* **15**, 1132-1139 (2003).
144. Gartmann, N.; Bruhwiler, D. Controlling and Imaging the Functional-Group Distribution on Mesoporous Silica. *Angew. Chem. Int. Ed.* **48**, 6354-6356 (2009).
145. Tanaka, S.; Kaihara, J.; Nishiyama, N.; Oku, Y.; Egashira, Y.; Ueyama, K. Incorporation of organic groups within the channel wall of spin-on mesostructured silica films by a vapor infiltration technique. *Langmuir* **20**, 3780-3784 (2004).
146. Acosta, E. J.; Carr, C. S.; Simanek, E. E.; Shantz, D. F. Engineering nanospaces: Iterative synthesis of melamine-based dendrimers on amine-functionalized SBA-15 leading to complex hybrids with controllable chemistry and porosity. *Adv. Mater.* **16**, 985-989 (2004).
147. Murata, S.; Kata, H.; Kimura, T.; Sugahara, Y.; Kuroda, K. Effective adsorption of chlorophyll a by FSM-type mesoporous silica modified with 1,4-butanediol. *Langmuir* **16**, 7106-7108 (2000).
148. Fukuoka, A.; Fujishima, K.; Chiba, M.; Yamagishi, A.; Inagaki, S.; Fukushima, Y.; Ichikawa, M. Photooxidation of cyclohexene and benzene with oxygen by fullerenes grafted on mesoporous FSM-16. *Catal. Lett.* **68**, 241-244 (2000).
149. Dufaud, V.; Davis, M. E.;. Design of heterogeneous catalysts via multiple active site positioning in organic-inorganic hybrid materials. *J. Am. Chem. Soc.* **125**, 9403-9413 (2003).
150. Corma, A.; Iborra, S.; Rodriguez, I.; Sanchez, F. Immobilized proton sponge on inorganic carriers: The synergic effect of the support on catalytic activity. *J. Catal.* **211**, 208-215 (2002).
151. Brunel, D.; Fajula, F.; Nagy, J. B.; Deroide, B.; Verhoef, M. J.; Veum,

L.; Peters, J. A.; Van Bekkum, H. Comparison of two MCM-41 grafted TEMPO catalysts in selective alcohol oxidation. *Appl. Catal. A* **213**, 73-82 (2001).
152. Motorina, I.; Crudden, C. M. Asymmetric dihydroxylation of olefins using cinchona alkaloids on highly ordered inorganic supports. *Org. Lett.* **3**, 2325-2328 (2001).
153. Mercier, L.; Pinnavaia, T. J. Access in mesoporous materials: Advantages of a uniform pore structure in the design of a heavy metal ion adsorbent for environmental remediation. *Adv. Mater.* **9**, 500-503 (1997).
154. Di Pasqua, A. J.; Sharma, K. K.; Shi, Y.-L.; Toms, B. B.; Ouellette, W.; Dabrowiak, J. C.; Asefa, T. Cytotoxicity of mesoporous silica nanomaterials. *Journal of Inorganic Biochemistry* **102**, 1416-1423 (2008).
155. Tao, Z.; Toms, B. B.; Goodisman, J.; Asefa, T. Mesoporosity and funtional group dependent endocytosis and cytotoxicity. *Chem. Res. Toxicol.* **22**, 1869-1880 (2009).
156. Verma, A.; Stellacci, F. Effect of surface properties on nanoparticle-cell interactions. *Small* **6**, 12-21 (2010).
157. Slowing, I. I.; Wu, C.-W.; Vivero-Escoto, J. L.; Lin, V.S-Y. Mesoporous silica nanoparticles for reducing hemolytic activity towards mammalian red blood cells. *Small* **5**, 57-62 (2009).
158. Veronese, F. M.; Pasut, G. PEGylation, successful approach to drug delivery. *Drug Discovery Today* **10**, 1451-1458 (2005).
159. Thomas, M. J. K.; Slipper, I.; Walunj, A.; Jain, A.; Favretto, M. E.; Kallinteri, P.; Douroumis, D. Inclusion of poorly soluble drugs in highly ordered mesoporous silica nanoparticles. *International Journal of Pharmaceutics* **387**, 272-277 (2010).
160. Heikkila, T.; Santos, H. A.; Kumar, N.; Murzin, D. Yu; Salonen, J.; Laaksonen, T.; Peltonen, L.; Hirvonen, J.; Lehto, V.-P. Cytotoxicity study of ordered mesoporous silica MCM-41 and SBA-15 microparticles on Caco-2 cells. *European Journal of Pharmaceutics and Biopharmaceutics* **74**, 483-494 (2010).
161. Yu, J.; Zhao, H.; Ye, L.; Yang, H.; Ku, S.; Yang, N.; Xiao, N. Effect of surface functionality of magnetic silica nanoparticles on the cellular uptake by glioma cells in vitro. *J. Mater. Chem.* **19**, 1265-1270 (2009).
162. Huang, D.-M.; Chung, T.-H.; Hung, Y.; Lu, F.; Wu, S.-H.; Mou, C.-Y.; Yao, M.; Chen, Y.-C. Internalization of mesoporous silica nanoparticles induces transient but not sufficient osteogenic signals in human mesenchymal stem cells. *Toxicol. Appl. Pharmacol.* **231**, 208-215

(2008).
163. Zhao, Y.; Trewyn, B. G.; Slowing, I. I.; Lin, V.S.-Y. Mesoporous silica nanoparticle-based double drug delivery system for glucose-responsive controlled release of insulin and cyclic AMP. *J. Am. Chem. Soc.* **131**, 8398-8400 (2009).
164. Slowing, I.; Trewyn, B. G.; Lin, V. S.-Y. Effect of surface functionalization of MCM-41-type mesoporous silica nanoparticles on the endocytosis by human cancer cells. *J. Am. Chem. Soc.* **128**, 14792-14793 (2006).
165. Wang, L.-S.; Wu, L.-C.; Lu, S.-Y.; Chang, L.-L.; Teng, I.-T.; Yang, C.-M.; Ho, J.-A. A. Biofunctionalized phospholipid-capped mesoporous silica nanoshuttles for targeted drug delivery: Improved water suspensibility and decreased nonspecific protein binding. *ACS Nano* **4**, 4371-4379 (2010).
166. Gao, H.; Shi, W.; Freund, L. B. Mechanics of receptor-mediated endocytosis. *PNAS* **102**, 9469-9474 (2005).
167. Trewyn, B. G.; Nieweg, J. A.; Zhao, Y.; Lin, V. S.-Y. Biocompatible mesoporous silica nanoparticles with different morphologies for animal cell membrane penetration. *Chemical Engineering Journal* **137**, 23-29 (2008).
168. Napierska, D.; Thomassen, L. C. J.; Rabolli, V.; Lison, D.; Gonzalez, L.; Kirsch-Volders, M.; Martens, J. A.; Hoet, P. H. Size-dependent cytotoxicity of monodisperse silica nanoparticles in human endothelial cells. *Small* **5**, 846-853 (2009).
169. Nel, A.; Xia, T.; Madler, L.; Li, N. Toxic potential of materials at the nanolevel. *Science* **311**, 622-627 (2006).
170. Tao, Z.; Morrow, M. P.; Asefa, T.; Sharma, K. K.; Duncan, C.; Anan, A.; Penefsky, H. S.; Goodisman, J.; Souid, A.-K. Mesoporous silica nanoparticles inhibit cellular respiration. *Nano Lett.* **8**, 1517-1526 (2008).
171. Eom, H.-J.; Choi, J. Oxidative stress of silica nanoparticles in human bronchial epithelial cell, Beas-2B. *Toxicology In Vitro* **23**, 1326-1332 (2009).
172. He, Q.; Shi, J.; Chen, F.; Zhu, M.; Zhang, L. An anticancer drug delivery system based on surfactant-templated mesoporous silica nanoparticles. *Biomaterials* **31**, 3335-3346 (2010).
173. Lin, Y.-S.; Haynes, C. L. Impacts of mesoporous silica nanoparticle size, pore ordering, and pore integrity on hemolytic activity. *J. Am. Chem. Soc.* **132**, 4834-4842 (2010).

174. Hudson, S. P.; Padera, R. F.; Langer, R.; Kohane, D. S. The biocompatibility of mesoporous silicates. *Biomaterials* **29**, 4045-4055 (2008).
175. Souris, J. S.; Lee, C.-H.; Cheng, S.-H.; Chen, C.-T.; Yang, C.-S.; Ho, J. A. A.; Mou, C.-Y.; Lo, L.-W. Surface charge-mediated rapid hepatobiliary excretion of mesoporous silica naoparticles. *Biomaterials* **31**, 5564-5574 (2010).
176. He, Q.; Shi, J.; Zhu, M.; Chen, Y.; Chen, F. The three-stage in vitro degradation behavior of mesoporous silica in simulated body fluid. *Microporous and Mesoporous Materials* **131**, 314-320 (2010).
177. Manzano, M.; Aina, V.; Arean, C. O.; Balas, F.; Cauda, V.; Colilla, M.; Delgado, M. R.; Vallet-Regi, M. Studies on MCM-41 mesoporous silica for drug delivery: Effect of particle morphology and amine functionalization. *Chemical Engineering Journal* **137**, 30-37 (2008).
178. Qu, F.; Zhu, G.; Huang, S.; Li, S.; Sun, J.; Zhang, D.; Qiu, S. Controlled release of Captopril by regulating the pore size and morphology of ordered mesoporous silica. *Microporous and Mesoporous Materials* **92**, 1-9 (2006).
179. Yang, P.; Gai, S.; Lin, J. Functionalized mesoporous silica materials for controlled drug delivery. *Chem. Soc. Rev.* **41**, 3679-3698 (2012).
180. Hata, H.; Saeki, S.; Kimura, T.; Sugahara, Y.; Kuroda, K. Adsorption of taxol into ordered mesoporous silicas with various pore diameters. *Chem. Mater.* **11**, 1110-1119 (1999).
181. Chen, L.; Zhu, G.; Zhang, D.; Zhao, H.; Guo, M.; Shi, W.; Qiu, S. Novel mesoporous silica spheres with ultra-large pore sizes and their application in protein separation. *J. Mater. Chem.* **19**, 2013-2017 (2009).
182. Katiyar, A.; Pinto, N. G. Visualization of size-selective protein separations on spherical mesoporous silicates. *Small* **2**, 644-648 (2006).
183. Gao, F.; Botella, P.; Corma, A.; Blesa, J.; Dong, L. Monodispersed mesoporous silica nanoparticles with very large pores for enhanced adsorption and release of DNA. *J. Phys. Chem. B* **113**, 1796-1804 (2009).
184. Andersson, J.; Rosenholm, J.; Areva, S.; Linden, M. Influences of material characteristics on ibuprofen drug loading and release profiles from ordered micro- and mesoporous silica matrices. *Chem. Mater.* **16**, 4160-4167 (2004).
185. Azais, T.; Tourne-Peteilh, C.; Aussenac, F.; Baccile, N.; Coelho, C.; Devoisselle, J.-M.; Babonneau, F. Solid-state NMR study of ibuprofen confined in MCM-41 material. *Chem. Mater.* **18**, 6382-6390 (2006).

186. Vallet-Regi, M.; Balas, F.; Arcos, D. Mesoporous Materials for Drug Delivery. *Angew. Chem. Int. Ed.* **46**, 7548-7558 (2007).
187. Xia, T.; Kovochich, M.; Liong, M.; Meng, H.; Kabehie, S.; George, S.; Zink, J. I.; Nel, A. E. Polyethyleneimine coating enhances the cellular uptake of mesoporous silica nanoparticles and allows safe delivery of siRNA and DNA constructs. *ACS Nano* **3**, 3273-3286 (2009).
188. Tourne-Peteilh, C.; Brunel, D.; Begu, S.; Chiche, B.; Fajula, F.; Lerner, D. A.; Devoisselle, J.-M. Synthesis and characterisation of ibuprofen-anchored MCM-41 silica and silica gel. *New J. Chem.* **27**, 1415-1418 (2003).
189. Katiyar, A.; Ji, L.; Smirniotis, P.; Pinto, N. G. Protein adsorption on the mesoporous molecular sieve silicate SBA-15: Effects of pH and pore size. *J. Chromatogr. A* **1069**, 119-126 (2005).
190. Okazaki, M.; Toriyama, K. Inhomogenous distribution and collective diffusion of solution molecules in the nanochannel of mesoporous silica. *J. Phys. Chem. B* **107**, 7654-7658 (2003).
191. Matsumoto, A.; Tsutsumi, K.; Schumacher, K.; Unger, K. K. Surface functionalization and stabilization of mesoporous silica spheres by silanization and their adsorption characteristics. *Langmuir* **18**, 4014-4019 (2002).
192. Liu, J.; Hartono, S. B.; Jin, Y. G.; Li, Z.; Lu, G. Q.; Qiao, S. Z. A facile vesicle template route to multi-shelled mesoporous silica hollow nanospheres. *J. Mater. Chem.* **20**, 4595-4601 (2010).
193. Angelos, S.; Khashab, N. M.; Yang, Y.-W.; Trabolsi, A.; Khatib, H. A.; Stoddart, J. F.; Zink, J. I. pH clock-operated mechanized nanoparticles. *J. Am. Chem. Soc.* **131**, 12912-12914 (2009).
194. Bae, Y.; Fukushima, S.; Harada, A.; Kataoka, K. Design of environment-sensitive supramolecular assemblies for intracellular drug delivery: Polymeric micelles that are responsive to intracellular pH change. *Angew. Chem. Int. Ed.* **42**, 4640-4643 (2003).
195. Kaihara, S.; Fisher, J. P.; Matsumura, S. Chemo-enzymatic synthesis of degradable PTMC-b-PECA-b-PTMC triblock copolymers and their micelle formation for pH-dependent controlled release. *Macromol. Biosci.* **9**, 613-621 (2009).
196. Tang, R.; Ji, W.; Panus, D.; Palumbo, R. N.; Wang, C. Block copolymer micelles with acid-labile ortho ester side-chains: Synthesis, characterization, and enhanced drug delivery to human glioma cells. *J. Controlled Release* **151**, 18-27 (2011).
197. Park, C.; Kim, H.; Kim, S.; Kim, C. Enzyme responsive nanocontainers

with cyclodextrin gatekeepers and synergistic effects in release of guests. *J. Am. Chem. Soc.* **131**, 16614-16615 (2009).
198. Vivero-Escoto, J. L.; Slowing, I. I.; Wu, C.-W.; Lin, V. S.-Y. Photoinduced intracellular controlled release drug delivery in human cells by gold-capped mesoporous silica nanosphere. *J. Am. Chem. Soc.* **131**, 3462-3463 (2009).
199. Aznar, E.; Marcos, Ma. D.; Martinez-Manez, R.; Sancenon, F.; Soto, J.; Amoros, P.; Guillem, C. pH- and photo-switched release of guest molecules from mesoporous silica supports. *J. Am. Chem. Soc.* **131**, 6833-6843 (2009).
200. Casasus, R.; Marcos, M. D.; Martinez-Manez, R.; Ros-Lis, J. V.; Soto, J.; Villaescusa, L. A.; Amoros, P.; Beltran, D.; Guillem, C.; Latorre, J. Toward the development of ionically controlled nanoscopic molecular gates. *J. Am. Chem. Soc.* **126**, 8612-8613 (2004).
201. Park, J.-H.; Lee, Y.-H.; Oh, S.-G. Preparation of thermosensitive PNIPAm-grafted mesoporous silica particles. *Macromol. Chem. Phys.* **208**, 2419-2427 (2007).
202. Chung, P.-W.; Kumar, R.; Pruski, M.; Lin, V. S.-Y. Temperature responsive solution partition of organic-inorganic hybrid poly(N-isopropylacrylamide)-coated mesoporous silica nanospheres. *Adv. Funct. Mater.* **18**, 1390-1398 (2008).
203. Sierocki, P.; Maas, H.; Dragut, P.; Richardt, G.; Vogtle, F.; De Cola, L.; Brouwer, F.; Zink, J. I. Photoisomerization of azobenzene derivatives in nanostructured silica. *J. Phys. Chem. B* **110**, 24390-24398 (2006).
204. Collier, C. P.; Mattersteig, G.; Wong, E. W.; Luo, Y.; Beverly, K.; Sampaio, J.; Raymo, F. M.; Stoddart, J. F.; Heath, J. R. A [2]catenane-based solid state electronically reconfigurable switch. *Science* **289**, 1172-1175 (2000).
205. Perez, E. M.; Dryden, D. T. F.; Leigh, D. A.; Teobaldi, G.; Zerbetto, F. A generic basis for some simple light-operated mechanical molecular machines. *J. Am. Chem. Soc.* **126**, 12210-12211 (2004).
206. Collin, J.-P.; Laemmel, A.-C.; Sauvage, J.-P. Photochemical expulsion of a Ru(phen)2 unit from a macrocyclic receptor and its thermal reco-ordination. *New J. Chem.* **25**, 22-24 (2001).
207. Murakami, H.; Kawabuchi, A.; Matsumoto, R. Ido, T.; Nakashima, N. A multi-mode-driven molecular shuttle: Photochemically and thermally reactive azobenzene rotaxanes. *J. Am. Chem. Soc.* **127**, 15891-15899 (2005).
208. Radu, D. R.; Lai, C.-Y.; Wiench, J. W.; Pruski, M.; Lin, V. S.-Y.

Gatekeeping Layer Effect: A Poly(lactic acid)-coated Mesoporous Silica Nanosphere-Based Fluorescence Probe for Detection of Amino-Containing Neurotransmitters. *J. Am. Chem. Soc.* **126**, 1640-1641 (2004).

209. Descalzo, A. B.; Jimenez, D.; Marcos, M. D.; Martinez-Manez, R.; Soto, J.; El Haskouri, J.; Guillem, C.; Beltran, D.; Amoros, P.; Borrachero, M. V. A new approach to chemosensors for anions using MCM-41 grafted with amino groups. *Adv. Mater.* **14**, 966-969 (2002).
210. Rodman, D. L.; Pan, H.; Clavier, C. W.; Feng, X.; Xue, Z.-L. Optical metal ion sensor based on diffusion followed by an immobilizing reaction. Quantitative analysis by a mesoporous monolith containing functional groups. *Anal. Chem.* **77**, 3231-3237 (2005).
211. Mercier, L.; Pinnavaia, T. J. Heavy metal ion adsorbents formed by the grafting of a thiol functionality to mesoporous silica molecular sieves: Factors affecting Hg(II) uptake. *Environ. Sci. Technol.* **32**, 2749-2754 (1998).
212. Kang, T.; Park, Y.; Choi, K.; Lee, J. S.; Yi, J. Ordered mesoporous silica (SBA-15) derivatized with imidazole-containing functionalities as a selective adsorbent of precious metal ions. *J. Mater. Chem.* **14**, 1043-1049 (2004).
213. Rodriguez-Lopez, G.; Marcos, M. D.; Martinez-Manez, R.; Sancenon, F.; Soto, J.; Villaescusa, L. A.; Beltran, D.; Amoros, P. Efficient boron removal by using mesoporous matrices grafted with saccharides. *Chem. Commun.* **10**, 2198-2199 (2004).
214. Mornet, S.; Vasseur, S.; Grasset, F.; Duguet, E. Magnetic nanoparticle design for medical diagnosis and therapy. *J. Mater. Chem.* **14**, 2161-2175 (2004).
215. d their micelle formation for pH-dependent controlled release. *Macromol. Biosci.* **9**, 613-621 (2009).

„New trends in supramolecular chemistry"
Edited by Volodymyr I. Rybachenko
Donetsk 2014, East Publisher House, ISBN 978-966-317-208-8

Chapter 6

Application of mesoporous silica nanoparticles for drug delivery

Dawid Lewandowski and Grzegorz Schroeder
Adam Mickiewicz University in Poznań, Faculty of Chemistry, Umultowska 89b, 61-614 Poznań

1. Introduction

Since the discovery of the MCM-41s silicas in 1992, the synthesis of mesoporous silica materials has developed rapidly. The best known families of mesoporous silicas include MCM-n[1], MSU-n (Michigan State University silica)[2], KIT-1 (Korean Institute of Technology)[3], SBA-n (Santa Barbara amorphous silica)[4], IBN (Institute of Bioengineering and Nanotechnology)[5], FDU-n (Fudan University)[6], KSW silicas[7], FSM[8] and HMS[9] silicas. Each of them has its own unique advantages and disadvantages, and all have found a variety of applications.

Mesoporous nanoparticles have been found particularly interesting from the point of view of applications in medicine because of their increased mechanical strength, chemical stability, tunable particle size, uniform and tunable pore sizes, high surface areas, large pore volumes, two functional surfaces – an internal one in the pores and an external one on the exterior particle surface, porous structure enabling controlled cargo delivery, biocompatibility and higher resistance to microbial attack comparing to their organic (polymeric) equivalents[10]. Additionally, the silica matrix protects entrapped molecules against denaturation or enzymatic degradation induced by external pH and temperature[11].

Multiple nanocomponents with diagnostic and therapeutic functions can be combined into a single nanosystem. These systems follow on the concept of a "theranostic" device, in which both diagnostic and therapeutic functions can be administered in a single dose[12].

2. Synthesis and surface properties of the mesoporous silica nanoparticles

2.1. General synthetic approaches

According to the International Union of Pure and Applied Chemistry (IUPAC), a mesoporous material is defined as a porous material with pore diameters between 2 and 50 nm.

There are three main synthetic routes to the synthesis of mesoporous silica nanoparticles. The first one, the so-called "modified Stöber method", involves the condensation of silicon source (TEOS, TMOS, etc.) in a basic medium in the presence of a cationic structure directing agent[13], which yields monodisperse spherical particles with sizes in the 50-200 nm range, containing pores of about 2 nm in diameter. More useful in plant-scale is the use of the spray-drying process[14]. This method involves spraying a homogenized precursor solution containing the inorganic compounds and relevant additives within a specially designed chamber at above the boiling point of the solvent. The particle size is determined mainly by the droplet size sprayed into a chamber, however diameters below 250 nm are difficult to achieve and the particle size distribution is poor[15]. Another method for the production of nanoparticles is microemulsion process. This approach has been used for synthesis of metallic nanoparticles[16] as well as magnetic and superconductor nanoparticles[17]. Microemulsions are produced spontaneously without the need for mechanical agitation, making it a rather simple technique. The technique is useful for large-scale production and uses relatively simple and inexpensive equipment that result in high yields with homogenous particle size distribution[18].

Two main approaches have been used to avoid secondary aggregation during the synthesis: a) carrying out the synthesis in highly diluted solutions and b) the use of particle growth quenchers. Performing the synthesis under dilute conditions gives reproducible results for producing monodisperse particles in the laboratory scale, but up-scaling of the synthesis may become difficult. In this case, the use of particle growth quenchers, like non-ionic surfactants or polymers[19,20], fluorocarbon-based cationic surfactants[21], triethanolamine[22], propanetriol[23] etc. is an alternative.

The last step of all synthetic approaches is the surfactant removal and it leads to two-dimensional hexagonal organization of cylindrical mesopores typical of MCM-41-type materials[1]. Elimination of the structure directing agent is normally carried out by solvent extraction, as calcination can lead to inter-particle condensation. Thermal decomposition can also lead to decomposition of organic moieties incorporated during the co-condensation reactions, which normally is undesired. Dialysis has also been shown to be an attractive method for surfactant removal in the case of very small nanoparticles (<20 nm), which

otherwise tend to aggregate irreversibly during repeated centrifugation and re-dispersion cycles[24].

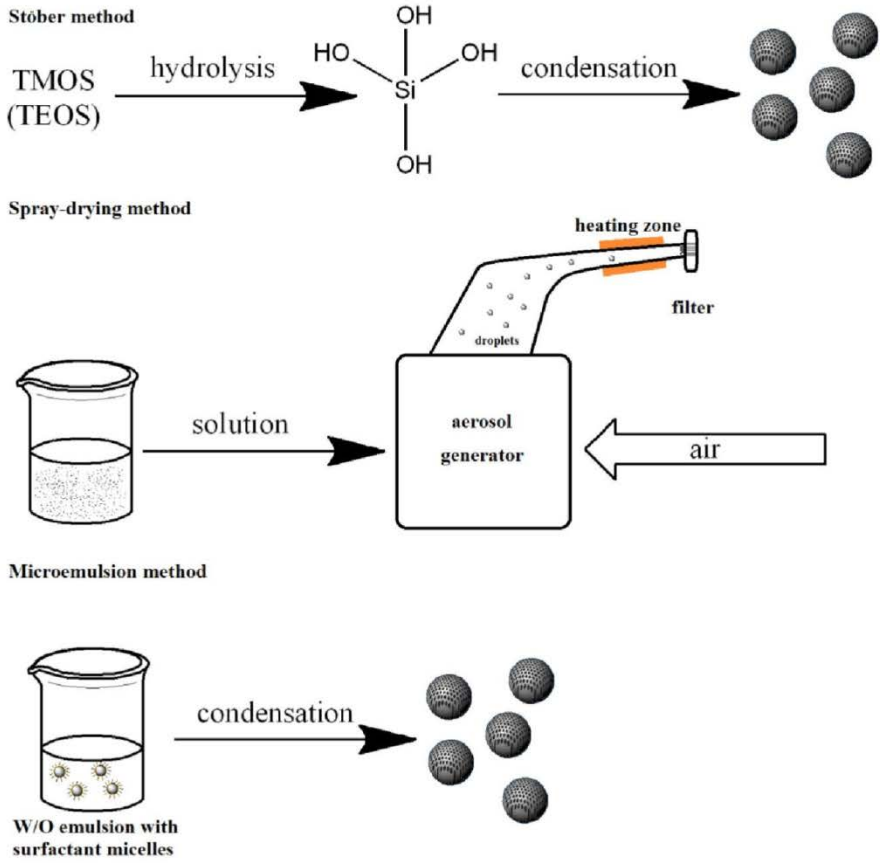

Figure 1. General synthetic approaches to the synthesis of mesoporous silica nanoparticles.

2.2. Surface properties and characterization

Nanoparticles are often defined as materials with two or three dimensions between 1 and 100 nm and showing specific properties related to their size, shape and chemical composition. Indeed, it is generally assumed that the size of nanoparticles allows them to easily enter and pass through tissues, cells and organelles as this size is comparable to that of many biological molecules and structures.

Native mesoporous silica nanoparticles typically have a high surface concentration of silanol groups (approximately 5 per nm^2, measured using the proton-deuterium exchange method[25]), especially when not calcined, and the process of the particles drying can easily lead to formation of siloxane bridges between the particles. Surface silanol groups show different acidic properties, for example SBA-15 silica analyzed by Rosenholm *et al.*[26] is characterized by two different pK_a values. One pK_a of 8.2 describes the $Si-(OH)_2$ groups that represent over 80% of all silanol moieties covering the silica nanoparticles surface. The other 18% of Si-(OH) groups are characterized by pK_a near 2.0. These two pK_a values result in silica's negative charge in most biological systems (≈7.4 in physiological pH and lower than 7.0 under most pathological conditions)[27].

The surface functional organic groups, which can be attached to the surface through the post-synthetic grafting process or by using the co-condensation method, are employed to fulfill specific tasks in medical appliations[28]: a) to increase the host-guest affinity when drugs are adsorbed in the mesoporous channels to enhance drug adsorption and/or slow down drug release rates, b) to chemically graft functional molecules inside or outside the pores, c) to control the surface electrical charge of particles, d) to link nanogates at the mesopore entrances to prevent premature release of entrapped cargo.

Characterization of unloaded mesoporous silica usually means specification of its chemical composition and pore network structure. Spectroscopic methods, such as nuclear magnetic resonance spectroscopy, Raman spectroscopy and Fourier transformation infrared spectroscopy have been widely used to characterize the chemical groups on the surfaces of these materials. High surface area and the high number of attached species make its characterization relatively easy although heterogeneity of the surface can complicate interpretation of results.

The pore structure is often characterized by electron microscopy imaging (transmission electron microscopy (TEM) or SEM) or nitrogen sorption measurements. Imaging methods provide valuable information about the morphology of the pores, unobtainable by other methods. Nitrogen sorption measurements give statistically strong results for pore sizes and can also characterize the pore volume and surface area of the materials. It also informs about pore blocking effects when reduction in pore diameter and pore volume is observed. Mesoporous structures can also be characterized by a few other methods such as mercury intrusion porosimetry, thermoporometry and NMR cryoporometry[29].

X-ray diffraction (XRD) is frequently used for characterization of ordered mesoporous silica materials. Although the pore walls consist of amorphous

silica, the pore order gives rise to a diffraction pattern following the Babinet's principle. XRD provides information about the regularity of the structure and the mean distance between adjacent pore centers. This repeat distance along with the pore diameter can be used to determine the pore wall thickness.

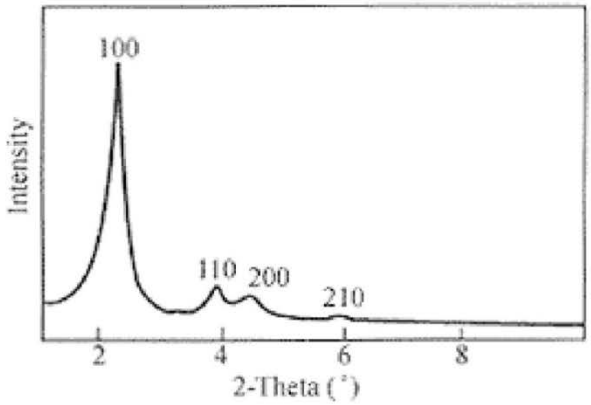

Figure 2. Typical XRD pattern of MCM-41 mesoporous silica.

Particle size and morphology can also play a role in drug delivery applications. Particle size is typically characterized by different techniques, e.g. imaging, sieving, dynamic light scattering and laser diffraction[29]. Particle morphology characterization relies mostly on imaging by optical or electron microscopy methods.

The characterization of drug loaded carriers is connected with drug-carrier interactions, the amount and physical characteristics of the loaded drug. Drug-carrier interactions can be determined with FTIR or by determining the adsorption isotherms of the model adsorbate (drug), which can provide important information about the possible sorption mechanism - chemisorption or physisorption.

Measuring the drug loading degree of the carrier includes extraction and thermogravimetry (TG) as the most commonly applied methods. In extraction, drug is released from the carrier and the drug concentration in the medium to which it has been released is measured by UV/VIS spectroscopy or other techniques. High performance liquid chromatography (HPLC) is frequently used for drug concentration assay since it is also able to provide information about the possible degradation of the cargo molecules. While using the extraction method, care should be taken that all of the cargo material has been extracted from the

silica; quite often the release is incomplete. In TG, the weight of the sample is measured as a function of temperature. The mass of the loaded drug can be calculated because the thermal decomposition of the organic drug takes place at lower temperatures than the degradation of the carrier[29].

Knowledge of the state of the drug in the mesoporous carrier is of the utmost importance. A poorly soluble drug located on the external surface of the carrier particle can inhibit or block the release of the drug from the pores by forming crystallites larger than the molecules inside the pores. This is usually characterized by XRD and differential scanning calorimeter (DSC). Both methods can be used to detect crystalline phases and size of the crystallites in the loaded materials. An advantage of DSC in this context is that it is more sensitive to detection of material of small crystallite size. In addition, pycnometry, nitrogen sorption and NMR can be used to obtain information about the loaded drugs[29].

3. Biocompatiblity and toxicology issues

The term "biocompatible" means that the nanoparticles must display limited toxicity to the organism at their effective dose, they must be able to accomplish their function without interference from the organism's defense mechanisms, and they must be able to circulate sufficiently long to perform their intended task – they should not be eliminated or undergo hydrolysis under biological conditions and the targeting or imaging groups attached to their surface, as well as the drug inside the pores, have to remain associated with the nanoparticles until it reaches its target site in order for the targeting/delivery to be efficient. A key requirement for intravenously administered nanotherapeutics is that they are able to circulate in the bloodstream for >2 hours; if they are filtered out by the liver or the kidneys they cannot make it to the intended site of action[30]. Shape, size and charge are all factors in determining how long a given nanoparticle will circulate before being absorbed by the cells and, after performing its task, eliminated by the liver, kidneys or spleen. The cellular uptake and distribution of the mesoporous silica nanoparticles can be studied by attaching fluorescent dye molecules (e.g. fluorescein isothiocyanate and Rhodamine B) to them, to permit visualization of the particles by fluorescence and confocal microscopy[31].

3.1. Factors influencing the cytotoxicity of mesoporous silica nanoparticles

Several articles have reported the influence of size dependent cellular uptake and toxicity, but the results have not proved whether larger or smaller particles are more toxic. For human monocyte-derived dendritic cells, the so-called size effect holds which means that larger micron sized silica particles (2.5 μm) are

more toxic than smaller submicron (270 nm) sized ones. Moreover, for particles of either size the toxicity increased with increasing concentration[32]. Size effect can also be observed when human endothelial cells are used with amorphous silica particles. Silica particles below 20 nm were much more toxic than those of 104 and 335 nm in size. These larger particles showed very little toxic effects[33]. The use of particles from the submicron range below 500 nm is recommended as they are easily taken up by the cell through endocytosis and can be seen localised in the lysosomes of the cell[34]. In another study, Mou and co-workers synthesized ordered monodispersed mesoporous silica nanoparticles of uniform sizes in the range from 30 to 280 nm (most of which had hexagonally ordered structures, except for the 30-nm sized particles, which had predominantly worm-like mesostructures), and they then investigated their uptake by HeLa cells. While the cell proliferation and viability were found to be unchanged at a dosage of 100 μg/mL for all the silica particles despite their differences in size, their cellular uptakes varied with sizes in the order of 50 > 30 > 110 > 170 nm[35]. These results clearly indicate that endocytosis of silica particles is virtually a complicated process, determined by many more factors than just the particle size of the mesoporous silicas. Also their *in vivo* biodistribution is influenced by the surface charge and size. To date, only a few authors have addressed the influence of these parameters on in vivo behavior of these potential drug carriers. Mesoporous nanoparticles in the size range of 50–100 nm possessing a relative positive charge have been shown to mainly be targeted to the liver after intravenous injections[36] while 50–200 nm non-porous silica particles were shown to be cleared to urine and bile over time, in a size dependent manner[37]. Smaller particles were preferably cleared by the urine and bile, whereas larger particles were trapped by macrophages and accumulated in the liver and spleen where they remained up to 4 weeks after injection. 130–180 nm mesoporous silicon particles were shown to be cleared from the body within 4 weeks after intravenous injections[38]. It was contributed to disintegration of the particles followed by renal clearance.

Particle cytotoxicity is also influenced by the surface charge. Cationically modified silica nanoparticles exhibit lower cytotoxicity in cellular assays than non-functionalized ones[39]. In the case of mesoporous silica nanoparticles, no significant cell death was observed to have been caused by amino-functionalized particles, indicating that positively charged amines reduce the toxicity of mesoporous silica in *in vitro* conditions. As-synthesized particles with negative surface charge in physiological conditions, influenced the cell growth with a recovery of cell viability over time, while exposure to amino-functionalized particles was not shown to induce a noticeable cell death until longer incubation

when a high dosage of 200 $\mu g*mL^{-1}$ was applied. Also Pasqua *et al.*[40] have found that unmodified mesoporous silica was more cytotoxic than thiol- or amino-functionalized silica.

Nanoparticles of different morphologies interacted differently with cell membranes that are the first physical barriers that need to be penetrated by silica particles. This hypothesis was tested and confirmed in several experimental papers. Huang *et al*[41] showed different cellular uptakes and subsequent cellular responses to mesoporous silica nanoparticles with three different aspect ratios. The particles of the aspect ratios 1:1, 2:1, and 4:1, with dimensions ranging from 100 × 100 nm to 100 × 450 nm and of surface areas ranging from 791 to 1169 m^2*g^{-1} were all effciently ingested by A375 human melanoma cells via encapsulation within endosomes, while the particles with higher aspect ratios entered the cells faster than those with lower aspect ratios. Moreover, the particles with higher aspect ratios destroyed the cytoskeleton of the cells and induced more cytotoxicity in a dose-dependent manner. The mesoporous silica-treated cells also expressed less melanoma adhesion proteins comparing to the untreated cells. The particles with higher aspect ratios resulted in much less protein expression, although they did not influence the levels of mRNA concentrations, suggesting that some damage to protein translation or post-translational modification was dependent on the shapes of the mesoporous silica nanoparticles. General conclusions about the effect of shapes of silica particles on cells cannot be easily drawn and require consideration of several other parameters including cell type and material composition.

3.2. Factors influencing the biodistribution and the hemolytic activity

As yet no detailed analyses of biodistribution of differently charged mesoporous silica nanoparticles have been made. Generally, negatively charged surfaces should be less bioreactive avoiding cellular interactions that can give rise to unspecific toxicity. Positively charged particles are expected to be more prone to interact with the reticuloendothelial system (RES) and induce an immune response. High absolute charge, either positive or negative, is prone to disable the so-called "stealth" properties of any particle[42], by increasing the protein adsorption (opsonization) on the particles, a property known to be induced also by hydrophobicity. Critical evaluation of how electrostatic charge of mesoporous silica nanoparticles affects biodistribution is needed to avoid accumulation in healthy organs, disruption of biological membranes and undesired activation of immune response.

Protein adsorption to the mesoporous silica nanoparticles under physiological conditions is an important problem that must be avoided because it would

decrease the targetability of the particles, as well as increase the recognition of the particles as foreign by the body defense mechanisms, which would lead to their rapid removal from the blood circulation. In addition, protein adsorption onto the silica's surface may also influence its toxicity. The PEGylation (PEG-functionalization) of nanoparticles has been frequently used as a general and effective approach to reduce the nonspecific binding of nanoparticles to blood proteins and macrophages. This reduction is caused by the steric hindrance and repulsion effects of PEG chains against blood proteins and macrophages, which are closely correlated to the PEG molecular weight, surface chain density and conformation[28].

The effect of mesoporous silica materials on hemolytic activity is important in order to understand how the materials will interact with blood. Lin and Haynes have found significant effects of silica particles size, porosity and dosage on the hemolytic activity. They reported that mesoporous silica nanoparticles with ordered structures show lower activity compared with the solid nonporous particles of similar size because of the smaller amount of silanol groups on the external surface. The addition of poly-ethylene glycol (PEG) coatings can help to overcome the hemolysis[43]. Hemolytic assays have recently been made with hollow mesoporous silica. Again, at low dosages (up to 1600μg*ml^{-1}) these hollow mesoporous silica showed no effect on the activity of the red blood cells[44]. He *et al.* obtained similar results, that is they reported a significant influence of PEGylated particles on the nonspecific serum binding and proved that these particles showed significantly reduced hemolysis rate compared to non PEGylated particles[45]. Tang *et al.* tested the *in vivo* effect of differently shaped and PEGylated MSNs on blood, hematology and serum biochemical indicators in 1 day and 18 days after the intravenous administration of MSNs[46]. All hematology markers, such as RBC, HGB, HCT, MCV, MCH, MCHC, PLT and WBC, took values mostly within the normal ranges and did not show significant trends of toxicity of all tested samples, indicating the excellent biocompatibility in hematology.

Due to the leaky vasculature and poorly operational lymph system of tumors, nanoparticles can exit the blood vessels and accumulate at the tumor site by passive targeting *via* the enhanced permeability and retention (EPR) effect. The diffusion rate in the extracellular spaces of the tumor is determined by the size and the surface charge of the particles. Small particles easily diffuse out and in of the tumor vasculature and within the tumor institium and the active concentration of the drug carrier at the tumor site might be low. Free movement is also affected by surface charge and negatively charged or weakly positively charged particles in the 50–150 nm range easily pass through the tumor tissue[47].

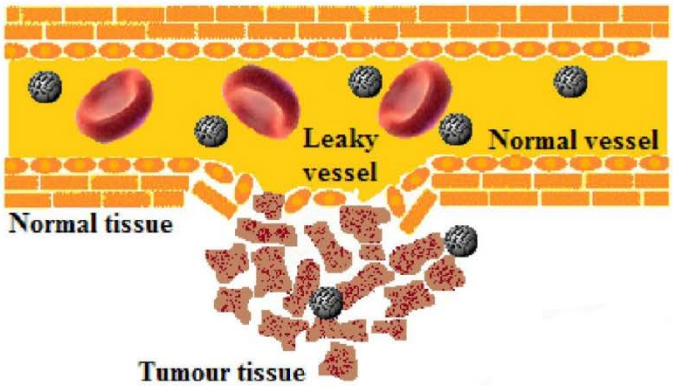

Figure 3. Scheme presenting enhanced permeability and retention effect in tumour tissues.

3.3. Elimination of mesoporous silica nanoparticles and their degradation in biological environment

Once the mesoporous silica nanoparticles have reached their target, it is important to know the kinetics of the particles removal from the cells. It is clear that the extracellular dissolution kinetics is different, probably much faster, than that of the intracellular one due to the limited liquid volume inside the cell, but this topic remains the focus of future studies[48].

Although only a few authors have studied the phenomenon of exocytosis of nanoparticles, there have been some reports on exocytosis of mesoporous silica nanoparticles in different cell lines. Slowing *et al.*[49] have studied the exocytosis of particles by normal (HUVEC) and cancerous (HeLa) cells and reported two interesting findings. The first is that, the particles were found to be ingested by the cells and reached a constant intracellular amount within 2 h, indicating the attainment of a balance between the rates of endocytosis and exocytosis of the particles (or equilibrium) in 2 h of incubation time. The second is that the exocytosis as well as transcytosis of mesoporous silica nanoparticles were found to be much more effcient in healthy HUVEC cells than in malignant HeLa cells.

Etienne and Walcarius[50] have studied the dissolution of mesoporous silica in water as a function of pH, both for as-synthesized silica and amino-functionalized one, and showed that amino-functionalized silica dissolved at a faster rate than pure silica particles under biologically relevant pH conditions. For the aminosilane functionalized particles as much as 2/3 of the amino- groups were already found in the supernatant 4h into the experiment, after which the concentration of amino species in solution reached a plateau. Thus, not all amino-functions were dissolved in solution, but clearly factors such as particle

surface charge could be expected to have dramatically influenced the process. He *et al.*[51] have reported a three-stage degradation behavior of mesoporous silica nanoparticles in simulated body fluid. Also this study revealed rapid initial bulk degradation, followed by the deposition of calcium/magnesium silicate layer, which drastically reduced (or counteracted) the degradation rate, similarly to the observations of Onida *et al.*[52]. The third stage involved a maintained slow diffusion of dissolved silica species detected as free Si, whereas the whole sample was degraded after 15 days when immersed in an aqueous solution at a concentration of 0.5 mg*ml-1. Importantly, the particle morphology remained intact after 24h even though hollowing out and enlargement of the mesopores was clearly observed.

Suspended silica is known to be adsorbed or excreted by the body. Several reports have supported elimination of MSNs through renal excretion. Mamaeva *et al.* have shown quite rapid renal clearance of particles (250–350 nm) injected both intravenously and peritumorally with a peak at 42–72 h depending on the functionalization. PEI functionalized particles were more rapidly eliminated than folate tagged particles[53]. He *et al.* have shown that differently modified amorphous silica nanoparticles (OH-Si, COOH-Si and PEG-Si) with a size of approximately 45 nm were all partly excreted through the urine[54].

Mesoporous silica nanoparticles have also been reported to be eliminated by hepatobiliary route although that process appeared to be slower and showed a peak at 4 days after intravenous injection[55]. Lo and coworkers have studied the effect of the surface charge on the two proposed elimination routes of mesoporous silica nanoparticles and found that particles (size 50–100 nm) with high positive charge showed rapid hepatobiliary excretion and reached the peak of excretion at 2 days post injection[56]. Although both particles were sequestered by the liver, the one with the higher charge could have been more opsonized by serum proteins and thus more amenable to hepatobiliary excretion into the gastrointestinal tract. In conclusion, this shows that the surface charge regulates the rate of excretion.

4. Application of mesoporous silica nanoparticles in drug delivery systems

4.1. General methods for preparation of drug delivery systems

In general there are two main approaches to incorporate a drug or diagnostic entity in a nanoparticle[30]: to stick it to the surface of a silica nanoparticle, or to encapsulate it in a porous nanostructure. These approaches can be illustrated by the two methods of carrying goods on ships in the macroscopic world: we either stack the cargo on the deck of a barge or we place it in the closed container of a tanker. As with shipping in a macroscopic world, the solution

chosen to carry a nanocargo depends on the characteristics of the cargo and the delivery requirements. A reactive or antigenic drug should be isolated from the environment in some sort of container vessel until it reaches its "port," whereas an imaging agent attached to the external surface of a barge-like vessel can be more readily accessed and more rapidly released in response to physiological stimuli.

One concept that does not translate well to the macroscopic shipping analogy, is the carrying capacity. For a macroscopic sphere, many more molecules can be contained in the inner volume than can be adsorbed on the surface. As the sphere gets smaller, the space available to load a drug in the interior volume decreases with the sphere radius to the third power and on the surface with its radius squared. That is why when the diameter of the sphere approaches the molecular dimensions, more molecules can be placed on the surface than can be contained in the inner volume.

Table 1. Comparison of the number of molecules trapped inside of a sphere and adsorbed on its surface at different radii values. The volume occupied by a single molecule assumed to be 2 nm^3 (1 nm X 1 nm X 2nm) and the surface - 1 nm^2 (1 nm X 1 nm)

Sphere radius	**Number of molecules trapped inside the sphere (N_I)**	**Number of molecules adsorbed on the external and internal sphere surface (N_S)**	**N_I:N_S ratio**
1 m	$2.618*10^{26}$	$6.284*10^{18}$	$4.166*10^{7}$
1 mm	$2.618*10^{17}$	$6.284*10^{12}$	$4.166*10^{4}$
100 nm	$2.618*10^{5}$	$6.284*10^{4}$	4.166

Nevertheless, nanoparticles of a size equal to 100 nm or more, with an empty interior, the so-called hollow mesoporous silica spheres, are known to store more cargo than conventional mesoporous silicas thanks to their voids inside the shells and mesoporous channels at the shells providing accessibility without blocking (channels in conventional mesoporous silica are much longer and can be easily blocked by molecules occupying pore entrances). Despite lower surface area ($436 m^2*g^{-1}$) relative to that of MCM-41 ($1152\ m^2*g^{-1}$) hollow mesoporous spheres can deliver as much cargo as conventional mesoporous silicas ($302\ mg*g^{-1}$ for hollow mesoporous silica and $358\ mg*g^{-1}$ for MCM-41)[57]. When surface areas are comparable, the hollow mesoporous silica's capacity is even much larger than that of MCM-41 ($1133\pm52.4\ mg*g^{-1}$ of ibuprofen adsorbed by hollow mesoporous silica and $337\ mg*g^{-1}$ by MCM-41)[58].

Until now, simple surface adsorption has been used much more often

than encapsulation of a cargo in the hollow mesoporous silica spheres. A few procedures for loading a cargo onto the silica's surface have been proposed. In the method of incipient wetness impregnation, a very concentrated drug solution is used to obtain a high loading degree, where the drug concentration is usually close to its solubility limit. Capillary action draws the solution into the pores together with the drug molecules. The interactions between the cargo molecules and the silica particle usually include hydrogen bonding and electrostatic interactions.

The impregnation method is preferred when only small amounts of the drug are available. It is easy to determine the amount of the loaded drug in advance, but a disadvantage of the method is the difficulty to control the uniformity of the drug distribution. Moreover, the residual drug can recrystallize on the external surface of mesoporous materials after repeatable solvent evaporation.

In the melt method, a physical mixture of drug and mesoporous carrier is heated above the melting point of the drug. To some extent, this method can be considered as a special case of the impregnation method. However, many drugs cannot withstand melting without degradation. In addition, the drug molecules loaded from melt are distributed less homogenously on the pore surfaces if the molten drug has high viscosity. In this case most of the drug molecules pack on the surface close to the pore opening and can undergo recrystallization. Thus, the drug materials loaded from the melt have a bit slower release rate. However, if the molten drug has low viscosity such as ibuprofen, the effect of the drug loading method on the physical state and release profile of the drug is minor[29]

Controlled release systems based on mesoporous silica nanoparticles are more useful than simple, unmodified silicas loaded with drug molecules. They have been developed by applying mechanical controls over the pore openings. First, polymers that are either adsorbed or covalently bonded to the surface of the silica particles have served as a mechanized controlled release system[59]. Under their "close" condition, the polymer chains tightly wrap around the particle surface, each blocking multiple pore openings. Then the polymers are induced by certain stimuli to undergo swelling or coiling so that the pore openings are re-exposed and cargo is released through the unblocked pores. The second method to achieve controllable release is to form chemical bonds directly over the pore openings so that they can later be cleaved upon stimulation[60]. The third way to mechanically block the pores is to attach bulky groups such as Au or CdS nanocrystals over the pore openings[61]. These bulky groups serve as gatekeepers for the encapsulated cargo. Removal of the bulky blocking groups *via* chemical methods initiates cargo release.

Targeting is especially relevant in the context of cancer therapies, as most of

the commonly used anticancer drugs have serious side-effects due to unspecific action on healthy cells. The selectivity is a key ability of the nanoparticles to be internalized by the targeted cell population. Active targeting requires the knowledge of which receptors are overexpressed on the outer cell membrane for a given cancer type. Different moieties, such as peptides, antibodies or more simple molecules, such as folic acid can be attached to the silica surface and used as targeting agents. The folate receptor has been found to be overexpressed on the surface of several cancer cell types, such as ovarian, endometrial, colorectal, breast, lung, renal cell carcinoma, brain metastases derived from epithelial cancer, and neuroendocrine carcinoma[62,63].

4.2. Factors influencing the adsorption and release of cargo molecules

There are many physicochemical parameters affecting adsorption and release of cargo from mesoporous silicas: pore size, particle size and morphology, pore structure, pore volume, surface area, surface functionalization, pH at which the adsorption is carried out, molecule's polarity and surface polarity[64].

The maximum loading degree, i.e., the ratio of the drug mass to the total mass of the drug loaded carrier when the pores are totally filled, can be estimated on the basis of the pore volume of mesoporous carriers and the packing density of the payload drug. However, the ultimate density of the drug is difficult to estimate as it usually differs from the density of the crystalline drug. Loading degrees as high as 60 wt.% can be obtained for the carriers with very high porosity. As the inorganic mesoporous carriers are denser than the organic drugs, the loading degrees higher than 60 wt.% is difficult to obtain. The loading method also affects the loading degree obtained, the packing of the molecules in the pores as well as their distribution in the carrier. This naturally affects the release kinetics; the more disordered the structure, the faster the release is taking place[29].

The drug molecules physically adsorbed on the surfaces of mesoporous materials from organic solvents form multilayers or (typically) monolayers can be modeled using a Langmuir adsorption isotherm[65]. Monolayer adsorption onto the pore walls has also been observed for proteins from aqueous solutions[66]. In the case of a monolayer, the loading capacity increases with increasing the surface area[65]. Thus, the pore volume of the materials has no effect on the drug loading.[29] For more hydrophilic drugs, the pH-matching in aqueous solvent can be used to reach higher drug loading levels than possible from organic media[67]. Many studies have highlighted the possibility of using these kinds of specific interactions between the drug and functional groups present on the pore wall also for controlling the drug release process. In most cases, the vast majority of

the groups present on the silica surface even functionalized mesoporous particles are still silanol groups, while the influence of the silanol groups on the overall surface chemistry of the pore surface should not be underestimated[67].

The pore size is crucial for drug loading because the mesopores act as molecular sieves and in this way they can determine the size of molecules that can be loaded into the carrier materials. Generally, the ratio of pore diameter/ drug molecule size should be >1 so that the pores will be accessible for drug molecules. Furthermore, the ratio should be greater than 3 if the full use of surface area and high drug loading is desired. Horcajada *et al.*[68] have prepared mesoporous MCM-41 with different pore sizes by using surfactant molecules with different lengths of alkyl chain and subsequently studied the effect of pore size on drug loading. After immersing mesoporous MCM-41 in a hexane solution with ibuprofen (molecule size 1.0 nm × 0.5 nm), more ibuprofen molecules were loaded into the carrier with the pore size of 3.6 nm (loading degree of 19 wt.%) than in that with the pore size of 2.5 nm (11 wt.%).

Pore size affects also the possibility of drug crystallization, which influences the drug solubility. In the classical theory of homogenous nucleation, crystal growth proceeds spontaneously once a critical nucleation size is reached[69]. If, however, the spatial constraints of a capillary are imposed on the clusters of molecules before they reach the critical size, nucleation and growth will be prevented and the system will exist in an intrinsically noncrystalline state. Mesoporous materials have pores with diameters lower than the critical nucleation size of many popular drugs, so they have been used to increase their solubility. Solubility improvement was observed for a wide range of compounds such as carbamazepine[70], danazol[70], cinnarizine[70], diazepam[70], indomethacin[70,71], griseofulvin[70], ketoconazole[70], phenylbutazone[70], nifedipine[70], fenofibrate[70,72], telimisartan[73], glibenclimide[74] and carvedilol[75]. Wang *et al.* have encapsulated poorly water soluble drug, telmisartan, into mesoporous silica nanoparticles and mesoporous silica microparticles to test the oral drug delivery potentials of mesoporous particles in beagle dogs[76]. After the administration of drugs by gavage, the mean plasma drug concentrations were determined by HPLC. After the pharmacokinetic calculations, they found that the relative bioavaibilities of telmisartan-loaded nano- and microparticles were 154.4 ± 28.4% and 129.1 ± 15.6%, respectively, of commercial product Micardis. This research demonstrated the significant potential of using mesoporous particles to promote drug dissolution and drug permeability, thus to enhance the oral bioavailability of drugs.

The loading and release efficiencies of the particles are also affected by the electrostatic interactions between the cargo molecules and the silica surface[77,78]. Various studies using silica materials as adsorbents have shown that the maximum

adsorption of protein occurs at or near the isoelectric (pI) point of the protein. For example, myoglobin, cytochrome c (cyt c) and bovine serum albumin (BSA) have been shown to have a higher adsorption capacity onto the materials at a pH equal or less than the pI point of the protein[66].

For adsorption to take place in the solution state, the chemical potential of the drug in the solution must be the same as the chemical potential of drug adsorbed on the surface of silica at equilibrium. The same is true for the solvent molecules as well. Depending on the collective properties of the silica surface, solvent, and drug compound, a competitive interaction with the silica surface between solvent and drug molecules can be expected. Charnay *et al.*[79] and Fernandez-Nunez *et al.*[80] have studied the effect of solvent polarity on the capacity of ibuprofen inclusion in MCM-41 and SBA-15 silicas. The amount of ibuprofen adsorbed showed an inverse trend with the polarity of the solvent. The less polar solvent the greater amount of ibuprofen adsorbed on both MCM-41 and SBA-15.

Dissolution rate depends on the volume of dissolution media, hydrodynamic conditions, and amount of drug present, among other factors. The volumes of the dissolution media used by various investigators reporting controlled release were between 10 and 100mL[52,81,82]. Because hydrodynamic conditions were not clearly specified, local supersaturation may have resulted in precipitation, followed by slow dissolution of precipitated drug into the bulk medium. Sustained release might be an outcome of slow dissolution from the crystallized drug. On the other hand, if the pore diameter of SiO_2 is similar to the dimensions of drug molecules, the diffusion of the molecules out of pores during dissolution can be kinetically hindered due to collisions between the drug and water molecules or the drug molecules and the pore wall. On the basis of this explanation, microporous SiO_2 with 0.4-nm mean pore diameter has been synthesized to develop controlled release formulations of ibuprofen[83] and chlorhexidine[84]. In addition, if the lengths of the pores are sufficiently long, the formulation may provide sustained release because of the diffusion path length.

4.3. Examples of drug delivery systems triggered by different stimuli

Generally, the release of poorly soluble drugs can be fitted with Higuchi or Korsmeyer–Peppas model:

$$Q = K_H * \sqrt{t} \tag{1}$$

$$F = \left(\frac{M_t}{M}\right) = K_m t^n \tag{2}$$

In the Higuchi equation (1), Q is the cumulative amount of drug released at time t and K_H is the Higuchi constant. In the Korsmeyer-Peppas equation (2), F is the fraction of drug released at time t, M_t is the amount of drug released at time t, M is the total amount of the loaded drug in mesoporous carriers, K_m is the kinetic constant and n is the release constant. If n equals to 1/2 in the Korsmeyer-Peppas equation, both of the models describe diffusion controlled release.

The Higuchi equation is used to describe the release of cargo molecules from an insoluble carrier. Fitting with Higuchi equation suggests that the drug release is limited by diffusion process. Unlike bioactive polymer-based drug carriers, the mesoporous materials are mostly prepared with inorganic compounds that are insoluble in aqueous solutions under biological condition, so the Higuchi equation could also be applied to the mesoporous silica materials to explain the drug release kinetics. The Korsmeyer–Peppas equation is a more comprehensive way to describe the drug release kinetics from the mesoporous carriers, which is indicated by the parameter n in Eq. (2)[29].

Table 2. Examples of biologically active compounds that have already been released from unmodified or modified mesoporous silicas[85,29]

MCM-41
ibuprofen, vancomycin, gentamycin, acetylsalicylic acid, sodium alendronate, camptothecin, atenolol, cytochrome C, bovine serum albumin, paclitaxel, vitamin-B_2, calcein, safranine O, cAMP, carvedilol, fenofibrate, indomethacin, telmisartan
FSM
taxol, flurbiprofen
SBA-15
gentamycin, amoxicillin, erythromycin, sodium alendronate, L-tryptophan, bovine serum albumin, nimodipine, ezetimibe, fenofibrate, glibenclamide, indomethacin, itraconazole, telmisartan, griseofulvin
MCM-48
erythromycin
hollow mesoporous nanoparticles
fluorescein, propidium iodide
other
atazanavir

4.3.1. Release from the unmodified particles

The effect of incorporation of three poorly soluble drugs from BSC class II (ibuprofen and griseofulvin) and class IV (furosemide) into mesoporous silicon microparticles[86] on their solubility and release was studied. After loading the cargo, the dissolution of these model drugs was clearly improved and the pH dependence of the dissolution was reduced. The drugs loaded into the unmodified mesoporous silicas show very fast initial drug release profiles; i.e., 50% of the loaded itraconazole was dissolved within 3 min and more than 80% of the drug was dissolved after 5 min compared to only 14% solution of pure itraconazole.

Ibuprofen is probably the most extensively studied hydrophobic drug in the applications involving adsorption in matrices of mesoporous silicas[65,77,87]. The loading capacity and the release rate of ibuprofen from these materials have been proved to be affected by the surface area, pore diameter and surface functionalization[88-90].

The *in vitro* applications of unmodified mesoporous silicas to deliver hydrophobic anti-cancer drugs, namely camptothecin and paclitaxel, to human cancer cells have been studied[91,92]. A suspension of camptothecin loaded particles in phosphate buffer saline (PBS) was added to a human pancreatic cancer cell culture PANC-1. The uptake of the mesoporous silica was confirmed by the fluorescence from the fluorescein isothiocyanate (FITC) labeled particles within the cells. The cytotoxic efficacy of the camptothecin-loaded silica is similar to that of the DMSO dissolved camptothecin, and much higher than the cytotoxicity of the PBS suspension of camptothecin.

Balkus *et al.* have reported lysozyme immobilisation within MCM-41 matrices. This study highlighted the importance of silica pore size to encapsulate the enzyme. But, MCM-41 could not encapsulate a biomolecule with a size greater than 40 kDa[93]. On the other hand, SBA-15 with larger pore sizes (5–30 nm) could encapsulate various larger proteins. Unfortunately, the amount of larger protein such as bovine serum albumin[94] adsorbed in SBA-15 materials (pore sizes 6.8 nm) was small.

Sun *et al.* have been able to perform highly accelerated lysozymes adsorption by enlarging the conventional SBA-15 pore. They synthesized a material with ordered large mesopores with a pore size of 13 nm. Adsorption of enzymes reached equilibrium after 10 min as compared to hours needed to reach equilibrium in the conventional SBA-15. They could confirm that most of the lysozymes were within the pores.

4.3.2. Release from modified particles

Fujiwara and co-workers have introduced light-responsive mesoporous silica

systems from which the release of the cargo could be controlled through the photo-controlled and reversible intermolecular dimerization of coumarin derivatives attached to the pore outlets[95]. The same group has developed a controlled storage and release system by attaching azobenzene groups to the mesopore outlets. The release was promoted by simultaneous irradiation with UV and visible light, which made the azobenzene molecules act as both impellers and gatekeepers. Other light-operated systems, developed by Zink and co-workers[96], uses differences in binding affinity between β-CD and both isomers (*cis*- and *trans*-) of azobenzene. Irradiation with 351 nm light causes the isomerisation of azobenzene to the *cis* conformation and therefore pore uncapping. Another example of light-sensitive systems includes Au nanoparticles anchored to the surface through thioundecyl-tetraethyleneglycoester-nitrobenzylethyldimethylammonium bromide (TUNA). Upon UV irradiation TUNA would lead to the negatively charged thioundecyltetraethyleneglycolcarboxylate (TUEC), leading to the dissociation of the Au NPs from the surface due to charge repulsion[97]. Lin and co-workers have loaded the mesopores of mercaptopropyl-functionalized silica with sulforhodamine 101 and the cargo molecules were entrapped by the presence of $Ru(bpy)_2(PPh_3)$-moieties, coordinated to mercaptopropyl functional groups[98]. Upon irradiation with visible light, Ru-S coordination bond was cleaved, triggering the release of capping species and loaded molecules.

The pH-sensitive supramolecular nanovalves with the N-methylbenzimidazole stalks have the ability to bind β-CD strongly at pH 7.4[99], trapping dye or drug molecules inside the mesopores of silica. Upon entering an endosomal compartment at pH<6, N-methylbenzimidazole becomes protonated and β-CD cap dissociates, allowing the cargo molecules to be released from the silica. Meng and co-workers[100] have loaded mesoporous silica with either Hoechst 33342 to cause nuclear staining in human differentiated myeloid cells (THP-1) or anticancer drug doxorubicin to induce cell apoptosis in squamous carcinoma (KB-31) cells. Cyclodextrin and polyethyleneimine complexes have been used by Kim and co-workers to achieve a pH-dependent cargo release. Calcein molecules were first loaded into pores and then cyclodextrin/polyethyleneimine inclusion complexes were attached onto the surface of mesoporous silica nanoparticles. Due to the size of these compounds the cargo is protected until polypseudorotaxane is split. In acidic conditions, the cyclodextrin complex can be broken and hence the cargo can be released.

Magnetic field can also be used as external stimulus to trigger the release of molecules – it can guide the drug delivery systems to the desired location, hold them until the therapy is complete, and then remove them. Chen *et al.*[101] have recently reported the capping of mesoporous silica with Fe_3O_4 magnetic nanoparticles. To

achieve this, silica was first functionalized with 3-aminopropyltrimethoxysilane and then loaded with camptothecin. The mesopore entrances were covalently capped through amidation of the 3-aminopropyltrimethoxysilane bound at the pore surface with *meso*-2,3-dimercaptosuccinic acid functionalized superparamagnetic iron oxide nanoparticles with an average diameter of 5.6 nm. When a magnetic trigger was applied, the Fe_3O_4 caps were removed due to the cleavage of chemical bonds and this subsequently led to a fast-responsive drug release. Also some rattle-type particles with large hollow interior spaces, functional cores and mesoporous silica shells have been prepared. Shi and co-workers[102] have prepared a series of rattle-type $Fe_3O_4/Fe_2O_3@mSiO_2$ hollow ellipsoids/spheres with a single or double mesoporous silica shell and loaded them with doxycycline (DOX). The excellent blood compatibility and the greater cytotoxicity of doxycycline loaded nanospheres than free doxycycline to induce MCF-7 cell death indicate that the $Fe_3O_4@mSiO_2$ nanocapsules are excellent anticancer drug carriers for diagnosis and chemotherapy applications.

It is known that the local temperature in many tumours is slightly higher than normal body temperature. This is why a temperature-sensitive delivery system able to release its cargo only at temperatures higher than 37°C, but preserving the drugs entrapped while in blood, is required. Thermo-sensitive polymers, such as poly(N-isopropylacrylamide) (PNIPAM) and its derivatives have been used in the design of thermo-responsive release systems, reported in the recent years[103,104]. PNIPAM changes its conformation responding to temperature in aqueous environments. Its chains are hydrated below the lower critical solution temperature (LCST) of 32°C and occupy more space near the pore entrances and this is what prevents the departure of the cargo loaded inside the mesopore channels. Increasing the temperature above the LCST dehydrates the polymer chains, collapses PNIPAM's conformation and opens the pores resulting in a release of the cargo. Increasing the LCST under physiological conditions would be desirable for biomedical applications and this can be achieved by modifying the polymer composition by copolymerization with other monomers (such as acrylamide[105] or N-isopropylmethacrylamide[106]). Baeza *et al.* created a novel nanodevice based on mesoporous silica with iron oxide nanoparticles inside the matrix and decorated on the outer surface with a thermo-responsive copolymer of poly(ethylenimine)-β-poly(N-isopropylacrylamide) that was able to deliver small molecules or proteins in response to an alternating magnetic field or temperature[107]. Other thermo-responsive systems that have been already prepared involve double-stranded DNA sequences attached to the pore openings of mesoporous silica melting at certain temperatures[108] or octadecyl chains interacting with a hydrophobic layer made of paraffin that melts at certain

temperature, specific for different paraffins[109].

Another stimulus that can be used in controlled delivery systems is the redox potential. Different redox potential-responsive systems have been developed until now. They use various gatekeepers, such as CdS[110], Au[111] or Fe_3O_4[112] nanoparticles or organic molecules such as cross-linked poly(N-acryloxysuccinimide)[113], collagen[114] or cyclodextrin[115], covalently attached to the silica through disulphide links. These caps can be removed by cleaving such links using disulphide-reducing agents, such as mercaptoethanol or dithiothreitol. Redox potential is an important stimulus as in most tumor cells the level of intracellular glutathione, a natural reducer, is 100-1000-fold higher than in the extracellular space.

Biomolecules are internal stimuli that can be used to trigger cargo release. Enzyme-responsive systems can be represented by cyclodextrin-capped mesoporous silica attached on the silica surface thanks to "click chemistry" reactions. The addition of α-amylase catalyzed the hydrolysis and allowed the release of calcein trapped inside the pores[116]. Another example of such systems can be the one prepared by Martínez-Máñez and co-workers. They described the capping of mesoporous silica with lactose and the selective uncapping in the presence of enzyme β-D-galactosidase[117]. The same group developed multi-enzyme-responsive capped mesoporous silica containing amide and urea links to block the pores. The addition of amidase and urease triggered the cargo release. Amidase induced an immediate, but not complete release and urease allowed a near total cargo release that was delayed in time[118]. Glucose-responsive systems can be used in the treatment of diabetes. Zhao *et al.*[119] have reported a double delivery system for both insulin and cyclic adenosine monophosphate (that activates Ca^{2+} channels of pancreas beta cells stimulating insulin secretion) with precise control over the sequence of release. cAMPs gluconic acid-modified insulin proteins were immobilized on the outermost surface of phenylboronic acid-functionalized silica particles *via* reversible covalent bonding. Modified insulin also served as caps to encapsulate cAMP molecules inside the mesoporous channels. Phenylboronic acid forms much more stable cyclic esters with the adjacent diols of saccharides than with acyclic diols. Thus, the presence of saccharides induced the release of modified insulin and cAMP trapped inside the pores. Examples of very interesting biomolecules-responsive systems include antigen-responsive reported by Climent *et al.*[120], where hapten-modified surface of the mesoporous silica is covered by antibody nanoscopic caps that can recognize a certain hapten releasing the cargo after displacement reaction, or aptamer-target-responsive system containing aptamers (single stranded, short oligonucleotide sequences that can bind specific targets with high affinity and specifity) releasing the cargo upon detection of certain guest molecules (i.e. ATP[121]).

4.3.3. Modified mesoporous silica nanosystems against cancer multidrug resistance

Nanoparticle-mediated delivery of a single cancer drug often serves as proof of concept. A clinically relevant alternative approach is to combine therapeutic agents targeting specific survival mechanisms of cancer cells with classical anticancer drugs. One of the problems, with potential to be solved by co-delivery of several compounds, is cancer multidrug resistance (MDR) which is a major cause of therapy failure in cancer patients. Design of a drug delivery system might be tailored to overcome MDR by focusing on the ability for targeted delivery of different cargos to combine circumvention of MDR mechanisms with chemotherapy. We want to underline that the problem of MDR in general is far from being resolved, but the attempts made to overlap it with nanoparticle drug delivery are worth considering[122].

Although the mechanisms of MDR are multifaceted, they can be roughly classified as pharmacological and cellular. Pharmacological MDR mechanism employs different circumstances resulting in therapeutically insufficient drug dosage, such as inadequate infusion, influence of tumor microenvironment, pharmacokinetics in the plasma and others. Cellular mechanisms, simply classified into pump and non-pump, such as ABC-transporters, apoptosis signaling pathways, and DNA repair pathways may be switched on and off during the development of a drug-resistant phenotype and are potentially "druggable". Many of these challenges could be overcome by using drug carriers.

For example, a combination of mesoporous silica, an anticancer drug (DOX or cisplatin (CIS)), a suppressor drug resistance (siRNA targeted to MRP1 transporter or BCL2 mRNA), and a tumor targeting moiety (LHRH peptide) has been used and revealed enhanced anticancer activity when compared to that of free drug mixtures[123].

A different approach to overcome drug resistance has been investigated by Huang *et al.*[124], who studied DOX attached to the surface through a pH-sensitive linker, hydrazone bonds, to provide sustained and proportionate release of DOX and its effectiveness against human uterine sarcoma MES-SA/DOX-resistant tumor cell line was tested. Its uptake and activity were higher than those of free doxycycline and doxycycline combined with verapamil (the inhibitor of drug efflux pump protein).

Another modification of pH-responsive silica nanoparticles able to overcome drug resistance has been published by He *et al.*[125] Their nanoparticles consisted of silica still containing the surfactant, cetyltrimethylammoniumbromide (CTAB), and doxycycline. The surfactant was used as a chemosensitizer for overcoming the multidrug resistance and enhancing the drug efficiency. The cytotoxicity of

these particles was tested on MCF-7 and MCF-7/ADR cell lines and composite mesoporous silica was shown to increase the MCF-7/ADR intracellular accessibility to doxycycline and presented much higher drug efficiencies *in vitro* against both cell lines compared to that of the free drug.

Dual stimuli-responsive systems are those able to respond to two stimuli, either in an independent or in a synergistic fashion. Martínez-Máñez *et al.*[126] attached suitable polyamines to the silica surface to obtain pH sensitive and anion-controllable gate-like ensembles capable of controlling the release of a ruthenium dye trapped inside the mesoporous matrix. To achieve this goal, they varied the pH value and content of certain anions in the release medium.

Acknowledgements

This work was partially supported from the funds of National Science Centre (grant no. 2011/03/B/ST5/01573).

References

1. Kresge, C. T.; Leonowicz, M. E.; Roth, W. J.; Vartuli, J. C.; Beck, J. S., Ordered mesoporous molecular sieves synthesized by a liquid-crystal template mechanism, *Nature* **1992**, *359*, 710.
2. Bagshaw, S. A.; Prouzet, E.; Pinnavaia, T. J., Templating of Mesoporous Molecular Sieves by Nonionic Polyethylene Oxide Surfactants, *Science* **1995**, *269*, 1242.
3. Ryoo, R.; Kim, J. M.; Ko, C. H.; Shin, C. H., Disordered Molecular Sieve with Branched Mesoporous Channel Network, *The Journal of Physical Chemistry* **1996**, *100*, 17718.
4. Zhao, D.; Feng, J.; Huo, Q.; Melosh, N.; Fredrickson, G. H.; Chmelka, B. F.; Stucky, G. D., Triblock Copolymer Syntheses of Mesoporous Silica with Periodic 50 to 300 Angstrom Pores, *Science* **1998**, *279*, 548.
5. Han, Y.; Ying, J. Y., Generalized Fluorocarbon-Surfactant-Mediated Synthesis of Nanoparticles with Various Mesoporous Structures, *Angewandte Chemie International Edition* **2005**, *44*, 288.
6. Huo, Q.; Margolese, D. I.; Ciesla, U.; Feng, P.; Gier, T. E.; Sieger, P.; Leon, R.; Petroff, P. M.; Schuth, F.; Stucky, G. D., Generalized synthesis of periodic surfactant/inorganic composite materials, *Nature* **1994**, *368*, 317.
7. Shigeno, T.; Nagao, M.; Kimura, T.; Kuroda, K., Direct Silylation of a Mesostructured Precursor for Novel Mesoporous Silica KSW-2, *Langmuir* **2002**, *18*, 8102.

8. Inagaki, S.; Fukushima, Y.; Kuroda, K., Synthesis of highly ordered mesoporous materials from a layered polysilicate, *Journal of the Chemical Society, Chemical Communications* **1993**, 680.
9. Zhang, W.; Pauly, T. R.; Pinnavaia, T. J., Tailoring the Framework and Textural Mesopores of HMS Molecular Sieves through an Electrically Neutral (S°I°) Assembly Pathway, *Chemistry of Materials* **1997**, *9*, 2491.
10. Avnir, D.; Coradin, T.; Lev, O.; Livage, J., Recent bio-applications of sol-gel materials, *Journal of Materials Chemistry* **2006**, *16*, 1013.
11. Gill, I., Bio-doped Nanocomposite Polymers: Sol−Gel Bioencapsulates, *Chemistry of Materials* **2001**, *13*, 3404.
12. Bromley, A. *Theranostics: the influence of diagnostics on pharmaceutical therapy*; P. J. B. Publications: Richmond, 2000.
13. Grün, M.; Lauer, I.; Unger, K. K., The synthesis of micrometer- and submicrometer-size spheres of ordered mesoporous oxide MCM-41, *Advanced Materials* **1997**, *9*, 254.
14. Vasiliev, P. O.; Faure, B.; Ng, J. B. S.; Bergström, L., Colloidal aspects relating to direct incorporation of TiO2 nanoparticles into mesoporous spheres by an aerosol-assisted process, *Journal of Colloid and Interface Science* **2008**, *319*, 144.
15. Trommelen, A. M.; Crosby, E. J., Evaporation and drying of drops in superheated vapors, *AIChE Journal* **1970**, *16*, 857.
16. Kishida, M.; Fujita, T.; Umakoshi, K.; Ishiyama, J.; Nagata, H.; Wakabayashi, K., Novel preparation of metal-supported catalysts by colloidal microparticles in a water-in-oil microemulsion; catalytic hydrogenation of carbon dioxide, *Journal of the Chemical Society, Chemical Communications* **1995**, 763.
17. Pileni, M.; Fendler, J. H. *Nanoparticles and Nanostructured Films*; Wiley-VCH: New York, 1998.
18. Vestal, C. R.; Zhang, Z. J., Synthesis of CoCrFeO4 Nanoparticles Using Microemulsion Methods and Size-Dependent Studies of Their Magnetic Properties, *Chemistry of Materials* **2002**, *14*, 3817.
19. Mizutani, M.; Yamada, Y.; Nakamura, T.; Yano, K., Anomalous Pore Expansion of Highly Monodispersed Mesoporous Silica Spheres and Its Application to the Synthesis of Porous Ferromagnetic Composite, *Chemistry of Materials* **2008**, *20*, 4777.
20. Suzuki, K.; Ikari, K.; Imai, H., Synthesis of Silica Nanoparticles Having a Well-Ordered Mesostructure Using a Double Surfactant System, *Journal of the American Chemical Society* **2003**, *126*, 462.

21. Gao, F.; Botella, P.; Corma, A.; Blesa, J.; Dong, L., Monodispersed Mesoporous Silica Nanoparticles with Very Large Pores for Enhanced Adsorption and Release of DNA, *The Journal of Physical Chemistry B* **2009**, *113*, 1796.
22. Möller, K.; Kobler, J.; Bein, T., Colloidal Suspensions of Nanometer-Sized Mesoporous Silica, *Advanced Functional Materials* **2007**, *17*, 605.
23. He, Q.; Cui, X.; Cui, F.; Guo, L.; Shi, J., Size-controlled synthesis of monodispersed mesoporous silica nano-spheres under a neutral condition, *Microporous and Mesoporous Materials* **2009**, *117*, 609.
24. Urata, C.; Aoyama, Y.; Tonegawa, A.; Yamauchi, Y.; Kuroda, K., Dialysis process for the removal of surfactants to form colloidal mesoporous silica nanoparticles, *Chemical Communications* **2009**, 5094.
25. Zhuravlev, L. T., The surface chemistry of amorphous silica. Zhuravlev model, *Colloids and Surfaces A: Physicochemical and Engineering Aspects* **2000**, *173*, 1.
26. Rosenholm, J. M.; Czuryszkiewicz, T.; Kleitz, F.; Rosenholm, J. B.; Lindén, M., On the Nature of the Brønsted Acidic Groups on Native and Functionalized Mesoporous Siliceous SBA-15 as Studied by Benzylamine Adsorption from Solution, *Langmuir* **2007**, *23*, 4315.
27. Asefa, T.; Tao, Z., Biocompatibility of Mesoporous Silica Nanoparticles, *Chemical Research in Toxicology* **2012**, *25*, 2265.
28. Colilla, M.; Gonzalez, B.; Vallet-Regi, M., Mesoporous silica nanoparticles for the design of smart delivery nanodevices, *Biomaterials Science* **2013**, *1*, 114.
29. Xu, W.; Riikonen, J.; Lehto, V.-P., Mesoporous systems for poorly soluble drugs, *International Journal of Pharmaceutics* **2013**, *453*, 181.
30. Sailor, M. J.; Park, J.-H., Hybrid Nanoparticles for Detection and Treatment of Cancer, *Advanced Materials* **2012**, *24*, 3779.
31. Li, Z.; Barnes, J. C.; Bosoy, A.; Stoddart, J. F.; Zink, J. I., Mesoporous silica nanoparticles in biomedical applications, *Chem. Soc. Rev.* **2012**, *41*, 2590.
32. Vallhov, H.; Gabrielsson, S.; Strømme, M.; Scheynius, A.; Garcia-Bennett, A. E., Mesoporous Silica Particles Induce Size Dependent Effects on Human Dendritic Cells, *Nano Letters* **2007**, *7*, 3576.
33. Napierska, D.; Thomassen, L. C. J.; Rabolli, V.; Lison, D.; Gonzalez, L.; Kirsch-Volders, M.; Martens, J. A.; Hoet, P. H., Size-Dependent Cytotoxicity of Monodisperse Silica Nanoparticles in Human Endothelial Cells, *Small* **2009**, *5*, 846.

34. Qianjun, H.; Zhiwen, Z.; Yu, G.; Jianlin, S.; Yaping, L., Intracellular localization and cytotoxicity of spherical mesoporous silica nano-/micro-particles, *Small* **2009**, *5*, 2722.
35. Lu, F.; Wu, S.-H.; Hung, Y.; Mou, C.-Y., Size Effect on Cell Uptake in Well-Suspended, Uniform Mesoporous Silica Nanoparticles, *Small* **2009**, *5*, 1408.
36. Lee, C.-H.; Cheng, S.-H.; Wang, Y.-J.; Chen, Y.-C.; Chen, N.-T.; Souris, J.; Chen, C.-T.; Mou, C.-Y.; Yang, C.-S.; Lo, L.-W., Near-Infrared Mesoporous Silica Nanoparticles for Optical Imaging: Characterization and In Vivo Biodistribution, *Advanced Functional Materials* **2009**, *19*, 215.
37. Cho, M.; Cho, W.-S.; Choi, M.; Kim, S. J.; Han, B. S.; Kim, S. H.; Kim, H. O.; Sheen, Y. Y.; Jeong, J., The impact of size on tissue distribution and elimination by single intravenous injection of silica nanoparticles, *Toxicology Letters* **2009**, *189*, 177.
38. Park, J.-H.; Gu, L.; Maltzahn, G. V.; Ruoslahti, E.; Bhatia, S. N.; Sailor, M. J., Biodegradable luminescent porous silicon nanoparticles for in vivo applications, *Nat. Mater.* **2009**, *8*, 331.
39. Tao, Z.; Toms, B. B.; Goodisman, J.; Asefa, T., Mesoporosity and Functional Group Dependent Endocytosis and Cytotoxicity of Silica Nanomaterials, *Chemical Research in Toxicology* **2009**, *22*, 1869.
40. Di Pasqua, A. J.; Sharma, K. K.; Shi, Y.-L.; Toms, B. B.; Ouellette, W.; Dabrowiak, J. C.; Asefa, T., Cytotoxicity of mesoporous silica nanomaterials, *Journal of Inorganic Biochemistry* **2008**, *102*, 1416.
41. Huang, X.; Teng, X.; Chen, D.; Tang, F.; He, J., The effect of the shape of mesoporous silica nanoparticles on cellular uptake and cell function, *Biomaterials* **2010**, *31*, 438.
42. Verma, A.; Stellacci, F., Effect of Surface Properties on Nanoparticle–Cell Interactions, *Small* **2010**, *6*, 12.
43. Lin, Y.-S.; Haynes, C. L., Impacts of Mesoporous Silica Nanoparticle Size, Pore Ordering, and Pore Integrity on Hemolytic Activity, *Journal of the American Chemical Society* **2010**, *132*, 4834.
44. Chen, Y.; Chen, H.; Guo, L.; He, Q.; Chen, F.; Zhou, J.; Feng, J.; Shi, J., Hollow/Rattle-Type Mesoporous Nanostructures by a Structural Difference-Based Selective Etching Strategy, *ACS Nano* **2009**, *4*, 529.
45. He, Q.; Zhang, J.; Shi, J.; Zhu, Z.; Zhang, L.; Bu, W.; Guo, L.; Chen, Y., The effect of PEGylation of mesoporous silica nanoparticles on nonspecific binding of serum proteins and cellular responses, *Biomaterials* **2010**, *31*, 1085.

46. Huang, X.; Li, L.; Liu, T.; Hao, N.; Liu, H.; Chen, D.; Tang, F., The Shape Effect of Mesoporous Silica Nanoparticles on Biodistribution, Clearance, and Biocompatibility in Vivo, *ACS Nano* **2011**, *5*, 5390.
47. Davis, M. E.; Chen, Z.; Shin, D. M., Nanoparticle therapeutics: An emerging treatment modality for cancer, *Nat. Rev. Drug Discovery* **2008**, *7*, 771.
48. Rosenholm, J. M.; Sahlgren, C.; Linden, M., Towards multifunctional, targeted drug delivery systems using mesoporous silica nanoparticles - opportunities & challenges, *Nanoscale* **2010**, *2*, 1870.
49. Slowing, I. I.; Vivero-Escoto, J. L.; Zhao, Y.; Kandel, K.; Peeraphatdit, C.; Trewyn, B. G.; Lin, V. S. Y., Exocytosis of Mesoporous Silica Nanoparticles from Mammalian Cells: From Asymmetric Cell-to-Cell Transfer to Protein Harvesting, *Small* **2011**, *7*, 1526.
50. Etienne, M.; Walcarius, A., Analytical investigation of the chemical reactivity and stability of aminopropyl-grafted silica in aqueous medium, *Talanta* **2003**, *59*, 1173.
51. He, Q.; Shi, J.; Zhu, M.; Chen, Y.; Chen, F., The three-stage in vitro degradation behavior of mesoporous silica in simulated body fluid, *Microporous and Mesoporous Materials* **2010**, *131*, 314.
52. Mortera, R.; Fiorilli, S.; Garrone, E.; Verné, E.; Onida, B., Pores occlusion in MCM-41 spheres immersed in SBF and the effect on ibuprofen delivery kinetics: A quantitative model, *Chemical Engineering Journal* **2010**, *156*, 184.
53. Mamaeva, V.; Rosenholm, J. M.; Bate-Eya, L. T.; Bergman, L.; Peuhu, E.; Duchanoy, A.; Fortelius, L. E.; Landor, S.; Toivola, D. M.; Linden, M.; Sahlgren, C., Mesoporous Silica Nanoparticles as Drug Delivery Systems for Targeted Inhibition of Notch Signaling in Cancer, *Mol Ther* **2011**, *19*, 1538.
54. He, X.; Nie, H.; Wang, K.; Tan, W.; Wu, X.; Zhang, P., In Vivo Study of Biodistribution and Urinary Excretion of Surface-Modified Silica Nanoparticles, *Analytical Chemistry* **2008**, *80*, 9597.
55. Lu, J.; Liong, M.; Li, Z.; Zink, J. I.; Tamanoi, F., Biocompatibility, Biodistribution, and Drug-Delivery Efficiency of Mesoporous Silica Nanoparticles for Cancer Therapy in Animals, *Small* **2010**, *6*, 1794.
56. Souris, J. S.; Lee, C.-H.; Cheng, S.-H.; Chen, C.-T.; Yang, C.-S.; Ho, J.-a. A.; Mou, C.-Y.; Lo, L.-W., Surface charge-mediated rapid hepatobiliary excretion of mesoporous silica nanoparticles, *Biomaterials* **2010**, *31*, 5564.
57. Zhao, W.; Chen, H.; Li, Y.; Li, L.; Lang, M.; Shi, J., Uniform Rattle-

type Hollow Magnetic Mesoporous Spheres as Drug Delivery Carriers and their Sustained-Release Property, *Advanced Functional Materials* **2008**, *18*, 2780.
58. Zhu, Y.; Shi, J.; Shen, W.; Chen, H.; Dong, X.; Ruan, M., Preparation of novel mesoporous silica spheres and their sustained-release property, *Nanotechnology* **2005**, *16*, 2633.
59. Fu, Q.; Rao, G. V.-R.; Ista, L. K.; Wu, Y.; Andrzejewski, B. P.; Sklar, L. A.; Ward, T. L.; Lopez, G. P., Control of molecular transport through stimuli-responsive ordered mesoporous materials, *Adv. Mater* **2003**, *15*, 1262.
60. Mal, N. K.; Fujiwara, M.; Tanaka, Y.; Taguchi, T.; Matsukata, M., Photo-switched storage and release of guest molecules in the pore void of coumarin-modified MCM-41, *Chem. Mater.* **2003**, *15*, 3385.
61. Vivero-Escoto, J. L.; Slowing, I. I.; Trewyn, B. G.; Lin, V. S.-Y., Mesoporous silica nanoparticles for intracellular controlled drug delivery, *Small* **2010**, *6*, 1952.
62. Sudimack, J.; Lee, R. J., Targeted drug delivery via the folate receptor, *Advanced Drug Delivery Reviews* **2000**, *41*, 147.
63. Elnakat, H.; Ratnam, M., Distribution, functionality and gene regulation of folate receptor isoforms: implications in targeted therapy, *Advanced Drug Delivery Reviews* **2004**, *56*, 1067.
64. Lewandowski, D.; Schroeder, G. In *From molecules to functional architecture - Supramolecular interactions*; Rybachenko, V. I., Ed.; East Publisher House: Donetsk, 2012, p 229.
65. Andersson, J.; Rosenholm, J.; Areva, S.; Linden, M., Influences of material characteristics on ibuprofen drug loading and release profiles from ordered micro- and mesoporous silica matrices, *Chem. Mater.* **2004**, *16*, 4160.
66. Vinu, A.; Murugesan, V.; Tangermann, O.; Hartmann, M., Adsorption of Cytochrome c on Mesoporous Molecular Sieves: Influence of pH, Pore Diameter, and Aluminum Incorporation, *Chemistry of Materials* **2004**, *16*, 3056.
67. Rosenholm, J. M.; Lindén, M., Towards establishing structure–activity relationships for mesoporous silica in drug delivery applications, *Journal of Controlled Release* **2008**, *128*, 157.
68. Horcajada, P.; Rámila, A.; Pérez-Pariente, J.; Vallet, R.; amp; x; M., Influence of pore size of MCM-41 matrices on drug delivery rate, *Microporous and Mesoporous Materials* **2004**, *68*, 105.
69. Klafter, J.; Drake, J. M. *Molecular dynamics in restricted geometries*;

1st ed. New York City ed.; Wiley: New York 1989.
70. Van Speybroeck, M.; Barillaro, V.; Thi, T. D.; Mellaerts, R.; Martens, J.; Van Humbeeck, J.; Vermant, J.; Annaert, P.; Van den Mooter, G.; Augustijns, P., Ordered mesoporous silica material SBA-15: A broad-spectrum formulation platform for poorly soluble drugs, *Journal of Pharmaceutical Sciences* **2009**, *98*, 2648.
71. Limnell, T.; Santos, H. A.; Mäkilä, E.; Heikkilä, T.; Salonen, J.; Murzin, D. Y.; Kumar, N.; Laaksonen, T.; Peltonen, L.; Hirvonen, J., Drug delivery formulations of ordered and nonordered mesoporous silica: Comparison of three drug loading methods, *Journal of Pharmaceutical Sciences* **2011**, *100*, 3294.
72. Van Speybroeck, M.; Mellaerts, R.; Mols, R.; Thi, T. D.; Martens, J. A.; Van Humbeeck, J.; Annaert, P.; Van den Mooter, G.; Augustijns, P., Enhanced absorption of the poorly soluble drug fenofibrate by tuning its release rate from ordered mesoporous silica, *European Journal of Pharmaceutical Sciences* **2010**, *41*, 623.
73. Zhang, Y.; Jiang, T.; Zhang, Q.; Wang, S., Inclusion of telmisartan in mesocellular foam nanoparticles: Drug loading and release property, *European Journal of Pharmaceutics and Biopharmaceutics* **2010**, *76*, 17.
74. van Speybroeck, M.; Mellaerts, R.; Thi, T. D.; Martens, J. A.; Van Humbeeck, J.; Annaert, P.; Van den Mooter, G.; Augustijns, P., Preventing release in the acidic environment of the stomach via occlusion in ordered mesoporous silica enhances the absorption of poorly soluble weakly acidic drugs, *Journal of Pharmaceutical Sciences* **2011**, *100*, 4864.
75. Planinšek, O.; Kovačič, B.; Vrečer, F., Carvedilol dissolution improvement by preparation of solid dispersions with porous silica, *International Journal of Pharmaceutics* **2011**, *406*, 41.
76. Zhang, Y.; Wang, J.; Bai, X.; Jiang, T.; Zhang, Q.; Wang, S., Mesoporous Silica Nanoparticles for Increasing the Oral Bioavailability and Permeation of Poorly Water Soluble Drugs, *Molecular Pharmaceutics* **2012**, *9*, 505.
77. Munoz, B.; Ramila, A.; Perez-Pariente, J.; Diaz, I.; Vallet-Regi, M., MCM-41 organic modification as drug delivery rate regulator, *Chem. Mater.* **2003**, *15*, 500.
78. Chung, T. H.; Wu, S. H.; Yao, M.; Lu, C. W.; Lin, Y. S.; Hung, Y.; Mou, C. Y.; Chen, Y. C.; Huang, D. M., The effect of surface charge on the uptake and biological function of mesoporous silica nanoparticles in

3T3-L1 cells and human mesenchymal stem cells, *Biomaterials* **2007**, *28*, 2959.
79. Charnay, C.; Bégu, S.; Tourné-Péteilh, C.; Nicole, L.; Lerner, D. A.; Devoisselle, J. M., Inclusion of ibuprofen in mesoporous templated silica: drug loading and release property, *European Journal of Pharmaceutics and Biopharmaceutics* **2004**, *57*, 533.
80. Fernández-Núñez, M.; Zorrilla, D.; Montes, A.; Mosquera, M. J., Ibuprofen Loading in Surfactant-Templated Silica: Role of the Solvent According to the Polarizable Continuum Model, *The Journal of Physical Chemistry A* **2009**, *113*, 11367.
81. Aiello, R.; Cavallaro, G.; Giammona, G.; Pasqua, L.; Pierro, P.; Testa, F. In *Studies in Surface Science and Catalysis*; R. Aiello, G. G., Testa, F., Eds.; Elsevier: 2002; Vol. Volume 142, p 1165.
82. Wang, G.; Otuonye, A. N.; Blair, E. A.; Denton, K.; Tao, Z.; Asefa, T., Functionalized mesoporous materials for adsorption and release of different drug molecules: A comparative study, *Journal of Solid State Chemistry* **2009**, *182*, 1649.
83. Aerts, C. A.; Verraedt, E.; Depla, A.; Follens, L.; Froyen, L.; Van Humbeeck, J.; Augustijns, P.; Van den Mooter, G.; Mellaerts, R.; Martens, J. A., Potential of amorphous microporous silica for ibuprofen controlled release, *International Journal of Pharmaceutics* **2010**, *397*, 84.
84. Verraedt, E.; Pendela, M.; Adams, E.; Hoogmartens, J.; Martens, J. A., Controlled release of chlorhexidine from amorphous microporous silica, *Journal of Controlled Release* **2010**, *142*, 47.
85. Popat, A.; Hartono, S. B.; Stahr, F.; Liu, J.; Qiao, S. Z.; Qing Lu, G., Mesoporous silica nanoparticles for bioadsorption, enzyme immobilisation, and delivery carriers, *Nanoscale* **2011**, *3*, 2801.
86. Salonen, J.; Laitinen, L.; Kaukonen, A. M.; Tuura, J.; Björkqvist, M.; Heikkilä, T.; Vähä-Heikkilä, K.; Hirvonen, J.; Lehto, V. P., Mesoporous silicon microparticles for oral drug delivery: Loading and release of five model drugs, *Journal of Controlled Release* **2005**, *108*, 362.
87. Vallet-Regi, M.; Ramila, A.; Real, R. P. d.; Perez-Pariente, J., A new property of MCM-41: Drug delivery system, *Chem. Mater.* **2001**, *13*, 308.
88. Qu, F. Y.; Zhu, G. S.; Lin, H. W.; Zhang, W. M.; Sun, J. Y.; Li, S. G.; Qiu, S. L., A controlled release of ibuprofen by systematically tailoring the morphology of mesoporous silica materials, *J. Solid State Chem,* **2006**, *179*, 2027.

89. Horcajada, P.; A., R.; Gerard, F.; M., V.-R., Influence of superficial organic modification of MCM-41 matrices on drug delivery rate, *Solid State Sci.* **2006**, *8*, 1243.
90. Manzano, M.; Aina, V.; Arean, C. O.; Balas, F.; Cauda, V.; Colilla, M. R.; Delgado, M.; M., V.-R., Studies on MCM-41 mesoporous silica for drug delivery: Effect of particle morphology and amine functionalization, *Chem. Eng. J.* **2008**, *137*, 30.
91. Lu, J.; Liong, M.; Zink, J. I.; Tamanoi, F., Multifunctional inorganic nanoparticles for imaging, targeting, and drug delivery, *Small* **2007**, *3*, 1341.
92. Lu, J.; Liong, M.; Sherman, S.; Xia, T.; Kovochich, M.; Nel, A.; Zink, J.; Tamanoi, F., Mesoporous Silica Nanoparticles for Cancer Therapy: Energy-Dependent Cellular Uptake and Delivery of Paclitaxel to Cancer Cells, *Nanobiotechnol* **2007**, *3*, 89.
93. Díaz, J. F.; Balkus Jr, K. J., Enzyme immobilization in MCM-41 molecular sieve, *Journal of Molecular Catalysis B: Enzymatic* **1996**, *2*, 115.
94. Yiu, H. H. P.; Botting, C. H.; Botting, N. P.; Wright, P. A., Size selective protein adsorption on thiol-functionalised SBA-15 mesoporous molecular sieve, *Physical Chemistry Chemical Physics* **2001**, *3*, 2983.
95. Mal, N. K.; Fujiwara, M.; Tanaka, Y., Photocontrolled reversible release of guest molecules from coumarin-modified mesoporous silica, *Nature* **2003**, *421*, 350.
96. Ferris, D. P.; Zhao, Y.-L.; Khashab, N. M.; Khatib, H. A.; Stoddart, J. F.; Zink, J. I., Light-Operated Mechanized Nanoparticles, *Journal of the American Chemical Society* **2009**, *131*, 1686.
97. Vivero-Escoto, J. L.; Slowing, I. I.; Wu, C.-W.; Lin, V. S. Y., Photoinduced Intracellular Controlled Release Drug Delivery in Human Cells by Gold-Capped Mesoporous Silica Nanosphere, *Journal of the American Chemical Society* **2009**, *131*, 3462.
98. Knezevic, N. Z.; Trewyn, B. G.; Lin, V. S. Y., Functionalized mesoporous silica nanoparticle-based visible light responsive controlled release delivery system, *Chemical Communications* **2011**, *47*, 2817.
99. Meng, H.; Xue, M.; Xia, T.; Zhao, Y.-L.; Tamanoi, F.; Stoddart, J. F.; Zink, J. I.; Nel, A. E., Autonomous in Vitro Anticancer Drug Release from Mesoporous Silica Nanoparticles by pH-Sensitive Nanovalves, *Journal of the American Chemical Society* **2010**, *132*, 12690.
100. Park, C.; Oh, K.; Lee, S. C.; Kim, C., Controlled Release of Guest Molecules from Mesoporous Silica Particles Based on a pH-Responsive

Polypseudorotaxane Motif, *Angewandte Chemie International Edition* **2007**, *46*, 1455.
101. Chen, P.-J.; Hu, S.-H.; Hsiao, C.-S.; Chen, Y.-Y.; Liu, D.-M.; Chen, S.-Y., Multifunctional magnetically removable nanogated lids of Fe3O4-capped mesoporous silica nanoparticles for intracellular controlled release and MR imaging, *Journal of Materials Chemistry* **2011**, *21*, 2535.
102. Chen, Y.; Chen, H.; Zeng, D.; Tian, Y.; Chen, F.; Feng, J.; Shi, J., Core/Shell Structured Hollow Mesoporous Nanocapsules: A Potential Platform for Simultaneous Cell Imaging and Anticancer Drug Delivery, *ACS Nano* **2010**, *4*, 6001.
103. Park, J.-H.; Lee, Y.-H.; Oh, S.-G., Preparation of Thermosensitive PNIPAm-Grafted Mesoporous Silica Particles, *Macromolecular Chemistry and Physics* **2007**, *208*, 2419.
104. Zhu, S.; Zhou, Z.; Zhang, D.; Jin, C.; Li, Z., Design and synthesis of delivery system based on SBA-15 with magnetic particles formed in situ and thermo-sensitive PNIPA as controlled switch, *Microporous and Mesoporous Materials* **2007**, *106*, 56.
105. Zintchenko, A.; Ogris, M.; Wagner, E., Temperature Dependent Gene Expression Induced by PNIPAM-Based Copolymers: Potential of Hyperthermia in Gene Transfer, *Bioconjugate Chemistry* **2006**, *17*, 766.
106. Keerl, M.; Smirnovas, V.; Winter, R.; Richtering, W., Copolymer Microgels from Mono- and Disubstituted Acrylamides: Phase Behavior and Hydrogen Bonds, *Macromolecules* **2008**, *41*, 6830.
107. Baeza, A.; Guisasola, E.; Ruiz-Hernández, E.; Vallet-Regí, M., Magnetically Triggered Multidrug Release by Hybrid Mesoporous Silica Nanoparticles, *Chemistry of Materials* **2012**, *24*, 517.
108. Schlossbauer, A.; Warncke, S.; Gramlich, P. M. E.; Kecht, J.; Manetto, A.; Carell, T.; Bein, T., A Programmable DNA-Based Molecular Valve for Colloidal Mesoporous Silica, *Angewandte Chemie International Edition* **2010**, *49*, 4734.
109. Aznar, E.; Mondragón, L.; Ros-Lis, J. V.; Sancenón, F.; Marcos, M. D.; Martínez-Máñez, R.; Soto, J.; Pérez-Payá, E.; Amorós, P., Finely Tuned Temperature-Controlled Cargo Release Using Paraffin-Capped Mesoporous Silica Nanoparticles, *Angewandte Chemie International Edition* **2011**, *50*, 11172.
110. Lai, C.-Y.; Trewyn, B. G.; Jeftinija, D. M.; Jeftinija, K.; Xu, S.; Jeftinija, S.; Lin, V. S. Y., A Mesoporous Silica Nanosphere-Based Carrier System with Chemically Removable CdS Nanoparticle Caps for

Stimuli-Responsive Controlled Release of Neurotransmitters and Drug Molecules, *Journal of the American Chemical Society* **2003**, *125*, 4451.

111. Torney, F.; Trewyn, B. G.; Lin, V. S.-Y.; Wang, K., Mesoporous silica nanoparticles deliver DNA and chemicals into plants, *Nat. Nanotechnol.* **2007**, *2*, 295.
112. Giri, S.; Trewyn, B. G.; Stellmaker, M. P.; Lin, V. S. Y., Stimuli-Responsive Controlled-Release Delivery System Based on Mesoporous Silica Nanorods Capped with Magnetic Nanoparticles, *Angewandte Chemie International Edition* **2005**, *44*, 5038.
113. Liu, R.; Zhao, X.; Wu, T.; Feng, P., Tunable Redox-Responsive Hybrid Nanogated Ensembles, *Journal of the American Chemical Society* **2008**, *130*, 14418.
114. Luo, Z.; Cai, K.; Hu, Y.; Zhao, L.; Liu, P.; Duan, L.; Yang, W., Mesoporous Silica Nanoparticles End-Capped with Collagen: Redox-Responsive Nanoreservoirs for Targeted Drug Delivery, *Angewandte Chemie International Edition* **2011**, *50*, 640.
115. Kim, H.; Kim, S.; Park, C.; Lee, H.; Park, H. J.; Kim, C., Glutathione-Induced Intracellular Release of Guests from Mesoporous Silica Nanocontainers with Cyclodextrin Gatekeepers, *Advanced Materials* **2010**, *22*, 4280.
116. Park, C.; Kim, H.; Kim, S.; Kim, C., Enzyme Responsive Nanocontainers with Cyclodextrin Gatekeepers and Synergistic Effects in Release of Guests, *Journal of the American Chemical Society* **2009**, *131*, 16614.
117. Bernardos, A.; Aznar, E.; Marcos, M. D.; Martínez-Máñez, R.; Sancenón, F.; Soto, J.; Barat, J. M.; Amorós, P., Enzyme-Responsive Controlled Release Using Mesoporous Silica Supports Capped with Lactose, *Angewandte Chemie International Edition* **2009**, *48*, 5884.
118. Agostini, A.; Mondragón, L.; Coll, C.; Aznar, E.; Marcos, M. D.; Martínez-Máñez, R.; Sancenón, F.; Soto, J.; Pérez-Payá, E.; Amorós, P., Dual Enzyme-Triggered Controlled Release on Capped Nanometric Silica Mesoporous Supports, *ChemistryOpen* **2012**, *1*, 17.
119. Zhao, Y.; Trewyn, B. G.; Slowing, I. I.; Lin, V. S. Y., Mesoporous Silica Nanoparticle-Based Double Drug Delivery System for Glucose-Responsive Controlled Release of Insulin and Cyclic AMP, *Journal of the American Chemical Society* **2009**, *131*, 8398.
120. Climent, E.; Bernardos, A.; Martínez-Máñez, R. n.; Maquieira, A.; Marcos, M. D.; Pastor-Navarro, N.; Puchades, R.; Sancenón, F. l.; Soto, J.; Amorós, P., Controlled Delivery Systems Using Antibody-Capped Mesoporous Nanocontainers, *Journal of the American Chemical*

Society **2009**, *131*, 14075.
121. Zhu, C.-L.; Lu, C.-H.; Song, X.-Y.; Yang, H.-H.; Wang, X.-R., Bioresponsive Controlled Release Using Mesoporous Silica Nanoparticles Capped with Aptamer-Based Molecular Gate, *Journal of the American Chemical Society* **2011**, *133*, 1278.
122. Mamaeva, V.; Sahlgren, C.; Lindén, M., Mesoporous silica nanoparticles in medicine—Recent advances, *Advanced Drug Delivery Reviews* **2013**, *65*, 689.
123. Taratula, O.; Garbuzenko, O. B.; Chen, A. M.; Minko, T., Innovative strategy for treatment of lung cancer: targeted nanotechnology-based inhalation co-delivery of anticancer drugs and siRNA, *Journal of Drug Targeting* **2011**, *19*, 900.
124. Huang, I.-P.; Sun, S.-P.; Cheng, S.-H.; Lee, C.-H.; Wu, C.-Y.; Yang, C.-S.; Lo, L.-W.; Lai, Y.-K., Enhanced Chemotherapy of Cancer Using pH-Sensitive Mesoporous Silica Nanoparticles to Antagonize P-Glycoprotein–Mediated Drug Resistance, *Molecular Cancer Therapeutics* **2011**, *10*, 761.
125. He, Q.; Gao, Y.; Zhang, L.; Zhang, Z.; Gao, F.; Ji, X.; Li, Y.; Shi, J., A pH-responsive mesoporous silica nanoparticles-based multi-drug delivery system for overcoming multi-drug resistance, *Biomaterials* **2011**, *32*, 7711.
126. Casasús, R.; Climent, E.; Marcos, M. D.; Martínez-Máñez, R.; Sancenón, F.; Soto, J.; Amorós, P.; Cano, J.; Ruiz, E., Dual Aperture Control on pH- and Anion-Driven Supramolecular Nanoscopic Hybrid Gate-like Ensembles, *Journal of the American Chemical Society* **2008**, *130*, 1903.